Plasmonic (Bio)sensors Based on Nanostructured Metallic Surfaces

Dissertation

zur Erlangung des

Doktorgrades der Naturwissenschaften

(Dr. rer. nat.)

an der Fakultät Chemie und Pharmazie

der Universität Regensburg

Deutschland

vorgelegt von

Christa Genslein

aus Dorgendorf

im Jahr 2018

Die vorliegende Dissertation entstand in der Zeit von Oktober 2015 bis September 2018 am Institut für Analytische Chemie, Chemo- und Biosensorik der Universität Regensburg.

Die Arbeit wurde angeleitet von Prof. Dr. Antje J. Bäumner und Dr. Thomas Hirsch.

Promotionsgesuch eingereicht am: 23.08.2018

Prüfungsausschuss

Vorsitzender: Prof. Dr. Oliver Tepner
Erstgutachterin: Prof. Dr. Antje J. Bäumner
Zweitgutachter: Prof. Dr. Jascha Repp
Drittprüfer: Prof. Dr. Joachim Wegener

DANKSAGUNG

Table of Contents

1 Nano(bio)sensors based on Plasmonic Effects of Nanostructured Metallic Surfaces: Concept, Fabrication and Applications

1.1 Abstract

Biosensors utilizing plasmonic features have become a rapid growing field of interest due to the improvements of cheap and easy fabrication techniques of nanostructured materials. Especially plasmonic fields generated by nanostructured metallic substrates enable the tailoring of highly sensitive label-free platforms. This review (with 131 references) covers the progress made on the past years. An introduction into the field (physical basis of plasmons and transducers) is followed by a section that covers progress made in design and fabrication techniques of nanostructured surfaces. (Bio)sensor applications of nanostructured surfaces, based on gold as an exemplary plasmonic material are introduced. Advantages and improvements of nanostructured sensing platforms for transduces like surface plasmon resonance, Raman, transmission and fluorescence spectroscopy will be identified, and underlined be examples. The review concludes with a discussion of future perspectives and current challenges.
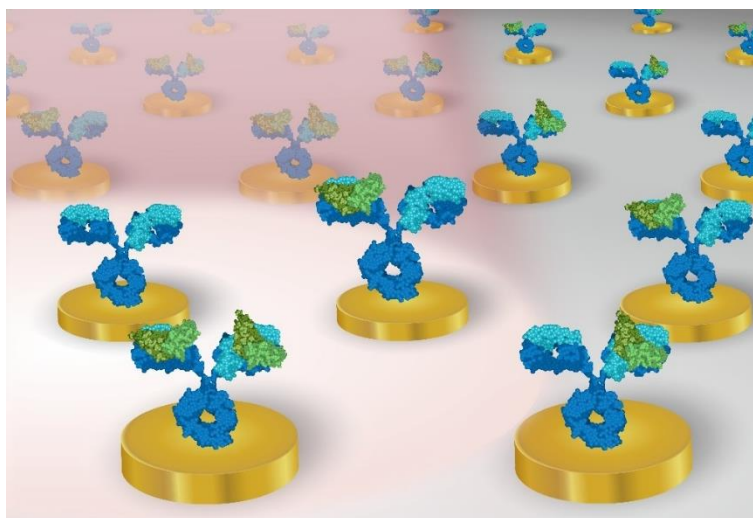
Figure 1.1│ Schema of a nanoplasmonic sensor surface consisting of a biofunctionalized gold nanodisk array.

This chapter is invited to be submitted.

Genslein Christa, Hirsch Thomas. *Invited to be submitted to Microchimica Acta.*

Author contributions

CG performed literature research and wrote the manuscript. The article was revised by CG and TH. TH is corresponding author.

1.2 Introduction

The field of nano(bio)sensors is emerging in the last years as a new frontier of science, technology and engineering. Applications are manifold and reach from point-of-care diagnostic to cancer detection with the focus on the implementation of plasmonic based sensors [1,2]. Nano(bio)sensors are sensors that use effects occurring in the nanometer-regime for improved performance. At the nano dimensions additional effects like plasmons occur, which can improve the sensor performance. One of the most promising phenomena for nanobiosensor development are plasmonic effects. Propagating surface plasmons polaritons (SPPs) appear in the presence of conducting materials and are defined as oscillations at the interface between a material with free electrons and a dielectric material [3]. SPPs have been applied for sensing for around half a century and from the basis for surface plasmon resonance (SPR) sensors [4]. The potential lies in the label-free and real-time monitoring of affinity binding and kinetics. In this regard, the scope of applications has extremely diversified and lead to the establishment of SPR sensing concepts in the analytical routine. Sensitivity, throughput and miniaturization are still difficult to realize with conventional SPR setups and pursuing to improve the drawbacks is important [5]. A large propagation length reduces the minimum sensing area and complicates multiplexing for the prize of large, multi-channel devices and less throughput. Another limitation results from the fundamental property of SPPs, having a penetration depth of several hundreds of nm in the dielectric layer on top of the nanostructure, which decreases the sensitivity, especially for small analytes. In most analytical fields, the target molecule is much smaller than this decay length and therefore only a small fraction of the sensitive layer will interact with the analyte, leading to low signals and not sufficient resolution of low concentrations [6]. Solutions for overcoming the problem use further steps or modifications. The addition of compounds or regents increase the molecular weight and lead to a signal enhancement. Such layer like systems are well known and a popular example is the secondary antibody sandwich assay with a for instance a modified gold nanoparticles (AuNP) [7]. Using this approach for improving the sensing performance, the procedure is more complex, highly error-prone and time consuming. Homola *et al.* additionally predict a limit of sensitivity for SPR sensors with reference to the angular, wavelength and intensity modulation and coupling modifications [8]. The most promising strategies, when taking into account the simplicity, are techniques modulating the optics and the metallic surface [8]. Nanomaterials are supposed to overcome the limitations and built the platform for high performance LSPR based biosensors. Until recently,

accompanied with the growth in nanofabrication technologies, nanostructured materials are boosted in many new applications as a consequence of the optical properties and a better understanding of the light-metal interactions [3]. Common nanostructures for nanobiosensors are metal nanoparticles (NPs). On the dielectric surface LSPs are excited and related to an enhancement of the EMF in vicinity of the NP: scattering and absorption of the light is improved [9]. In solution-based assays, NPs deal as a kind of label which is not suitable for online monitoring in microfluidic systems, due to high particle consumption. Therefore, a promising approach for next-generation plasmonic sensors are nanostructured surfaces. For the excitation of LSPs no bulky coupling techniques are needed, since their EMF can be directly excited, and enable multiplexing and miniaturization [10]. The presence of a solid metal interface on a substrate allow for easy incorporation in a microfluidic system necessary for continuous online measurements [11].

1.2.1 Principles of Plasmonics

Plasmons are defined as collective oscillations of free electrons in metals [9]. These movements have a well-defined frequency. In a more pictorial way, they can be described as an electron gas displacement of a metal, which mechanically vibrates around the fixed ionic core in the presence of an electrical field [12]. The repetitive variations around a central point of the free electrons occurs, as for all oscillators with a characteristic frequency, for bulk plasmons at the plasma frequency: [13]

$$w_p = \sqrt{\frac{ne^2}{m_{\text{eff}} \cdot \varepsilon_0}} \qquad (1)$$

where m_{eff} is the effective mass, ε_0 is the permittivity of free space, n is the density of electrons and e is the charge of the electron. The effective mass represents the ability of an electron to move in response to an incident field [13]. Electrons will not oscillate if the light has a higher frequency than the plasma frequency. In this case the light will be absorbed or transmitted into interband transitions [9]. If the frequency of the incident light is smaller than the plasma frequency electrons will move 180° out of the phase and leading to a strong reflection [13]. The characteristic color of a metal is a result of the plasma frequency and the interband transitions of the metal [14].

The situation changes if the bulk metal is now shrunk to a thin film. Oscillations will only occur at the surface and result in a propagating charge wave, which is called surface plasmon polaritons (SPPs) [15]. It can be imagined as charge waves traveling along the interface of the surrounding dielectric and a metal (Fig. 1.2). The electromagnetic field (EMF) of the metallic surface and the coupling of the collective movements give rise to the SPPs [16]. As the occurrence at the interface constrains the frequencies of the electron oscillations in the incident field, the resonance conditions for SPP excitation are described as [15],

$$k_{SPP} = \frac{w}{c} \sqrt{\frac{\varepsilon_{metal} \cdot \varepsilon_{diel}}{\varepsilon_{metal} + \varepsilon_{diel}}} \qquad (2)$$

where ε_{metal} is the relative permittivity of the metal, ε_{diel} is the relative permittivity of the dielectric medium at the metal surface, w is the light frequency, c is the speed of light and k_{SPP} is the wave vector (or momentum) of the SPPs. The dispersion curve (Equation 2) reveals that the k_{SPP} is always greater than the wave vector of free-space electrons in air at the same frequency [16]. Hence, the direct excitation of SPPs is not achievable. A coupling of the wave vector with a grating or prism in the Kretschmann configuration allows for excitation [15]. For sensor design the dependency of the SPP frequency on the dielectric permittivity (also known as the dielectric constant) at the interface is helpful. A change of the dielectric constant within the local EMF created by the SPP oscillations into the dielectric (100 - 200 nm [17]), influences the resonance conditions and shifts the frequency of the plasmons compared to air [18]. Substitution of the thin layer by structures in the nano-regime such as nanoparticles or nanostructured films overcomes this issue. When a surface plasmon is confined to a structure comparable to the light wavelength, the free electron of the nanostructure contributes to the collective oscillations (Fig 1.2). The phenomenon is termed localized surface plasmon (LSP) [19]. For other objects the models described here can easy be deducted. A more detailed explanation is reported by Maier [9] and Hafner *et al.* [19].The excitations of LSP coupled to the EMF are non-propagating, in contrast to SPP. Modes occur from the scattering problem of sub-wavelength structures in an oscillating EMF [9]. Because of the geometry, LSPs have an additionally momentum and can be direly exited by the incident field [16]. A change in the environment shifts the LSP resonance peak, that is detectable without any additional coupling. Mie theory provides an exact solution of the resonance conditions for LSP [20]. Scattering is negligible with respect to absorption and the extinction cross section, if the nanoparticles are around ten times smaller than the

incident light wavelength. In this case only the dipole term in the expression is significant, resulting in a simplified extinction the cross section: [21]

$$\sigma = \frac{18 \, \pi \, V \, \varepsilon_{diel}^{3/2}}{\lambda} \frac{\varepsilon_2}{(\varepsilon_1 + 2 \, \varepsilon_{diel})^2 + \varepsilon_2^{\,2}} \qquad (3)$$

where V is the volume of the nanoparticle, ε_{diel} is the relative permittivity of the dielectric medium, λ is the wavelength and $\varepsilon_1 + i \, \varepsilon_2$ is the complex dielectric function of the metal [22]. The resonance conditions are met when $\varepsilon_1 = -2 \, \varepsilon_{diel}$ [21] The LSPs have two important effects, that are utilized for sensors. First, the EMF extent is much short into the surrounding medium for nanoparticles (10 - 30 nm [17]) and hence is greatly enhanced at the surface with the highest enhancement directly at the surface. Second, an optical extinction maximum occurs at the plasmon resonance frequency [19].
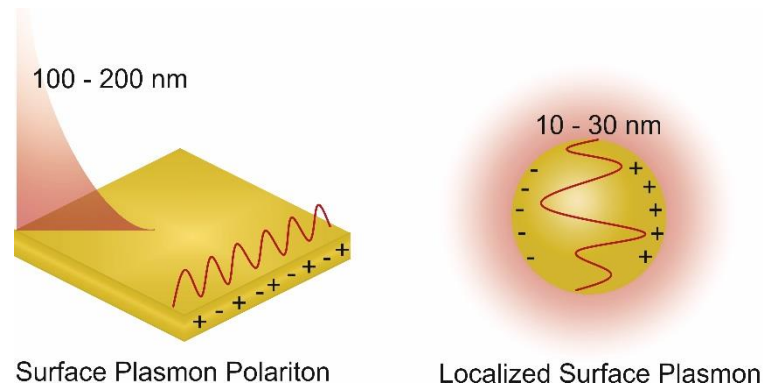
Figure 1.2│ Illustration of the different plasmonic modes: surface plasmons polaritons (left) and localized surface plasmon (right).

1.2.2 Principles of Transducers

For understanding how plasmons can improve nano(biosensor), a fundamental knowledge of the most prominent transducers used, such as surface plasmon resonance spectroscopy (SPR), transmission, Raman spectroscopy and fluorescence spectroscopy is required. In this review they will be shortly introduced. For more detailed information on these techniques some excellent reviews have been published [6,23-27].

Transmission spectroscopy is a well-established technique. Light of an intensity I_0 passes through a sample and is detected in an 180° angle to the incidence with a lower intensity I. The amount of light that is absorbed within the sample correlates with the concentration of the light-absorbing substances. Lambert-Beer law describes the light

absorption process physically [28]. For detection of low concentrations a certain volume of sample is necessary. Nanostructures with a high surface sensitivity are expected to confine the volume close to the surface.

Light emission from a substance is called luminescence and occurs from electronically excited states. Fluorescence is one typ of luminescence. From an excited singlet state the electron returns rapidly by emission of a photon to the ground state. The transition is fast as it is spin allowed. Also, the electron in the excited orbital is paired (by opposite spin) to the second electron in the ground-state orbital [29]. Strategies for enhanced emission and decreased lifetimes are needed to expand the field of fluorescence. It would allow for weak quantum emitters to be incorporated, photobleaching can be reduced and imaging with higher resolution is possible [30]. Plasmons can improve the emission and absorption properties of molecules placed on nanostructures via enhancement of the incident electromagnetic field intensity and/or the radiative emission rates [31,32]. The combination of fluorophores with plasmonic surfaces is termed as surface enhanced fluorescence (SEF).

Raman spectroscopy is a label-free and non-invasive technique to analyze the chemical composition. It utilizes the inelastic scattering of light, also known as Raman effect. A monochromatic light beam is illuminated on the sample. Spectral analysis of the scattered light reveals, that not only scattering without change of the energy of the incident light (Rayleigh scattering) is present but also discrete components of altered energy. Subtraction of those energies from the Rayleigh scattering gives the vibrational states of a molecule. Compared to fluorescence, Raman is a relatively weak scattering phenomena [33] and research is focused on improving the signal for sensors applications with high sensitivity. Interaction with plasmonic nanostructures is one way, which is derived from the electromagnetic field and chemical enhancement. Improved Raman-signal by nanostructures is referred to as surface enhanced Raman spectroscopy (SERS) [34].

Surface plasmon resonance (SPR) is a charge-density oscillation that occurs at the interface of dielectric constants of opposite signs, *e.g.* a metal and dielectric medium. If the resonance conditions are met by the incident light, the conduction electrons start to oscillate. A light wave can couple to a surface plasmon if the wavevector of light matches that of the surface plasmon. This is only achievable by coupling of the surface plasmons (SP), for instance, with a prism. Interaction of a molecule at the surface of the metal, affects the SPR signal, as it strongly depends on the refractive index of the dielectric

medium [23]. Sensing based on SPR offers advantages like label-free detection and online monitoring. The penetration depth of the SPP is often a drawback of this method in the case of small molecule detection at low concentrations. Introducing LSP to SPR, allows for variations of the plasmonic field, leading to better sensing performances.

1.2.3 Nanoplasmonic Sensing Strategies

Plasmonic (bio)sensors consist in general of a receptor (biorecognition element) and a metal or metal-dielectric nanostructure supporting plasmons [35]. The label-free nature of plasmons is especially interesting as the intrinsic features of an analyte can be exploited, which makes them suitable for long-time usage as no recovery of a receptor layer is required [36].

Basically, two different phenomena are responsible for the enhanced sensing capabilities of nanostructures: localized surface plasmons (LSP) and extraordinary optical transmission (EOT) (Fig1.3). On a film perforated with long-range or short range ordered holes, light interacts with the nanostructures and gives rise to EOT. It is caused by grating coupling of the incident light with surface plasmon modes and leads to the enhancement of the light transmission. The resulting transmission spectra is characterized by specific dips and peaks [37]. On non-interacting random arrangement of nanostructures (*e.g.* particles) LSPR emerge from the light interaction. Nanostructures smaller than the wavelength of the incident light are needed to generate LSPR. The resulting localized plasmon oscillations enhance the electromagnetic field and have a maximum at a specific plasmon resonance frequency [38].

A main advantage of nanostructures compared to a continuous film is the shorter and tunable plasmonic evanescent field, resulting in a smaller sensitive layer [39]. Molecules are occupying a much larger area of penetration depth in the dielectric medium close to the surface relatively to the classical approaches and lead to higher signal to noise ratio [40]. Optical processes like fluorescence and Raman scattering are influenced and improved by the EMF of both plasmonic modes [17]. The promising part are LSPs with the intense EMF confined to the structures, leading to a strong signal enhancement [41]. These region with a high EMF are called hot spots [42] and are important for SERS and SEF. The strongly enhanced light at the edges of nanostructures is able to interact with a fluorophore and enhances the absorption of photons next to the metal surfaces [43,44]. If the frequency of the plasmons overlaps with the fluorophore, the absorption process as well as the emission of photons are both getting enhanced by the plasmonic

nanostructures [45]. The SERS mechanism is resulting from a charge transfer resonance between the nanostructures, the analyte and the Raman scattering [46].
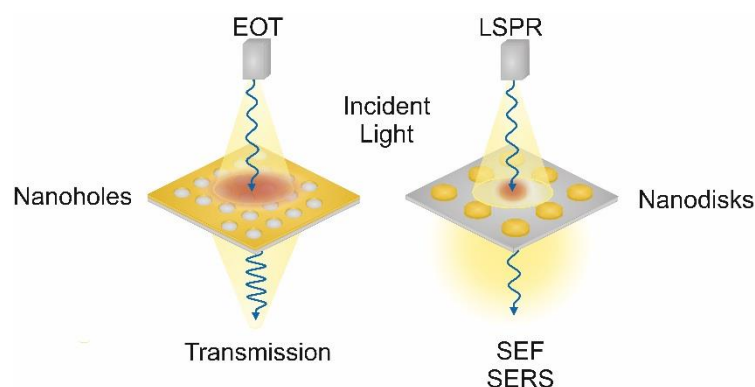
Figure 1.3│ Schema of the main nanoplasmonic sensing strategies. On nanohole arrays EOT is present. Free standing nanostructures like nanodisks are characterized by LSP modes.

The presence of an analyte at the surface alter the resonance conditions (k_{SPP}) or interacts with the EMF at the dielectric metal interface, shifting or modulating the signal. For read-out of the analyte induced signal change, a few characteristics of the light can be used: angular, wavelength, intensity and phase modulations [47] (Fig 1.4). In SPR sensors most commonly used is the angular modulation, where the reflectivity is monitored as a function of the angle of incident of a monochromatic light source [48]. At the SPR resonance angle the reflectivity has a minimum. At this position the resonance conditions are met. An interaction of molecules at the surface changes the resonance conditions and shifts the SPR response [49]. Wavelength modulation is performed by excitation of SP with a polychromatic light source at a fixed angle [50].

The signal is measured as a function of wavelength with a spectrometer. At the resonance wavelength a spectral absorption minimum occurs. As the environment of the dielectric medium at the surface is changed, similar to angular modulation, the resonance wavelength is affected. Intensity modulation uses the alteration of the intensity at a constant angle or wavelength. The interaction of a molecule at the surface shifts the SP resonance angle and wavelength accompanied by a strong intensity variation at other angles of wavelength position [51]. In contrast to the angular or wavelength modulations, the intensity-based approaches are capable for integration into imaging systems [52]. The basis for phase modulation is the phase change of the light beam that is linked with the reflection of the light at a metal surface [53]. Interference is observed as a spatial

displacement of the light beam and results in a phase difference that is sensitive to molecule interaction at the surface [54]. For a more detailed overview including resolution and sensitivity refer to *Aguilar et al.* [47].
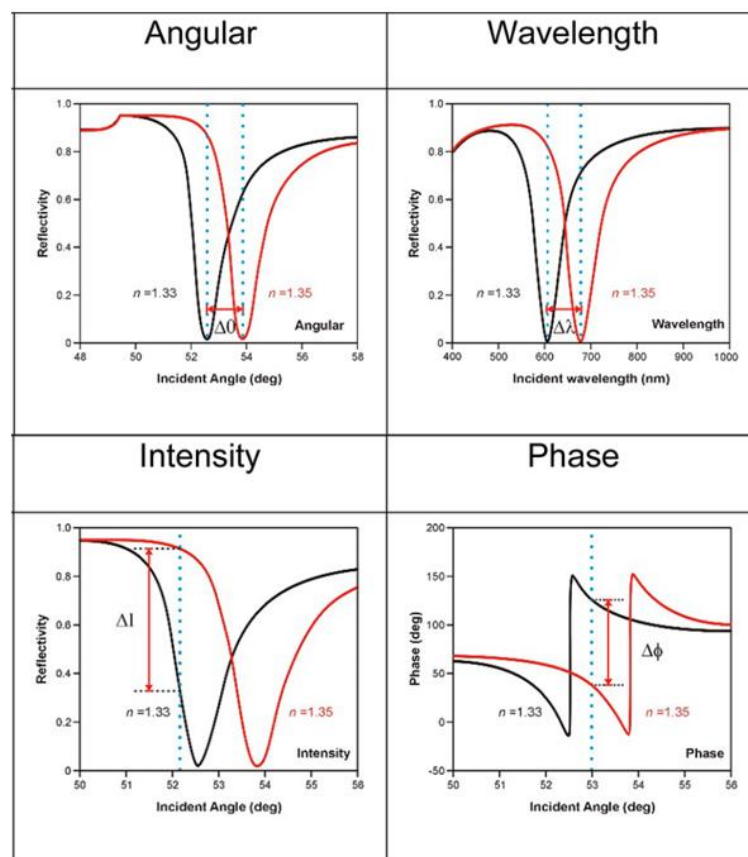
Figure 1.4│ Schematic of the different signal read-outs. Picture adapted with permission from Ref [47] © (2018) American Chemical Society.

1.3 Design of Nanostructured Plasmonic Surfaces

The design of a nanostructured surface describes on the one hand the type of material(s) and on the other hand the structural dimensions such as shape size and density, all together orchestrating the plasmonic features. The main discrimination of nanostructured surfaces is introduced in Figure 1.5. Nanostructured films exhibit SPP on the gold film and LSP close to the structuring element, *e.g.* the holes in the film. On a nanostructured film SPP are present on the continuous part of the film. LSP are directly located at the structures, giving rise to a mixed plasmonic feature. A free-standing nanostructure is characterized only by LSP and the EMF strongly confined to the metal surface.
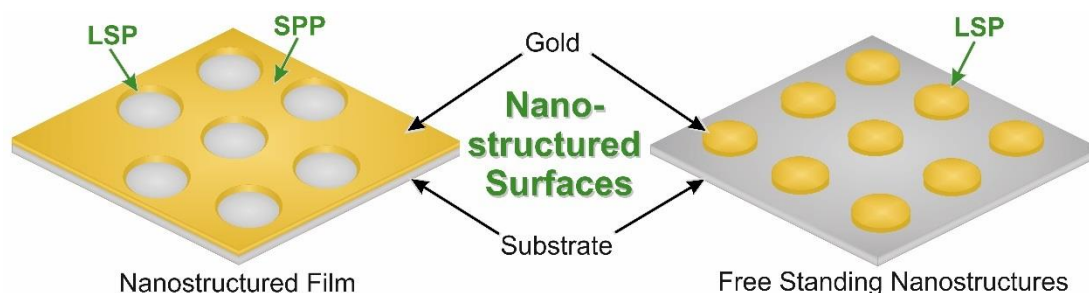
Figure 1.5│ Schema of nanostructured surfaces. The two variations are: a) nanostructured films, characterized by LSP and SPP and b) free standing nanostructures, were only LSP are present.

Before designing a nanoplasmonic sensor not only the composition, size and shape of the nanostructure must be well thought, the supporting material and its structure is also an important point. Structural changes of the carrier substrate result in different sensing applications and implementations in the systems. An overview of some concepts was published by Dahlin *et al.* [55]. Variations within the etching step at the end of the fabrication of nanostructures, *e.g.* nanoholes, enable the preparation of different pore structures. A structural change of the supporting platform facilitates the design of very specific sensors with the same analytical performance. For example, nanoholes can be used to study the behavior of molecules in a confined volume, nanowells offers an artificial biological nanopore and membrane pores are useful for analyzing molecular transport through nanopores. The plasmonic response is not effected by the structure of the support, though a change in the underlaying material shifts the resonance peak if the new support has a different refractive index [55].

A better understanding of the plasmonic feature of the materials and their variation with the specific design of the surface, will lead to improvements in the sensing capabilities. In this chapter the classical and recently developed plasmonic materials are depicted along with their advantages and drawbacks. The influence of the dimensional changes in the plasmonic repose will be discussed. An overview of the different design approaches is given in Figure 1.6. A lot more nanostructures as the here mentioned exists like stars [56], flowers [57] and raspberries [58]. They are all defined by the presence of LSP arising from the nanometer regime. The effect of the specific structure is difficult to discuss, but the effects can be traced by back to the well-known geometries.
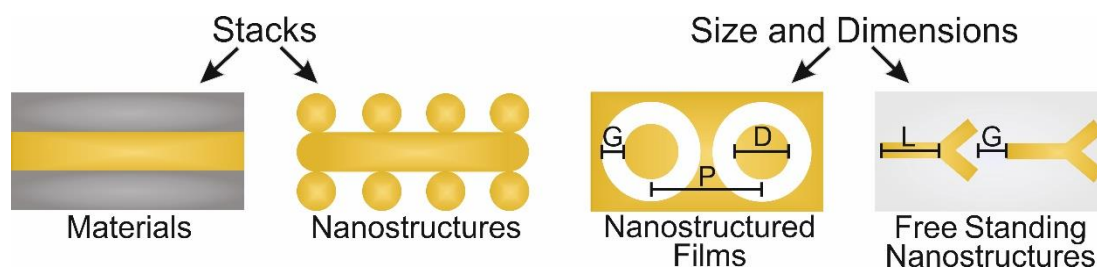
Figure 1.6| Schema of the most important design possibilities for nanostructured substrates. Parameters for characterization of the dimension are indicated: gap size (G), diameter (D) length (L) and periodicity (P).

1.3.1 Materials Giving Plasmonic Effects

The frequency of a plasmon mainly depends on the dielectric constant of the metal and therefore influences the spectral response and the sensitivity. A key role for sensor development plays the stability of the plasmonic surface in complex media and the possible functionalization. Some metals are sensitive against oxygen and moisture, others offer only challenging routes for introducing selectivity by chemical surface modifications. For sensor design a compromise between sensitivity, stability and functionalization needs to be found [59]. The most studied metals for plasmonics are gold [60] and silver because of their higher near-field enhancement factor and unique optical properties [61]. Other materials like copper are not common as they are extremely sensitive to oxygen [62], though they exhibit auspicious promising plasmonic features. Aluminum and Cu form efficient nanostructures when directly compared to Au and Ag within surface-enhanced Raman spectroscopy [63]. Not only noble metals are employed as plasmonic material. Surface plasmon modes can be present on any material, which has a sufficiently high carrier density as *e.g.* metamaterials such as nanoscale metal oxides and chalcogenides. They allow for plasmonic absorbance over a large optical range to include the visible, near-infrared (NIR), and mid-infrared regions [64] (Fig 1.7), and provide the possibility to tune the plasmonic modes by particle doping, shape and compositions [65]. Therefore, they offer the option for sensor development with highly tunable plasmonic modes over a large range of dielectric constants.
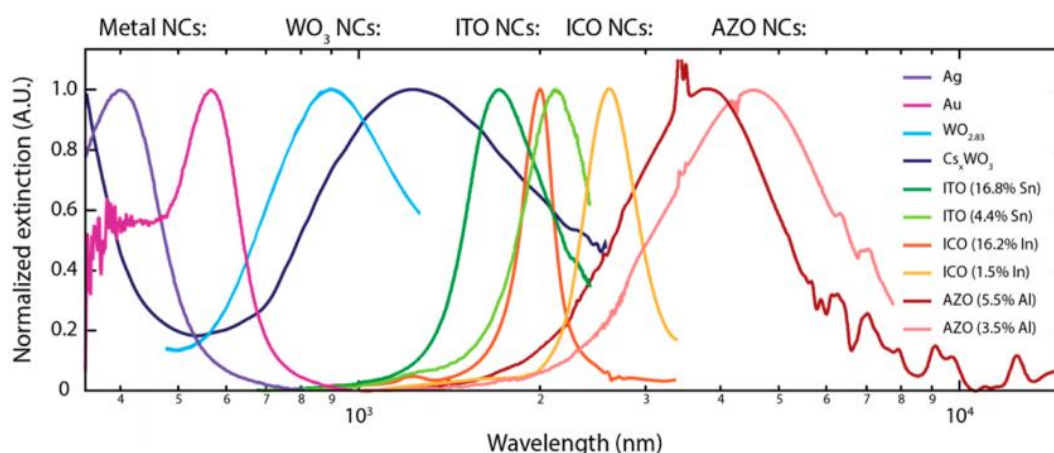
Figure 1.7 │ A absorbance spectra of metal and chalcogenide plasmonic materials spanning a large spectral range. Presented materials are silver (Ag), gold (Au), tungsten oxide ($WO_{2.83}$), cesium tungsten bronze Cs_xWO3, tin-doped indium oxide (ITO), indium doped cadmium oxide (ICO) and aluminum-doped zinc oxide (AZO). Picture adapted with permission from Ref [64] © (2014) American Chemical Society.

The use of multilayered materials is a more complex approach for variation and improvement of the plasmonic properties due to the elaborate fabrication processes. Plasmonic coupling of the materials and the connection of different material properties are exploited. The combination of ferromagnetic and noble metals enhances the sensing capabilities. Theoretically a stack of Au-Cu-Au film perforated with a periodic nanohole array results in two-times larger bulk figures of merit (FOM) compared to other plasmonic sensors. It needs to be taken into account, that such alloy arrangements tend to mix [66], leading to a reduced long-term stability. This issue is often not addressed but needs to be taken into account for sensor development. The nanohole array has a hole size of 203 nm and a lattice parameter of 400 nm. For the copper layer a thickness of 110 nm was used in the multilayer system with a thickness of 250 nm. The sensor performance is boosted by interplay of the plasmonic properties of the Au with the magneto optical features of the ferromagnetic membrane [67]. A metal-insulator-nanohole array metasurface, built up from Al_2O_3, Cu and Al was investigated. Nanoholes in a Cu layer (20 nm) have a size of 158 nm and are protected from oxidation by Al_2O_3 coating (20 nm). As a spacer Al_2O_3 (75 to 115 nm) is used between the nanohole array and an Al mirror. Due to the relatively similar permittivity of Au and Cu, both nanohole arrays show similar spectra and resonance features are only slightly broadened. This substrate shows a high chromaticity depending on the thickness of the Al_2O_3 spacer, which changes the resonance wavelength of the surface plasmons and cavity modes due to coupling between the metal films [68]. The combination of a metal-insulator-metal

nanocup array with a cavity of 80 nm consisting of Au (90 nm), TiO_2 (100 nm) and Au (90 nm) (Fig 1.8 A, B and C) demonstrates a high sensitivity for the detection of cancer biomarker carcinoembryonic antigen an LOD of 10 ng·mL^{-1} [69], which is in the relavent range (>10 ng·mL^{-1}) for the early diagnosis of several cancers [70]. Sensitivity arises from the degree of cavity-plasmon coupling and the plasmonic feature of the metal-insulator-metal materials. Spectrometer-free refractometric detection and imaging based on transmission is realizable with this nanostructure. The peak resonance wavelength does not change and only the transmission depends on the refractive index value (Fig 1.8 B). The transmission value is monitored with an objective and a camera [69].
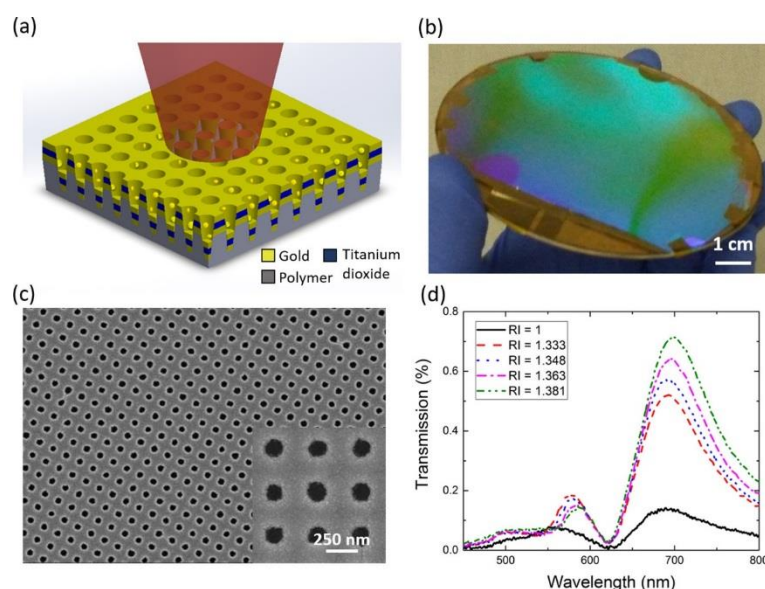
Figure 1.8 Schematic of Au-TiO_2-Au nanocup arrays. (a) and camera image of a wafer-scale fabricated array(b). The reflected light off the surface is diffracted due to the periodic nanostructures. SEM image of the multilayer system (c). Experimental transmission spectra with increasing RI values. Transmission intensity at the resonance wavelength increases with a fixed spectral location with RI increase (d). Picture adapted with permission from Ref [69] © (2018) American Chemical Society.

1.3.2 Geometrical Properties of the Nanostructured Surfaces

Size and shape of the nanostructures highly influences the plasmonic field. Resonance wavelength and penetration depth differ with various nanostructures and hence change the analytical parameters. Varying the nanostructures allows for tailored sensors with high signal-to-noise ratio regarding the type of analyte [71].

For a nanostructured film geometries which have an impact on the plasmonic features are the diameter, size and distance. Oh *et al.* investigated the effect of structural changes for a coaxial nanocavities in gold films. Decreasing the gap size from 10 to 2 nm results in a strong red shift of the resonance peak and increased area-normalized transmission within the mid-infrared region [72]. A decrease in the diameter of coaxial nanocavities with a constant gap size of 10 nm leads also to a decrease in the resonance wavelength. The concept can be used for multiband sensing, if mixed coaxial diameters are fabricated side-by-side [73]. For nanohole arrays the hole size has a strong effect on the SPR peak position (change of ~200 nm), whereas the periodicity only slightly shifts (~30 nm) the response wavelength. Both parameters have a strong effect on the peak shape. With decreasing hole size at a constant periodicity, the peak sharpens and gets more intense as the array resembles in a continuous gold film. If the diameter to periodicity ratio is constant and the periodicity decreased, the peak broadens and weakens [74]. Within sensing a sharp and intense peak is important as small changes can be monitored very accurate, which is crucial 0for high sensitivity. For SERS a only few laser wavelengths (mainly 532 nm and 785 nm) are used in commercial devices for excitation. Applications can profit from adjusted nanostructure design matching the exactions wavelengths.

It is very difficult to extract a general trend for size changes on nanostructured films and the resulting plasmonic feature. The large range of structures, their different dimensions and the lack of an all-embracing detailed analytical study complicates the selection of the most suitable substrates for a specific application. Nevertheless, knowing the influencing parameter of the size and shape is an important aspect for developing nano(bio)sensors with high sensing performance.

In contrast for freestanding nanostructures on a substrate, the distance between the structures has little impact on the sensitivity compared to the length/size of the nanostructures. A larger length of the structures shifts the resonance wavelength to longer values and to a higher extent compared to a decrease in the distance between the nanostructures. Iso-Y-shaped-nanopillars show a 30% higher LSPR sensitivity when the length is increased from 70 nm to 100 nm, whereas a variation of the distance does not change the sensitivity. The structures enable sensor design in the visible or near infrared region with the possibility to realize threshold or high sensitivity devices [75].

The thickness of the nanostructures has smaller effects on the plasmon resonance wavelength and the sensing properties like sensitivity, FOM and full width at half-maximum (FWHM) compared to the strong spectral changes with varying in the geometries. For gold-

coated nanodisk arrays the overall best performance, which only slightly differed from other systems, was found for the thickest nanodisk of 75 nm deposited on a film array of 75 nm [76]. It has to be considered for nanosensor design, that a transition to PSP is found to be at around 100 nm thickness. For a nanohole array with constant hole size and periodicity thicknesses smaller than 100 nm the plasmonic response is similar to LSP. Thickness changes from 20 to 90 nm slightly red shift the spectra from around 500 to 540 nm. For thicknesses larger than 100 nm the plasmonic response is comparable to the one obtained by a continuous film [74]. For even larger thicknesses the layer has again bulk plasmonic properties.

Very promising for future sensor designs is the concept using of stacks, especially nanostructure stacks, creating multiple hotspots advantageous for signal enhancement in SERS and fluorescence. The increasing number of hot spots is a promising feature that comes with the use of muli-stacked nanostructures. Plasmonic responses of gold nanowire stacks was studied by Jung *et al.* [77]. More stacks provide more hot spots, which allow for strong plasmonic coupling. The SERS signal increases with the number of stacks and the highest signal, was found for five-layer samples. Higher stack numbers did not further enhance the signal. Here, the finite penetration depth of light needs to be considered, as there is a maximum depth that the incident light can enter into the 3D structure and from which the Raman-scattered photons can get out [77].

1.4 Fabrication Techniques

In addition to the large structural variations, there is also a broad range of different fabrication techniques, from bottom-up methods to nanolithography. Main aspects for evaluation are here, resolution, reproductivity, the complexity of the fabrication process and the possibility to fabricate different structures.

1.4.1 Electron-beam Lithography and Focused Ion Beam Milling

Established techniques like electron-beam lithography (EBL) [78] and focused ion beam (FIB) milling [79] ensure high control of the process resolution and precision. Within FIB, first a thin metal layer is deposited before a focused ion beam locally splitters off the metal. The EBL process involves basically four steps: (1) deposition of a resist, (2) exposure and development of the resist with an electron-beam, (3) thin metal layer deposition and (4) lift-off of remaining residual and cleaning. Both techniques are suitable

for fabrication of sub-10-nm structures but are very time consuming with fabrication times of serval days [80]. In some applications, like single molecule analysis, a very high accuracy of the optimized nanostructures is inevitable to ensure a precise read-out with low variations. Edel *et al.* reported *e.g.* on a free standing nanopore of 20 nm ± 3 nm size surrounded by a plasmonic bullseye structure for single molecule detection. For preparing the very precise nanostructures a combination of gallium and helium FBI was essential [81]. Those techniques suffer from low throughput, limited scalability and high expenditure of time [82]. Laser interference lithography is an alternative, capable of large are patterning of up to a few cm^2 with the possibility of manipulation of the geometries, like periodicity and diameter to some extent. This maskless technique is based on the optical interference of two laser beams to imprint a nanostructure into a photoresist [83].

1.4.2 Nanotransfer

Nanotransfer approaches have received considerable attraction because they preserve the high reproducibility and precision of the lithographic methods. Solvent-assisted nanotransfer realizes sub-20 nm pattern with high accuracy in replication. Nanostructures are duplicated and transferred from a master mold fabricated by photolithography (0.2 – 200 µm) or block copolymers (8 – 15 nm). With injection of a solvent the adhesion between the replicas and a polyimide film is switched off and enables the release of the nanostructures on diverse and unconventional substrates, *e.g.* skin or an apple [84]. For a simple and easy transfer onto a substrate of choice, template-stripping can be applied. On a nanostructured photoresist-template a metal layer is evaporated, pressed against a glass slide modified with an epoxy adhesive, and after curing the patterned metallic structure is detached from the original template [83]. A transfer method to fabricate multi-layered nanostructures with high aspect-ratio utilizes an EBL-master for a covalent bonding-assisted nanotransfer lithography. The replica preparation and the nanotransfer procedure rests on the formation of a covalent bond between an adhesive layer on the substrate and transferring materials. Nanostructures dimensions down to ~20 nm are realizable on an area of ~100 cm^2 and the process is not affected by the shape of the structure [85]. For rapid prototyping the classic lithographic techniques are beneficial due to the high precision and resolution [86]. Disadvantages of those methods for sensor design are still the dependence on beam-based lithography, limited structural variations, residual layers and long manufacturing times.

1.4.3 Self-Assembly

To improve nanofabrication techniques and make them accessible for a large community, techniques like colloidal or nanoimprint lithography have been developed. Among those approaches colloidal lithography [87] is a strategy with high potential for nanosensor fabrication. This bottom-up methods are versatile tools for fabrication of nanostructured surfaces on a large scale with simple adjustability of the size and dimension. Here, the self-assembly properties of colloidal particles are exploited. As an example, Pacholski *et al.* published a method for bottom-up fabrication of gold-capped hydrogel microspheres in periodic hole arrays. First a colloidal mask of hexagonal arranged microspheres was generated by self-assembly of a hydrogel on a glass substrate. For the formation of the metal nanostructure the substrate is placed in a gold nanoparticle dispersion. After an electroless deposition and a photochemical metal deposition the final structure is yielded. The holes have a diameter of 1.04 ± 0.02 µm and microspheres of 0.72 ± 0.03 µm. A long-range symmetry with regions in the mm^2 range is achieved [88]. This method demonstrates the benefits of colloidal lithography as it is scalable (covering areas of cm^2) and only standard laboratory equipment is required. Different structural changes are not easy achievable since the nanostructure is defined by the hydrogel microspheres and the hole fabrication process is with ~1.5 days relatively long. Addressing the problem to adjust size and dimensions, the construction of nanostructures utilizing the self-assembly of nanoparticles, acting as plasmonic material or as a sphere mask, have been invented. Simple variations of the particle size or shape alter the dimensions of the nanostructures. Implementations of this principle are the direct formation of nanostructures by immobilizing of structures like Au nanoparticles on the substrate [89] or using the nanoparticles as a template *e.g.* for the fabrication of nanodisks [90].

The dimensions range from ~20 to ~150 nm and depend on the size of the nanoparticles with act as a sphere mask. Introducing an etching step before metal deposition on the particle sphere mask overcomes this issue. For instance, nanohole arrays were fabricated by a modified nanosphere lithography. Polystyrene particles self-assemble in a closed-packed hexagonal monolayer and their diameter can be reduced with reactive ion etching, leading to variation of the size of the nanoholes [91]. With at least 20 h most of the fabrication time takes up the particle synthesis. This issue is can be overcome as a large variety of monodisperse nanoparticles of different size are commercial available. The resolution mainly is defined by the dispersity and shape variations of the nanoparticles. Diameters with low deviations from the nanometer (1.6 ± 0.3 nm [92]) up

to the micrometer (20 ± 0.5 µm [93]) regime are possible. The large range of available diameters of particles ranges, allows for the fabrication of nanostructures with in the same dimensional range, as the particles act as a mask for the nanostructures.

In the case of structural variations an even higher degree of freedom is given by techniques using block copolymers [94] or colloidal nanocrystal superlattices [95]. They act as nanostructure building blocks and offer the opportunity to transfer the nanostructures. Depending on the environment and the polymer/nanocrystal a large variety of structures, consisting of different plasmonic materials, can be fabricated. *E.g.* nanoholes can be prepared with a diameter of 15 nm, a resolution ~1.5 nm, and a density over 400 holes·µm^2 by solvent assisted direct pattering of block copolymer master templates [82]. The resolution was improved to a limit comparable with classic lithography approaches. A high density of the nanostructures provides a high number of hot spots within the sensing spot, further enhancing the signal for SERS and SEF. Other structures like rings-in-mesh [96], lines and crosswires [97] in dimensions from 5 to 20 nm can be fabricated. The templates are reusable and the transfer process ensures a high-yield transfer without further surface treatment [82]. The block copolymer master template formation is the time limiting factor (~14 h) and a lot of complex steps are necessary to yield the nanostructures. A variety of hierarchical material structures, like gold nanocrystals assembled in grids or lines, are prepared with self-assembled binary nanocrystal superlattices and pattern transfer printing. Size, shape and arrangement of the nanocrystals can be controlled by changing conditions such as temperature and solvent. Prepatterned PDMS molds are used for transferring self-assembled nanostructures via a liquid–interfacial assembly technique. Dimension of the gold nanocrystal are of 5.4 nm ± 0.4 nm on an area of ~400 µm2 [98]. The method is easily scalable as binary nanocrystals can cover areas of a few mm2 [99]. A fast fabrication time of ~ 5 h makes them attractive for nanosensor development.

1.4.4 Summary

Comparing the different fabrication approaches for nanostructured surfaces, FBI and EBL yield a very high resolution but self-assembly techniques are emerging and similarly low dimension of ~5 nm are realizable. In Table 1.1 the most important fabrication techniques are summarized along with the main advantages and disadvantages. As self-assembly approaches do not require high equipment, almost every laboratory is able to fabricate nanostructured substrates and hence pushing this research field to a new level.

Better flexibility, faster production and cheaper manufacturing costs are present in colloidal approaches especially when combined with nanotransfer methods. They offer a sufficient resolution for read-out methods with micro- or millimeter measurement spot size and can be scaled up easily. In summary, for most applications like SEF, SERS or EOT techniques based on colloidal lithography are effective in case of sensor performance. Roughness of the surface or structural defects in the µm-range are not a drawback for those methods as the laser spot covers a larger area, which outperforms such variations. For SPR a roughness of the surface would lead to reflectivity loss and hence a lower sensitivity. Imaging approaches in the same dimensional regime as the nanostructures suffers from small structural defects, as the signal is not uniform over the sensing area.

Table 1.1 │ Overview of the most important fabrication techniques for nanostructured surfaces listed by their resolution.

Technique	Reso-lution	Time	Scal-ability	Advantages	Disadvantages	Refer-ences
EBL/FIB	<10 ± 0.1nm	day(s)	no	ultimate precision	equipment, limited flexibility	[80]
binary nanocrystal superlattice	5.4 ± 0.4 nm	~5 h	Yes	structural variations, high resolution	complex fabrication	[98, 99]
block copolymer assembly	15 ± 1.5 nm	~15 h	Yes	structural variations, reusable master	complex fabrication	[82]
nanoparticle assembly	17 ± 2nm	>24 h	Yes	low resolution	limited structures and dimensions	[89, 90]
laser interference lithography	>100 ± 8 nm	~5 h	no	tunable dimensions	limited structures	[83, 100]
nanosphere lithography	250 ± 20 nm	~10 h	Yes	tunable dimensions	limited structures, resolution	[91, 101, 102]

1.5 (Bio)sensor Applications

The following section summarizes the (bio)sensing approaches based on nanostructured gold surfaces with SPR, Raman, EOT and fluorescence techniques.

For a large variety of fields like food safety and medical diagnostics SPR has been applied, due to the ability to measure kinetic interaction. Compared to a continuous gold film, nanostructured surfaces detect refractive index changes only in a short volume close to the surface and hence show a higher surface sensitivity. Recently randomly distributed nanostructures like nanoislands or nanorods have been utilized as sensor platform due the exclusive presence of LSPR. With nanostructures the determination of concentrations is with an order of magnitude lower compared to a continuous gold based SPR sensor, as it has been shown for the analytes ssDNA [103] and Pb^{2+} [104]. From an instrumental point of view, parallelization is easy, as one surface can hold more than one receptor. The limitations come with a suitable technique in the chemical modification of the sensor array. Sensing spots need to be printed. An analogy can be found for monitoring volatile organic compounds (VOCs) were 72 spots can be assembled in high density for SPR readout. The features of a cross-sensitive microarray are combined with SPR. A high sensitivity allows to discriminate between VOCs by only a single carbon atom [105]. So far there are only a few examples to use this technology in plasmonic sensing. Proof of concept mainly done for dual sensing such as for ordered gold islands on glass, which are modified by self-assembly of SH-functionalities on the gold and NH_2-funcionaliatzion of the glass substrate. The separated spatial functionalities are selective receptors for the detection of heavy metals ions Hg^{2+} and Cu^{2+}, respectively [106]. The implementation of nanostructured surfaces makes high-throughput analysis with improved sensing performance feasible.

The effect and potential of coupling fluorophores to nanoengineered surfaces has been demonstrated, but applications are limited up to now often by the time consuming or expensive fabrication of such substrates. As a result there are only a few reports on the implementation of such sensing systems [107]. The outstanding sensor properties in the presented examples, depicts the high potential of SEF platforms as very sensitive surfaces in nanobiosensors, which are achieved even with simple and cheap fabrication techniques, like nanosphere lithography. Applying this principle, for Au nanoparticle arrays interacting with upconversion (UC) nanorods [108] and for Au nanopillar arrays combined with UC nanoparticles [109], emission enhancements of around 2 to 5 can be achieved. Enhancing the quantum dot emission with gold nanopillars enables a low limit

of detection (LOD) for prostate specific antigen (PSA) of around 10 pg·mL^{-1} [110] (Fig 1.9 C). Single-strand DNA, a common biomarker, has been used as a model concept. For a ssDNA modified with Cyanine 3 on a nanoporous Au disk a detection down to ~1500 molecules (estimated) and up to 1 nM was shown [111]. Using a gold nanorod array and a ssDNA probe modified with Quasar 670 a linear relationship is realizable from 10 pM to 10 nM [112] (Fig 1.9 B). Plasmonic Au nanotriangles improve the single-molecule fluorescence intensity by a factor of two for living *vibrio cholerae* cells expressing photoactivatable fluorescent proteins [113] (Fig 1.9 A).
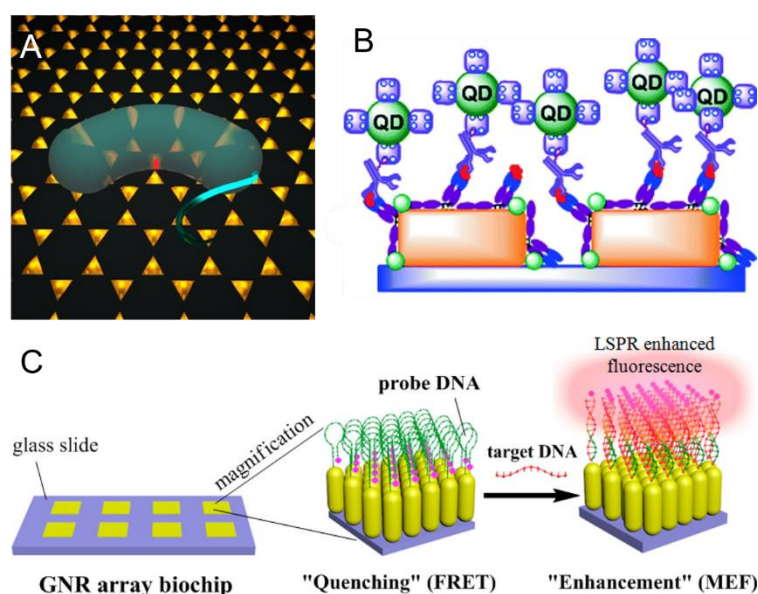
Figure 1.9 | Examples of SEF applications. (A) Gold nanotriangle arrays fabricated by nanosphere lithography enhance the single molecule fluorescence intensity for imaging applications. (B) Schematic illustration of a nanopillar array applied for the PSA detection with a sandwich immunoassay and enhanced fluorescence of quantum dots [110]. (C) An ordered nanorod array chip is used for ssDNA detection upon hybridization with a tagged reporter probe. Picture (A) adapted with permission from Ref [113] © (2018) American Chemical Society. Picture (B) adapted with permission from [110] © (2015) Royal Society of Chemistry. Picture (C) adapted with permission from Ref [112] © (2018) American Chemical Society.

Improved sensing capabilities of SERS with nanostructured surfaces have been shown. A high selective and portable SERS for the analysis of the Pb^{2+} concentration in water was published by Ayoko *et al.* [114]. The sensor surface consists of a solid substrate coated with gold nanoparticles and is functionalized with an aminobenzo-18-crown-6 as a selective recognition molecule, allowing for the detection of 0.69 pM Pb^{2+} [114]. SERS techniques based on AuNP are only able to detect 0.3 nM of Pb^{2+}, indicating three orders

of magnitude lower LOF for nanostructured surfaces [115]. For cell analysis not only excellent sensitivity is needed, also the nanostructured surface should be highly reproduceable, yielding a homogeneous SERS response over the sensing area. Gold triangular nanoprism arrays, fabricated by electron beam lithography, show an enhancement factor (EF) of ~5·10^5 especially in the characteristic frequency range of protein fraction and utilizes mapping experiments with compatible standard deviations of the SERS signal [116]. A gold nanorod array, modified with sensitive bovine serum albumin-coated 4-mercaptopyridine-linked as a receptor layer, exhibits an EF of ~6·10^7. With the nanostructured platform, which is fabricated by evaporative self-assembly method, it is possible to determine the pH value in blood with good reliability and accuracy [117]. These examples point out the feasibility of nanostructured surfaces as sensitive platforms for the design of biosensors in various fields. Besides the simple concept of using nanostructured surfaces directly as SERS substrate, there are also more complex setups for further improving the Raman signal or other objectives. A lot of effort was made to find optimized geometries of nanostructures to enhance the signals for better LODs. The group of Vo-Dinh investigated a DNA bioassay-on-chip based on a bimetallic film over nanospheres [118]. For such structures, particularly high EF of 10^6 to 10^8 are enabled. By combination of nanowave structures with a thiolated reporter probe tagged with a Raman active dye, ~3.6·10^6 molecules of the target ssDNA was detected [118] (Fig. 1.10 C). The detection of 100 pM Rhodamine 6G was achieved by plasmonic trapping via laser excitation of Au nanoparticles in the middle of a nanobowtie structure. Hot spots arise from the trapped nanoparticles and act as additional SERS sites [119] (Fig. 1.10 B). Nanostructured substrates have also been used in super-resolution chemical imaging. A stochastic optical reconstruction microscopy (STORM) algorithm can be applied for processing the blinking behavior of SERS hot spots. The phenomena results from the large field enhancement of plasmonic nanoholes and enables localization to within 10 nm and high resolution imaging [120]. Additionally, nanostructures, as *e.g.* nanobaskets, can concentrate molecules or objects in the surrounding medium. A bubble, that acts as a fastmoving net, is generated by an ultrafast IR laser pulse and gains a locally high density of the analyte, making a detection at extremely low concentrations more effectively and requires no sample treatment [121] (Fig. 1.10 A). It needs to be considered that, SERS yields much narrower peaks compared to fluorescence, which are highly specific and therefore it has a great potential for multiplexed detection [118]. Taking this into account, the crucial point for the design and application of high performance SERS biosensors is the fabrication of reproducible and sensitive (high EFs) plasmonic nanostructures. The field of inexpensive and versatile

fabrication techniques shows tremendous progress, thereby paving the way for realization of commercial SERS sensors based on nanostructured surfaces.
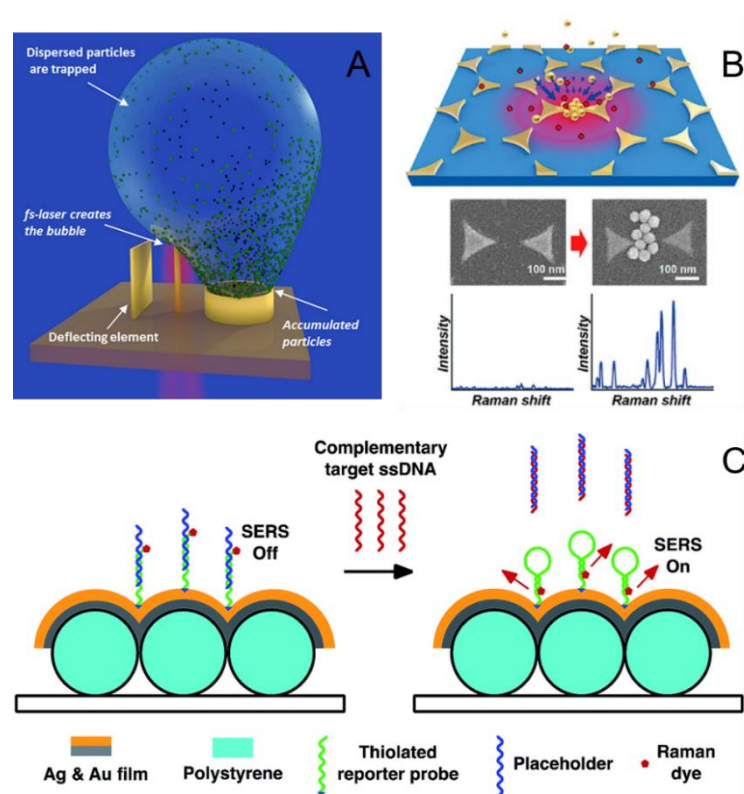
Figure 1.10│ Examples of SERS applications. (A) Sketch of the 3D nanostructured surfaces with the antennas, deflecting panels and target sites. The triggered nanobubble formation acts as a net for analyte molecules. (B) The Raman scattering is enhanced by plasmonic trapping of nanoparticles due to laser excitation at a nanobowtie structure. (C) Scheme of the detection of ssDNA on a multilayer nanowave structure, fabricated by the metal deposition on a clos packed polystyrene monolaye. Picture (A) adapted with permission from Ref [121]) © (2018) American Chemical Society. Picture (B) adapted with permission from Ref [119] © (2016) American Chemical Society. Picture (C) adapted with permission from Ref [118] © (2014) The Roylal Society of Chemstry.

Transmission and reflectance monitoring of binding events in real-time are very attractive, since they offer high sensitivity in accordance with simple, inexpensive and scalable setups [122]. The response of such sensors results from LSPR and EOT, depending on the nanostructured substrate. In contrast to conventional SPR systems, which are still lacking in throughput compared to 96 well-plate or in resolution and array fabrication for imaging formats, transmission sensing is compatible with mulitwell plate readers [123]. Hence nanoplasmonic substrates are considered as next generation sensing platform and a lot of sensors are devolved in the last years [5]. Nanohole arrays

are a very common and attractive nanostructure for EOT. The group of Hatice Altug
works on an integration of nanohole arrays in a multichannel microfluidic system. The
design makes a fast, simple and highly sensitive point-of-care system possible.
Multiplexed detection of bacteria by immobilization of specific antibodies in a one-step
assay with outstanding sensitivities was demonstrated [37] (Fig. 1.11 A). Cytokine
secretion of single-cells in real-time is shown with an antibody modified multifunctional
optofluidic system and an outstanding LOD of 39 pg·mL^{-1}[11]. The system was further
improved with the coupling of Au nanoparticles (NPs) to the nanohole arrays. Under
bright-field imaging plasmonic heatmaps can visualize single labeled Au NPs and thus
can quantify a single analyte binding event on the surface [124] (Fig. 1.11 B). Another
possibility for improving the plasmonic sensing properties is the coupling of Au NPs on
a gold-coated nanodisk arrays. The Bragg modes, which strongly interact with the
AuNPs, induce an enhancement of the electromagnetic field and 7-fold lower LOD for
ssDNA [125]. Structures utilizing LSPR are manifold, but most frequently used are
nanorod arrays [126], nanodisk arrays [127] and nanoislands [128]. For the detection of
the relevant cancer biomarkers prostate specific antigen (PSA) nanorod arrays with an
antibody as recognition element [126] and nanodisk arrays functionalized with a DNA
aptamer have been used and can analyze concentrations of PSA as low as ~1 ng·mL
[127]. Nanoparticle arrays as a sensing platform in combination with a cis-jasmone (CJ)
selective nanocomposite-imprinted are able to detect 3.5 ppm of CJ in air [129]. A
molecularly imprinted polymer film on a nanoisland structure allow the fast, reversible
and highly selective detection of α-pinene γ-terpinene, and limonene vapors [128]. For
nanorod arrays conjugated with a chelating agent of Co^{2+} ions a LOD of 100 pM is
realizable [130].

Reflectivity setups are also very promising but not so common up to now. Lechuga *et al.*
studied a periodic nanoslit array of commercial Blu-ray discs as a biosensor platform in
the reflection mode. Under an oblique angle the sensitive is improved and an LOD in the
pM range for a tumor associated antigen is achieved [131]. Most authors do not see any
limitations in transferring their proof-of-concept sensing schemes into real world
applications, as transducer can be miniaturized, and surface can be industrially
fabricated. This points out the high potential of transmission or reflectance systems as
portable biosensor. They offer other benefits such as real-time monitoring, integration
with microfluidics and label-free detection.
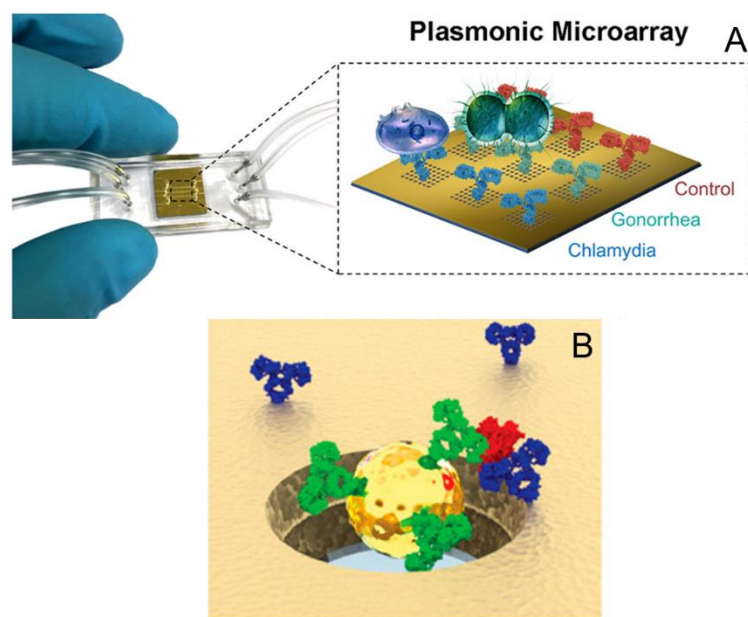
Figure 1.11│ Examples of transmission applications. (A) Schematics of the plasmonic microarray sensor and a picture of the implementation with PDMS in a microfluidic system. Nanohole arrays are modified with neisseria gonorrhoeae (NG) (green), anti-chlamydia trachomatis (CT) (blue) and a control antibody (red). (B) For improved digital imaging of biomarkers on a nanohole array nanoparticles are used. The capture antibody (blue) is immobilized on the nanohole array and recognizes the antigen (red). A detection antibody is bound to the NPs and also for capturing of the NPs by the antigen at the nanohole array. Picture (A) adapted with permission from Ref [37] © (2017) Elsevier. Picture (B) adapted with permission from Ref [124] © (2016) American Chemical Society.

For comparison of the performance of the different approaches are summarized in Table 1.2, with respect to the analyte class and sorted by the LOD. The detection of ssDNA is remarkably low for SEF and SERS when compared to other sensing techniques. Those values were calculated taking into account the solution volume and the laser spot size [111,118] and not the intrinsic signal is taken. Other techniques achieve similar LODs in the pM-range with the larger dynamic range for SPR and SEF. Heavy metal ion detection is possible over a large dynamic range of around six orders of magnitude and with a pM-low LOD for SERS and transmission spectroscopy. In the case of protein detection transmission measurements with nanohole arrays offer a pg·mL^{-1} low detectable concentration, comparable to SEF using nanopillars but here a larger dynamic range with three orders of magnitude is present.

Table 1.2│ General overview of nanostructured surfaces for nano(bio)sensors used for ssDNA, heavy metal and protein detection sorted by their LOD.

Analyte		LOD	Dynamic Range	Technique	Structure	Refer-ence
ssDNA		2.4 zmole	2.4 zM – 1 nM	SEF	Nanoporous Disk	[111]
		6 amoles	0 – 30 amoles	SERS	Bimetallic Nanowave	[118]
		0.7 pM	20 pM – 20 nM	SPR	Nanorods	[103]
		7 pM	20 – 200 pM	Transmission	Nanodisk on a Film	[125]
		10 pM	10 pM – 10 nM	SEF	Nanorod	[112]
Heavy Metals	Pb^{2+}	0.69 pM	10^{-12} M – 10^{-6} M	SERS	Particles on a Film	[114]
	Cu^{2+}	100 pM	100 pM – 1 μM	Transmission	Nanorods	[130]
	Pb^{2+}	0.011 ppb	0.011 ppb – 5 ppm	SPR	Nano-islands	[104]
	Hg^{2+}	0.01 ppm	0.01 – 0.04 ppm	SPR	Nano-islands	106]
Protein	PSA	10 pg·mL^{-1}	100 pg·mL^{-1} – 100 ng·mL^{-1}	SEF	Nanopillars	[110]
	bBSA*	10 pg·mL^{-1}	500 pg·mL^{-1} – 10 ng·mL^{-1}	Transmission	Nanoholes	[124]
	cytokine	39 pg·mL^{-1}	50 pg·mL^{-1} – 1 ng·mL^{-1}	Transmission	Nanoholes	[11]
	PSA	1.49 ng·mL^{-1}	1.7 – 20.4 ng·mL^{-1}	Transmission	Nanodisk	[127]
	GTF2b	3.4 ng·mL^{-1}	25 - 1000 ng·mL^{-1}	Reflectance	Periodic Nanoslit	[131]

*biotinylated bovine serum albumin (bBSA)

In summary the presented sensing techniques show comparable sensing performance, for this reason the limiting factor is the equipment needed for excitation and signal collection. For successfully designing a high-performance biosensor, low cost components and the possibility for miniaturization are very important. Additionally, a simple protocol for functionalizing and selective analyte detection should be available. Ultimately, there is not the perfect transducing technique for a particular for analyte, the

circumstances of a specific application need to be considered, keeping in mind the stated pros and cons of each transducer.

1.6 Conclusions and Perspectives

Nanostructured surface sensing strategies are useful for a large variety of transducers due to the LSP or EOT. For a sensor application the design, in context of the plasmonic material and nanostructure, needs to be considered. Important aspects are the penetration depth of the plasmonic field, density of the nanostructures and the spectral position of the plasmonic band. One of the main issues within fabrication of nanostructured surfaces is the reproducible and high-resolution over large areas. Most promising are self-assembly approaches. They allow for tailored dimensions, shape and composition with a high scalability and do not depend on expensive laboratory equipment. In the near future the current drawback of resolution, when compared to established lithography methods, will be overcome, leading to large range of (bio)sensor with nanostructured surfaces. The diversity of fabrication techniques gives rise to all sort of structures, mainly subdivided into nanostructured films and free-standing nanostructures. The plasmonic properties and characteristics are in the focus of research at the moment. Often the application as nano(bio)sensor are still in the proof-of-concept stage. Basic aspects for nanostructured surfaces are the improved sensing performance, high-throughput possibility and microfluidic implementation compared to conventional plasmonic sensors. The successful accomplishment of super-resolution chemical imaging, single-cell analysis and single molecule detection should be emphasized as it is paving the way for point-of-care diagnostics and label-free online monitoring applications. The use of nanostructured surfaces would be very beneficial for daily-use applications, since they allow for integrated devices utilizing low-cost and facile experimental setups.

Regardless all the existing challenges, which need to be addressed, nano(bio)sensors utilizing nanostructured surfaces as sensing platform is an interesting research field with enormous opportunities.

1.7 References

[1]   Sugumaran S, Jamlos MF, Ahmad MN, Bellan CS, Schreurs D (2018)
Nanostructured materials with plasmonic nanobiosensors for early cancer
detection: A past and future prospect. Biosens Bioelectron 100:361–373.

[2]   Dodson SL, Cao C, Zaribafzadeh H, Li S, Xiong Q (2015) Engineering plasmonic
nanorod arrays for colon cancer marker detection. Biosens Bioelectron 63:472–
477.

[3]   Brolo AG (2012) Plasmonics for future biosensors. Nat Photon 6:709–713.

[4]   Mauriz E, García-Fernández MC, Lechuga LM (2016) Towards the design of
universal immunosurfaces for SPR-based assays: A review. Trends Analyt Chem
79:191–198.

[5]   Estevez M, Otte MA, Sepulveda B, Lechuga LM (2014) Trends and challenges
of refractometric nanoplasmonic biosensors: a review. Anal Chim Acta 806:55–
73.

[6]   Homola J (2008) Surface plasmon resonance sensors for detection of chemical
and biological species. Chem Rev 108:462–493.

[7]   Uludag Y, Tothill IE (2012) Cancer biomarker detection in serum samples using
surface plasmon resonance and quartz crystal microbalance sensors with
nanoparticle signal amplification. Anal Chem 84:5898–5904.

[8]   Piliarik M, Homola J (2009) Surface plasmon resonance (SPR) sensors:
approaching their limits? Opt Express 17:16505–16517.

[9]   Maier SA (2006) Plasmonics fundamentals and applications. Springer, New York.

[10]   Couture M, Live LS, Dhawan A, Masson J (2012) EOT or Kretschmann
configuration? Comparative study of the plasmonic modes in gold nanohole
arrays. Analyst 137:4162–4170.

[11]   Li X, Soler M, Szydzik C, Khoshmanesh K, Schmidt J, Coukos G, Mitchell A, Altug
H (2018) Label-Free Optofluidic Nanobiosensor Enables Real-Time Analysis of
Single-Cell Cytokine Secretion. Small 1800698.

[12]   Kittel C (1976) Introduction to Solid State Physics. WILEY, New York.

[13]   Ashcroft NW, Mermin ND (1976) Solid state physics. Cengage Learning, New
Delhi.

[14]   Oates T, Wormeester H, Arwin H (2011) Characterization of plasmonic effects in thin films and metamaterials using spectroscopic ellipsometry. Prog Surf Sci 86:328–376.

[15]   Lakowicz JR (2006) Plasmonics in Biology and Plasmon-Controlled Fluorescence. Plasmonics 1:5–33.

[16]   Dostálek J, Knoll W (2008) Biosensors based on surface plasmon-enhanced fluorescence spectroscopy. Biointerphases 3:FD12-22.

[17]   Li M, Cushing SK, Wu N (2015) Plasmon-enhanced optical sensors: a review. Analyst 140:386–406.

[18]   Shalaev VM (2007) Nanophotonics with surface plasmons. Elsevier, Amsterdam.

[19]   Mayer KM, Hafner JH (2011) Localized surface plasmon resonance sensors. Chem Rev 111:3828–3857.

[20]   Mie G (1908) Beiträge zur Optik trüber Medien, speziell kolloidaler Metallösungen. Ann Phys 330:377–445.

[21]   Nehl CL, Hafner JH (2008) Shape-dependent plasmon resonances of gold nanoparticles. J Mater Chem 18:2415-2419.

[22]   Link S, El-Sayed MA (1999) Size and Temperature Dependence of the Plasmon Absorption of Colloidal Gold Nanoparticles. J Phys Chem B 103:4212–4217.

[23]   Homola J, Yee SS, Gauglitz G (1999) Surface plasmon resonance sensors. Sens Actuators B Chem 54:3–15.

[24]   Stiles PL, Dieringer JA, Shah NC, van Duyne RP (2008) Surface-enhanced Raman spectroscopy. Ann Rev Anal Chem (Palo Alto, Calif.) 1:601–626.

[25]   Sharma B, Frontiera RR, Henry A, Ringe E, van Duyne RP (2012) SERS: Materials, applications, and the future. Mater Today 15:16–25.

[26]   Bünzli JG (2010) Lanthanide luminescence for biomedical analyses and imaging. Chem Rev 110:2729–2755.

[27]   Berezin MY, Achilefu S (2010) Fluorescence lifetime measurements and biological imaging. Chem Rev 110:2641–2684.

[28]   Perkampus H-H (2012) Uv-vis spectroscopy and its applications. Springer, Berlin.

[29]   Lakowicz JR (2010) Principles of fluorescence spectroscopy. Springer, New York.

[30]   Li J, Li C, Aroca RF (2017) Plasmon-enhanced fluorescence spectroscopy. Chem
         Soc Rev 46:3962–3979.

[31]   Di Wu M, García-Etxarri A, Salleo A, Dionne JA (2014) Plasmon-Enhanced
         Upconversion. J Phys Chem Lett 5:4020–4031.

[32]   Nicol A, Knoll W (2018) Characteristics of Fluorescence Emission Excited by
         Grating-Coupled Surface Plasmons. Plasmonics in press doi: 10.1007/s11468-
         018-0757-8.

[33]   Chalmers J, Griffiths PR (2002) Handbook of vibrational spectroscopy. Wiley,
         Chichester.

[34]   Lee J, Lee T, Choi J (2016) Nano-Biosensor for Monitoring the Neural
         Differentiation of Stem Cells. Nanomaterials 6:24.

[35]   Spackova B, Wrobel P, Bockova M, Homola J (2016) Optical Biosensors Based
         on Plasmonic Nanostructures: A Review. Proc IEEE 104:2380–2408.

[36]   Tu L, Li X, Bian S, Yu Y, Li J, Huang L, Liu P, Wu Q, Wang W (2017) Label-free
         and real-time monitoring of single cell attachment on template-stripped plasmonic
         nano-holes. Sci Rep 7:11020.

[37]   Soler M, Belushkin A, Cavallini A, Kebbi-Beghdadi C, Greub G, Altug H (2017)
         Multiplexed nanoplasmonic biosensor for one-step simultaneous detection of
         Chlamydia trachomatis and Neisseria gonorrhoeae in urine. Biosens Bioelectron
         94:560–567.

[38]   Jackman JA, Rahim Ferhan A, Cho N (2017) Nanoplasmonic sensors for
         biointerfacial science. Chemi Soc Rev 46:3615–3660.

[39]   Mazzotta F, Johnson TW, Dahlin AB, Shaver J, Oh S, Höök F (2015) Influence
         of the Evanescent Field Decay Length on the Sensitivity of Plasmonic Nanodisks
         and Nanoholes. ACS Photonics 2:256–262.

[40]   Stockman MI (2015) Nanoplasmonic sensing and detection. Science 348:287–
         288.

[41]   Hering K, Cialla D, Ackermann K, Dörfer T, Möller R, Schneidewind H, Mattheis
         R, Fritzsche W, Rösch P, Popp J (2008) SERS: a versatile tool in chemical and
         biochemical diagnostics. Anal Bioanal Chem 390:113–124.

[42]   Correia-Ledo D, Gibson KF, Dhawan A, Couture M, Vo-Dinh T, Graham D,
         Masson J (2012) Assessing the Location of Surface Plasmons Over Nanotriangle
         and Nanohole Arrays of Different Size and Periodicity. J Phy Chem C Nanomater
         Interfaces 116:6884–6892.

[43]   Saboktakin M, Ye X, Chettiar UK, Engheta N, Murray CB, Kagan CR (2013)
        Plasmonic enhancement of nanophosphor upconversion luminescence in Au
        nanohole arrays. ACS Nano 7:7186–7192.

[44]   Saboktakin M, Ye X, Oh SJ, Hong S, Fafarman AT, Chettiar UK, Engheta N,
        Murray CB, Kagan CR (2012) Metal-enhanced upconversion luminescence
        tunable through metal nanoparticle-nanophosphor separation. ACS Nano
        6:8758–8766.

[45]   Pelton M, Aizpurua J, Bryant G (2008) Metal-nanoparticle plasmonics. Laser
        Photonic Rev 2:136–159.

[46]   Farrell ME, Strobbia P, Pellegrino PM, Cullum B (2017) Surface regeneration and
        signal increase in surface-enhanced Raman scattering substrates. Appl Opt
        56:B198-B213.

[47]   Lee T, Hirst DJ, Kulkarni K, Del Borgo MP, Aguilar M (2018) Exploring Molecular-
        Biomembrane Interactions with Surface Plasmon Resonance and Dual
        Polarization Interferometry Technology: Expanding the Spotlight onto
        Biomembrane Structure. Chem Rev 118:5392–5487.

[48]   Matsubara K, Kawata S, Minami S (1988) Optical chemical sensor based on
        surface plasmon measurement. Appl Opt 27:1160–1163.

[49]   Akimoto T, Sasaki S, Ikebukuro K, Karube I (2000) Effect of incident angle of light
        on sensitivity and detection limit for layers of antibody with surface plasmon
        resonance spectroscopy. Biosens Bioelectron 15:355–362.

[50]   Liu X, Song D, Zhang Q, Tian Y, Ding L, Zhang H (2005) Wavelength-modulation
        surface plasmon resonance sensor. Trends Analyt Chem 24:887–893.

[51]   Sepúlveda B, Calle A, Lechuga LM, Armelles G (2006) Highly sensitive detection
        of biomolecules with the magneto-optic surface-plasmon-resonance sensor. Opt
        Lett 31:1085.

[52]   Wong CL, Olivo M (2014) Surface Plasmon Resonance Imaging Sensors: A
        Review. Plasmonics 9:809–824.

[53]   Nelson SG, Johnston KS, Yee SS (1996) High sensitivity surface plasmon
        resonace sensor based on phase detection. Sens Actuators B Chem 35:187–191

[54]   Nikitin P, Grigorenko A, Beloglazov A, Valeiko M, Savchuk A, Savchuk O, Steiner
        G, Kuhne C, Huebner A, Salzer R (2000) Surface plasmon resonance
        interferometry for micro-array biosensing. Sens Actuators A Phys 85:189–193.

[55]   Emilsson G, Xiong K, Sakiyama Y, Malekian B, Ahlberg Gagnér V, Schoch RL,
Lim RYH, Dahlin AB (2018) Polymer brushes in solid-state nanopores form an
impenetrable entropic barrier for proteins. Nanoscale 10:4663–4669.

[56]   Nehl CL, Liao H, Hafner JH (2006) Optical properties of star-shaped gold
nanoparticles. Nano Lett 6:683–688.

[57]   Song CY, Zhou N, Yang BY, Yang YJ, Wang LH (2015) Facile synthesis of
hydrangea flower-like hierarchical gold nanostructures with tunable surface
topographies for single-particle surface-enhanced Raman scattering. Nanoscale
7:17004–17011.

[58]   Manivannan S, Ramaraj R (2013) Electrodeposited nanostructured raspberry-like
gold-modified electrodes for electrocatalytic applications. J Nanopart Res
15:1323.

[59]   Solanki PR, Kaushik A, Agrawal VV, Malhotra BD (2011) Nanostructured metal
oxide-based biosensors. NPG Asia Mater 3:17–24.

[60]   Chao J, Lin Y, Liu H, Wang L, Fan C (2015) DNA-based plasmonic
nanostructures. Mater Today 18:326–335.

[61]   Asapu R, Ciocarlan R, Claes N, Blommaerts N, Minjauw M, Ahmad T, Dendooven
J, Cool P, Bals S, Denys S, Detavernier C, Lenaerts S, Verbruggen SW (2017)
Plasmonic Near-Field Localization of Silver Core-Shell Nanoparticle Assemblies
via Wet Chemistry Nanogap Engineering. ACS Appl Mater interfaces 9:41577–
41585.

[62]   Kanninen P, Johans C, Merta J, Kontturi K (2008) Influence of ligand structure on
the stability and oxidation of copper nanoparticles. J Colloid Interface Sci 318:88–
95.

[63]   Rodriguez RD, Sheremet E, Nesterov M, Moras S, Rahaman M, Weiss T,
Hietschold M, Zahn DR (2018) Aluminum and copper nanostructures for surface-
enhanced Raman spectroscopy: A one-to-one comparison to silver and gold.
Sens Actuators B Chem 262:922–927.

[64]   Lounis SD, Runnerstrom EL, Llordés A, Milliron DJ (2014) Defect Chemistry and
Plasmon Physics of Colloidal Metal Oxide Nanocrystals. J Phys Chem Lett
5:1564–1574.

[65]   Mattox TM, Ye X, Manthiram K, Schuck PJ, Alivisatos AP, Urban JJ (2015)
Chemical Control of Plasmons in Metal Chalcogenide and Metal Oxide
Nanostructures. Adv Mater 27:5830–5837.

[66]   Divi S, Agrahari G, Kadulkar SR, Kumar S, Chatterjee A (2017) Improved
         prediction of heat of mixing and segregation in metallic alloys using tunable
         mixing rule for embedded atom method. Modelling Simul Mater Sci Eng
         25:85011.

[67]   Caballero B, García-Martín A, Cuevas JC (2016) Hybrid Magnetoplasmonic
         Crystals Boost the Performance of Nanohole Arrays as Plasmonic Sensors. ACS
         Photonics 3:203–208.

[68]   Xiong K, Tordera D, Emilsson G, Olsson O, Linderhed U, Jonsson MP, Dahlin
         AB (2017) Switchable Plasmonic Metasurfaces with High Chromaticity
         Containing Only Abundant Metals. Nano Lett 17:7033–7039.

[69]   Hackett LP, Ameen A, Li W, Dar FK, Goddard LL, Liu GL (2018) Spectrometer-
         Free Plasmonic Biosensing with Metal-Insulator-Metal Nanocup Arrays. ACS
         Sens 3:290–298.

[70]   Hernández L, Espasa A, Fernández C, Candela A, Martín C, Romero S (2002)
         CEA and CA 549 in serum and pleural fluid of patients with pleural effusion. Lung
         Cancer 36:83–89.

[71]   Negru B, McAnally MO, Mayhew HE, Ueltschi TW, Peng L, Sprague-Klein EA,
         Schatz GC, van Duyne RP (2017) Fabrication of Gold Nanosphere Oligomers for
         Surface-Enhanced Femtosecond Stimulated Raman Spectroscopy. J Phys
         Chem C 121:27004–27008.

[72]   Yoo D, Nguyen N, Martin-Moreno L, Mohr DA, Carretero-Palacios S, Shaver J,
         Peraire J, Ebbesen TW, Oh S (2016) High-Throughput Fabrication of Resonant
         Metamaterials with Ultrasmall Coaxial Apertures via Atomic Layer Lithography.
         Nano Lett 16:2040–2046.

[73]   Yoo D, Mohr DA, Vidal-Codina F, John-Herpin A, Jo M, Kim S, Matson J, Caldwell
         JD, Jeon H, Nguyen N, Martin-Moreno L, Peraire J, Altug H, Oh S (2018) High-
         Contrast Infrared Absorption Spectroscopy via Mass-Produced Coaxial Zero-
         Mode Resonators with Sub-10 nm Gaps. Nano Lett 18:1930–1936.

[74]   Live LS, Bolduc OR, Masson J (2010) Propagating surface plasmon resonance
         on microhole arrays. Anal Chem 82:3780–3787.

[75]   Rippa M, Castagna R, Tkachenko V, Zhou J, Petti L (2017) Engineered
         nanopatterned substrates for high-sensitive localized surface plasmon
         resonance: An assay on biomacromolecules. J Mater Chem B 5:5473–5478.

[76]   Couture M, Brulé T, Laing S, Cui W, Sarkar M, Charron B, Faulds K, Peng W,
         Canva M, Masson J (2017) High Figure of Merit (FOM) of Bragg Modes in Au-
         Coated Nanodisk Arrays for Plasmonic Sensing. Small 13:1700908.

[77]   Jeong JW, Arnob MMP, Baek K, Lee SY, Shih W, Jung YS (2016) 3D Cross-Point Plasmonic Nanoarchitectures Containing Dense and Regular Hot Spots for Surface-Enhanced Raman Spectroscopy Analysis. Adv Mat 28:8695–8704.

[78]   Vieu C, Carcenac F, Pepin A, Chen Y, Mejias M, Lebib A, Manin-Ferlazzo L, Couraud L, Launois H (2000) Electron beam lithography: resolution limits and applications. Appl Surf Sci. 164:111–117.

[79]   Reyntjens S, Puers R (2001) A review of focused ion beam applications in microsystem technology. J Micromech Microeng 11:287.

[80]   Horák M, Bukvišová K, Švarc V, Jaskowiec J, Křápek V, Šikola T (2018) Comparative study of plasmonic antennas fabricated by electron beam and focused ion beam lithography. Sci Rep 8:9640.

[81]   Crick CR, Albella P, Kim H, Ivanov AP, Kim K, Maier SA, Edel JB (2017) Low-Noise Plasmonic Nanopore Biosensors for Single Molecule Detection at Elevated Temperatures. ACS Photonics 4:2835–2842.

[82]   Yim S, Jeon S, Kim JM, Baek KM, Lee GH, Kim H, Shin J, Jung YS (2018) Transferrable Plasmonic Au Thin Film Containing Sub-20 nm Nanohole Array Constructed via High-Resolution Polymer Self-Assembly and Nanotransfer Printing. ACS Appl Mater Interfaces 10:2216–2223.

[83]   Hong KY, Menezes JW, Brolo AG (2018) Template-Stripping Fabricated Plasmonic Nanogratings for Chemical Sensing. Plasmonics 13:231–237.

[84]   Jeong JW, Yang SR, Hur YH, Kim SW, Baek KM, Yim S, Jang H, Park JH, Lee SY, Park C, Jung YS (2014) High-resolution nanotransfer printing applicable to diverse surfaces via interface-targeted adhesion switching. Nat Commun 5:5387.

[85]   Hwang SH, Jeon S, Kim MJ, Choi D, Choi J, Jung J, Kim K, Lee J, Jeong JH, Youn JR (2017) Covalent bonding-assisted nanotransfer lithography for the fabrication of plasmonic nano-optical elements. Nanoscale 9:14335–14346.

[86]   Chen Y, Bi K, Wang Q, Zheng M, Liu Q, Han Y, Yang J, Chang S, Zhang G, Duan H (2016) Rapid Focused Ion Beam Milling Based Fabrication of Plasmonic Nanoparticles and Assemblies via "Sketch and Peel" Strategy. ACS Nano 10:11228–11236.

[87]   Ai B, Möhwald H, Wang D, Zhang G (2017) Advanced Colloidal Lithography Beyond Surface Patterning. Adv Mater Interfaces 4:1600271.

[88]   Weiler M, Menzel C, Pertsch T, Alaee R, Rockstuhl C, Pacholski C (2016)
        Bottom-Up Fabrication of Hybrid Plasmonic Sensors: Gold-Capped Hydrogel
        Microspheres Embedded in Periodic Metal Hole Arrays. ACS applied materials &
        interfaces 8:26392–26399.

[89]   Zhang T, Li H, Hou S, Dong Y, Pang G, Zhang Y (2015) Construction of
        Plasmonic Core-Satellite Nanostructures on Substrates Based on DNA-Directed
        Self-Assembly as a Sensitive and Reproducible Biosensor. ACS Appl Mater
        Interfaces 7:27131–27139.

[90]   Liang Z, Liang W, Shao W, Huang J, Guan T, Wen P, Cao G, Jiang L (2018)
        Fabrication of tunable aluminum nanodisk arrays via a self-assembly
        nanoparticle template method and their applications for performance
        enhancement in organic photovoltaics. J Mater Chem A 6:3649–3658.

[91]   Correia-Ledo D, Gibson KF, Dhawan A, Couture M, Vo-Dinh T, Graham D,
        Masson J (2012) Assessing the Location of Surface Plasmons Over Nanotriangle
        and Nanohole Arrays of Different Size and Periodicity. J Phys Chem C
        Nanomater Interfaces 116:6884–6892.

[92]   Kim Y, Oh S, Crooks RM (2004) Preparation and Characterization of 1−2 nm
        Dendrimer-Encapsulated Gold Nanoparticles Having Very Narrow Size
        Distributions. Chem Mater 16:167–172.

[93]   Kuntaegowdanahalli SS, Bhagat AAS, Kumar G, Papautsky I (2009) Inertial
        microfluidics for continuous particle separation in spiral microchannels. Lab Chip
        9:2973–2980.

[94]   Sarkar B, Alexandridis P (2015) Block copolymer–nanoparticle composites:
        Structure, functional properties, and processing. Prog Polym Sci 40:33–62.

[95]   Boles MA, Engel M, Talapin DV (2016) Self-Assembly of Colloidal Nanocrystals:
        From Intricate Structures to Functional Materials. Chem Rev 116:11220–11289.

[96]   Baek KM, Kim JM, Jeong JW, Lee SY, Jung YS (2015) Sequentially Self-
        Assembled Rings-in-Mesh Nanoplasmonic Arrays for Surface-Enhanced Raman
        Spectroscopy. Chem Mater 27:5007–5013.

[97]   Jeong JW, Hur YH, Kim H, Kim JM, Park WI, Kim MJ, Kim BJ, Jung YS (2013)
        Proximity injection of plasticizing molecules to self-assembling polymers for
        large-area, ultrafast nanopatterning in the sub-10-nm regime. ACS Nano 7:6747–
        6757.

[98]   Paik T, Yun H, Fleury B, Hong S, Jo PS, Wu Y, Oh S, Cargnello M, Yang H,
        Murray CB, Kagan CR (2017) Hierarchical Materials Design by Pattern Transfer
        Printing of Self-Assembled Binary Nanocrystal Superlattices. Nano Lett 17:1387–
        1394.

[99]   Dong A, Chen J, Vora PM, Kikkawa JM, Murray CB (2010) Binary nanocrystal
        superlattice membranes self-assembled at the liquid-air interface. Nature
        466:474–477.

[100]   Gisbert Quilis N, Lequeux M, Venugopalan P, Khan I, Knoll W, Boujday S, Lamy
        de la Chapelle, Marc, Dostalek J (2018) Tunable laser interference lithography
        preparation of plasmonic nanoparticle arrays tailored for SERS. Nanoscale
        10:10268–10276.

[101]   Live LS, Dhawan A, Gibson KF, Poirier-Richard H, Graham D, Canva M, Vo-Dinh
        T, Masson J (2012) Angle-dependent resonance of localized and propagating
        surface plasmons in microhole arrays for enhanced biosensing. Anal Bioanal
        Chem 404:2859–2868.

[102]   Murray-Méthot M, Ratel M, Masson J (2010) Optical Properties of Au, Ag, and
        Bimetallic Au on Ag Nanohole Arrays. J Phys Chem C 114:8268–8275.

[103]   Špačková B, Lynn NS, Slabý J, Šípová H, Homola J (2017) A Route to Superior
        Performance of a Nanoplasmonic Biosensor: Consideration of Both Photonic and
        Mass Transport Aspects. ACS Photonics 5:1019–1025.

[104]   Qiu G, Ng SP, Liang X, Ding N, Chen X, Wu CL (2017) Label-Free LSPR
        Detection of Trace Lead(II) Ions in Drinking Water by Synthetic Poly(mPD-co-
        ASA) Nanoparticles on Gold Nanoislands. Anal Chem 89:1985–1993.

[105]   Brenet S, John-Herpin A, Gallat FX, Musnier B, Buhot A, Herrier C, Rousselle T,
        Livache T, Hou Y. (2018) Highly-Selective Optoelectronic Nose Based on
        Surface Plasmon Resonance Imaging for Sensing Volatile Organic Compounds.
        Anal Chem in press 10.1021/acs.analchem.8b02036

[106]   Choi Y, Shin SH, Hong S, Kim Y (2016) A combined top-down/bottom-up
        approach to structuring multi-sensing zones on a thin film and the application to
        SPR sensors. Nanotechnology 27:345302.

[107]   Wiesholler LM, Hirsch T (2018) Strategies for the design of bright upconversion
        nanoparticles for bioanalytical applications. Opt Mater 80:253–264.

[108]   Wang P, Li Z, Salcedo WJ, Sun Z, Huang S, Brolo AG (2015) Surface plasmon
        enhanced up-conversion from $NaYF_4$:Yb/Er/Gd nano-rods. Phys Chem Chem
        Phys 17:16170–16177.

[109]   Luu Q, Hor A, Fisher J, Anderson RB, Liu S, Luk T, Paudel HP, Farrokh Baroughi
M, May PS, Smith S (2014) Two-Color Surface Plasmon Polariton Enhanced
Upconversion in NaYF$_4$:Yb:Tm Nanoparticles on Au Nanopillar Arrays. J Phys
Chem C 118:3251–3257.

[110]   Song HY, Wong TI, Sadovoy A, Wu L, Bai P, Deng J, Guo S, Wang Y, Knoll W,
Zhou X (2015) Imprinted gold 2D nanoarray for highly sensitive and convenient
PSA detection via plasmon excited quantum dots. Lab Chip 15:253–263.

[111]   Santos GM, Zhao F, Zeng J, Li M, Shih W (2015) Label-free, zeptomole cancer
biomarker detection by surface-enhanced fluorescence on nanoporous gold disk
plasmonic nanoparticles. J Biophotonics 8:855–863.

[112]   Mei Z, Tang L (2017) Surface-Plasmon-Coupled Fluorescence Enhancement
Based on Ordered Gold Nanorod Array Biochip for Ultrasensitive DNA Analysis.
Anal Chem 89:633–639.

[113]   Lee SA, Biteen JS (2018) Interplay of Nanoparticle Resonance Frequency and
Array Surface Coverage in Live-Cell Plasmon-Enhanced Single-Molecule
Imaging. J Phys Chem C 122:5705–5709.

[114]   Sarfo DK, Izake EL, O'Mullane AP, Ayoko GA (2018) Molecular recognition and
detection of Pb(II) ions in water by aminobenzo-18-crown-6 immobilised onto a
nanostructured SERS substrate. Sens Actuators B Chem 255:1945–1952.

[115]   Shi X, Gu W, Zhang C, Zhao L, Li L, Peng W, Xian Y (2016) Construction of a
Graphene/Au-Nanoparticles/Cucurbit7uril-Based Sensor for Pb(2+) Sensing.
Chemistry 22:5643–5648.

[116]   Petti L, Capasso R, Rippa M, Pannico M, La Manna P, Peluso G, Calarco A,
Bobeico E, Musto P (2016) A plasmonic nanostructure fabricated by electron
beam lithography as a sensitive and highly homogeneous SERS substrate for
bio-sensing applications. Vib Spectrosc 82:22–30.

[117]   Bi L, Wang Y, Yang Y, Li Y, Mo S, Zheng Q, Chen L (2018) Highly Sensitive and
Reproducible SERS Sensor for Biological pH Detection Based on a Uniform Gold
Nanorod Array Platform. ACS Appl Mater Interfaces 10:15381–15387.

[118]   Ngo HT, Wang H, Fales AM, Nicholson BP, Woods CW, Vo-Dinh T (2014) DNA
bioassay-on-chip using SERS detection for dengue diagnosis. Analyst 139:5655–
5659.

[119]   Hong S, Shim O, Kwon H, Choi Y (2016) Autoenhanced Raman Spectroscopy
via Plasmonic Trapping for Molecular Sensing. Anal Chem 88:7633–7638.

[120] Olson AP, Ertsgaard CT, Elliott SN, Lindquist NC (2016) Super-Resolution Chemical Imaging with Plasmonic Substrates. ACS Photonics 3:329–336.

[121] Tantussi F, Messina GC, Capozza R, Dipalo M, Lovato L, Angelis F de (2018) Long-Range Capture and Delivery of Water-Dispersed Nano-objects by Microbubbles Generated on 3D Plasmonic Surfaces. ACS Nano 12:4116–4122.

[122] Anker JN, Hall WP, Lyandres O, Shah NC, Zhao J, van Duyne RP (2008) Biosensing with plasmonic nanosensors. Nat Mater 7:442–453.

[123] Couture M, Ray KK, Poirier-Richard H, Crofton A, Masson J (2016) 96-Well Plasmonic Sensing with Nanohole Arrays. ACS Sens 1:287–294.

[124] Belushkin A, Yesilkoy F, Altug H (2018) Nanoparticle-Enhanced Plasmonic Biosensor for Digital Biomarker Detection in a Microarray. ACS Nano 12:4453-4461.

[125] Lu M, Hong L, Liang Y, Charron B, Zhu H, Peng W, Masson J (2018) Enhancement of gold nanoparticle coupling with a 2D plasmonic crystal at high incidence angles. Anal Chem 90:6683-6692.

[126] Aćimović SS, Ortega MA, Sanz V, Berthelot J, Garcia-Cordero JL, Renger J, Maerkl SJ, Kreuzer MP, Quidant R (2014) LSPR chip for parallel, rapid, and sensitive detection of cancer markers in serum. Nano Lett 14:2636–2641.

[127] Khan Y, Li A, Chang L, Li L, Guo L (2018) Gold nano disks arrays for localized surface plasmon resonance based detection of PSA cancer marker. Sens Actuators B Chem 255:1298–1307.

[128] Chen B, Liu C, Ge L, Hayashi K (2016) Localized surface plasmon resonance gas sensor of Au nano-islands coated with molecularly imprinted polymer: Influence of polymer thickness on sensitivity and selectivity. Sens Actuators B Chem 231:787–792.

[129] Shang L, Liu C, Chen B, Hayashi K (2018) Development of molecular imprinted sol-gel based LSPR sensor for detection of volatile cis -jasmone in plant. Sens Actuators B Chem 260:617–626.

[130] Hong Y, Jo S, Park J, Park J, Yang J (2018) High sensitive detection of copper II ions using D-penicillamine-coated gold nanorods based on localized surface plasmon resonance. Nanotechnology 29:215501.

[131] López-Muñoz GA, Estevez M, Peláez-Gutierrez EC, Homs-Corbera A, García-Hernandez MC, Imbaud JI, Lechuga LM (2017) A label-free nanostructured plasmonic biosensor based on Blu-ray discs with integrated microfluidics for sensitive biodetection. Biosens Bioelectron 96:260–267.

2 Aim of the Work

Nanostructured surfaces offer unique plasmonic properties. The plasmonic field can be tuned and optimized by changing the geometries of the nanostructured surfaces. This seems to be promising in SPR (bio)sensor applications. A higher surface sensitive is expected to yield in better signal-to-noise ratios for the detection of small molecules. This postulation should be investigated in this work by the investigation of gold nanohole arrays of different hole diameters. The aim was to demonstrate the impact of the higher surface sensitivity in a sensor application for the detection of small molecules using SPR readout. When the sensing volume gets significantly decreased and highest sensitivity is expected next to the gold surface it becomes challenging to design a receptor for the detection of target analytes. Two-dimensional carbon nanomaterials, especially graphene, would be the best candidate to fulfil the requirement of providing a thin receptor layer. As this material is only one atom thick and possess large areas of sp^2 hybridization, it was planned to investigate the detection of small molecules via π-stacking on such a graphene-plasmon hybrid. Alternatively, the plasmonic effect of nanostructured surfaces is also known for a strong confined electromagnetic field close to the surface located at the edges of the structures. These so-called hot spots enhance sensing techniques based on transmission. A sensor concept utilizing the enhancement of nanostructured surface should be designed to proof the capabilities of such systems for (bio)analytical applications.

3 Graphene-enhanced Plasmonic Nanohole Arrays for Environmental Sensing in Aqueous Samples

3.1 Abstract

The label-free nature of surface plasmon resonance techniques (SPR) enables a fast, specific, and sensitive analysis of molecular interactions. However, detection of highly diluted concentrations and small molecules is still challenging [M]. It is shown here that in contrast to continuous gold films, gold nanohole arrays can significantly improve the performance of SPR devices in angle-dependent measurement mode, as a signal amplification arises from localized surface plasmons at the nanostructures. This leads consequently to an increased sensing capability of molecules bound to the nanohole array surface [M]. Furthermore, a reduced graphene oxide (rGO) sensor surface was layered over the nanohole array. Reduced graphene oxide is a 2D nanomaterial consisting of sp^2-hybridized carbon atoms and is an attractive receptor surface for SPR as it omits any bulk phase and therefore allows fast response times. In fact, it was found that nanohole arrays demonstrated a higher shift in the resonance angle of 250–380% compared to a continuous gold film [M]. At the same time the nanohole array structure as characterized by its diameter-to-periodicity ratio had minimal influence on the binding capacity of the sensor surface. As a simple and environmentally highly relevant model, binding of the plasticizer diethyl phthalate (DEP) via π-stacking was monitored on the rGO gold nanohole array realizing a limit of detection of as low as 20 nM. The concentration-dependent signal change was studied with the best performing rGO-modified nanohole arrays. Compared to continuous gold films a diameter-to-periodicity ratio (D/P) of 0.43 lead to a 12-fold signal enhancement. Finally, the effect of environmental waters on the sensor was evaluated using samples from sea, lake and river waters spiked with analytically relevant amounts of DEP during which significant changes in the SPR signal are observed. It is expected that this concept can be successfully transferred to enhance the sensitivity in SPR sensors.
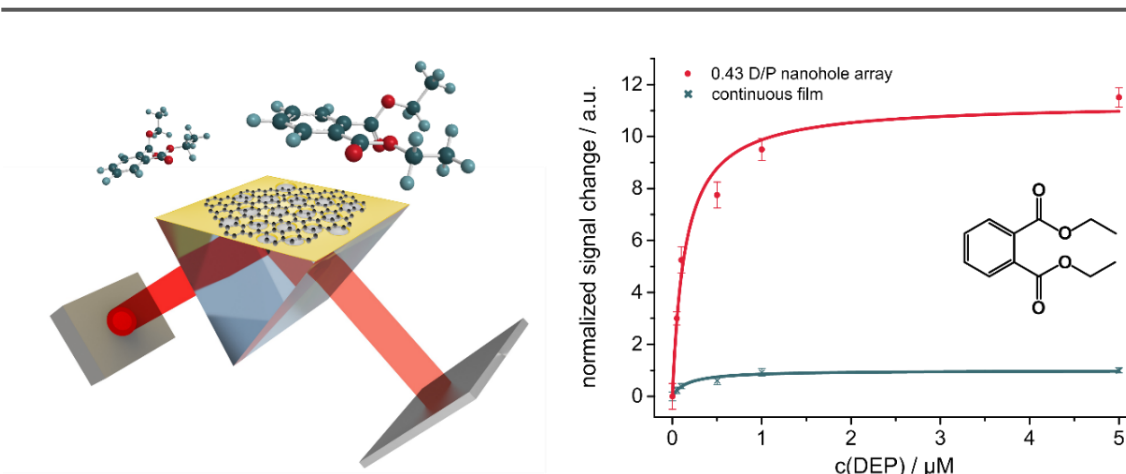
Figure 3.1 Scheme of the SPR setup with a plasmon-graphene hybrid as substrate used for DEP detection (Left). Normalized signal change at a constant angle in response to binding of DEP to rGO-modified nanohole arrays (*D/P* = 0.43) covering a concentration range from 0.05 to 5 µM aside with the chemical structure of DEP.

This chapter has been published.

Genslein C, Hausler P, Kirchner EM, Bierl R, Baeumner AJ, Hirsch T (2016) Graphene-enhanced plasmonic nanohole arrays for environmental sensing in aqueous samples. Beilstein J Nanotechnol, 7:564-1573

This paper contains research results that were in part described already in Christa Genslein's Master's thesis. This includes a paragraph within the introduction subchapter and descriptions of substrate fabrication and characterization. The Master's thesis is entitled "Nanostructured Substrates for Bioanalytical Applications Based on Plasmonic Effects" and was submitted at the 10th of August, 2015 to the Faculty of Chemistry and Pharmacy at the University of Regensburg. As the new work done during the Ph.D. project relied on previous results and as these combined are presented in the published work, the combination is presented here as chapter 3.

Also, those sections and data found in the Master's thesis are listed here in detail:

(1) Data taken from M.Sc. work:

– Page (P) 46, Figure 3.2 (outline scheme) is very similar (introduction)

– P 47, Figure 3.3 (results and discussion)

– P 48, Figure 3.4 (results and discussion)

– P 49, Figure 3.5 (results and discussion)

– P 50, Figure 3.6 (results and discussion)

– P 52, Table 3.1 (results and discussion)

(2) Text that is identical or similar to the M.Sc. thesis.:

- P 41, sentence one, two, four and seven (abstract)
- P 44(-45), paragraph two (introduction)
- P 45, paragraph two and paragraph three, sentence two to five (introduction)
- P 46, paragraph one, sentence five and paragraph two, sentence one (introduction)
- P 47, paragraph two, sentence two to four and paragraph three, sentence two and three (results and discussion)
- P 48, paragraph two, sentence two (results and discussion)
- P 49, paragraph one, sentence one and two and paragraph two, sentence three (results and discussion)
- P 51, paragraph two, sentence one (results and discussion)
- P 56, paragraph two (experimental)
- P 56-57, paragraph three (experimental)
- P 57, paragraph two to four (experimental)
- P 58, paragraph one, sentence one and two and paragraph two, sentence one and two (experimental)

These parts are indicated in the following by the citation "M".

Author contributions:

Most of the experimental work was carried out by CG. PH and CG performed the RIE and the SEM analysis. EMK synthesized the graphene oxide. CG wrote the manuscript. The article was revised by CG, PH, EMK, RB, AJB and TH. TH is corresponding author.

3.2 Introduction

Plasticizers are additives used in plastic industry, personal care products and especially in polyvinyl chloride (PVC) products. The most common plasticizers are phthalate acid esters (PAEs) [1]. Since PAEs are not chemically bound to the polymeric matrix, they can leach into the environment. The resulting wide distribution in aqueous systems, such as lakes and rivers, and disturbances of the ecological environment are caused by accumulation of PAEs in natural waters [2,3]. It has been reported that PAEs trigger adverse effects on human health and are readily absorbed through the skin. They can cause feminization of male infants, impact genital development and testes maturation. Metabolic products are also potential thyroid hormone disruptors [4-6]. Because of their carcinogenic and toxic characteristics determination of PAEs in environmental water is an urgent task. Most widely used techniques are gas chromatography and high performance liquid chromatography coupled with mass spectrometry (GC–MS and HPLC–MS), however often enrichment and extraction steps prior to the analysis are necessary [7]. An online detection system for natural water with detection limits in the environmental interesting concentration is important for water safety and direly needed.

Surface plasmon resonance spectroscopy (SPR) is a widely-used technique for quantifying and characterizing biomolecular interactions in biosensors for medical diagnostics, food safety and environmental monitoring [M] providing important features such as real time measurements, high sensitivity and label-free assay [8]. The detection of highly diluted concentrations and small molecules (<200 Da) remains challenging within SPR sensing [9,M]. For (bio)analytical applications the sensitivity needs to be enhanced to achieve low detection limits. To address this issue nanomaterials ranging from metallic nanoparticles, carbon-based structures to liposomes were used [10-12,M]. Plasmonic transducers are sensitive to changes of optical properties such as the dielectric constant and hence the refractive index next [M] to their surface. The exponential decay of the plasmonic field generates a response affected by the penetrated volume [M] within the solution [13]. Within conventional SPR sensing propagating surface plasmons (PSP) are the main parameter, defined as propagating charge oscillations on the surface of a thin metal film. At a visible wavelength the decay of PSP on a planar surface is approximately half of the excitation wavelength and in the range of a few hundred nanometers [14,M]. For localized surface plasmons (LSP) occurring at nanostructures, the values are significantly smaller and are in the range of 5–60 nm [14,15,M]. An enhancement of local electromagnetic fields and intense

absorption bands due to excitations of electrons at the nano-structures, results in a high sensitivity towards local changes of the refractive index [16,M]. A variety of nanostructured substrates, such as nanostructured arrays, has been designed and applied to bioanalytical sensing applications [17-20]. Nanohole arrays, which are characterized by combining localized and propagating surface plasmons, offer a possibility to tune the plasmonic features and therefore optimize the sensing performance for a specific application [21,M]. They have been shown to provide better sensitivity in wavelength [M] dependent SPR sensing. However, most commercial SPR devices are based on angle scanning by illumination at a constant wavelength and no studies are available investigating this interesting plasmonic effect [17, 22].

Nanohole arrays have been first fabricated 1995 by Masuda and Fukuda using a replication process of an anodized alumina structure [23,M]. Since then, a vast number of techniques has been invented. For example, as focused ion beam (FBI) milling allows a control of the size and shape of the nanoholes with good reproducibility it has been applied for biosensor development and theoretical studies [M]. With high fabrication costs and long milling times it is not adaptable to large volume manufacturing [24-26,M]. Standard lithography techniques can instead be used such as soft embossing. An imprinting mask is prepared by e-beam lithography and by printing numerous times on a surface, large areas of nanoholes are created [27-30,M]. Since for each different nanohole layout a new mask needs to be fabricated, this method is still time consuming and unfavorable for, optimization studies [M]. To provide tunability, rapid fabrication and low manufacturing cost that can also easily be done in low-class clean room areas, techniques such as polymer blend lithography or a modified nanosphere lithography (NSL) technique were recently developed [31,32,M]. Using colloidal lithography disordered nanoholes can be obtained. A combination of NSL with electrochemical deposition, ion-polishing, plasma treatment and glancing-angle deposition produces ordered nanohole arrays. Therefore, NSL is a promising tool to produce nanostructured substrates [M].

Here, nanohole arrays were prepared by a modified nanosphere lithography (Figure 3.2). The dominating parameters for sphere mask formation are the evaporation rate and the particle content [M]. Both can be tuned very precisely [33,M]. The most characteristic parameter for nanohole arrays is the diameter- to-periodicity ratio (D/P) [M], as visualized below in Figure 4B. Hole diameter (D) and periodicity (P, distance between the centres of neighbouring holes [M]) both significantly affect the plasmonic properties and therefore the sensitivity of nanohole arrays [34].
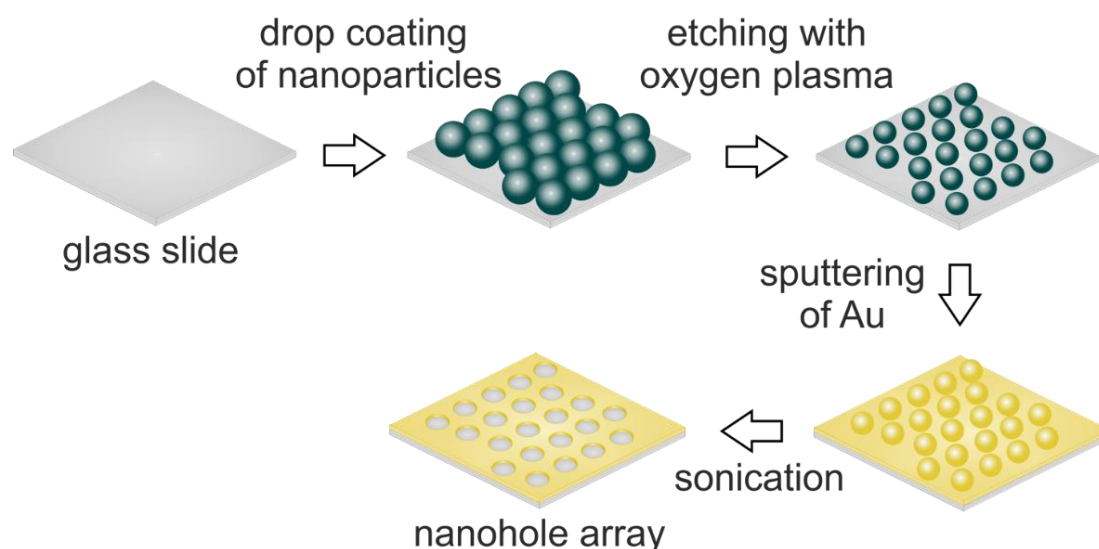
Figure 3.2│ Outline of the fabrication steps to form a nanohole array with a modified nanosphere lithography technique [M].

For an analytical application the gold layer needs to be modified with a receptor layer. Reduced graphene oxide (rGO) is very interesting receptor layer as it serves two purposes. On the one hand, it improves the sensing performance as its high surface- to-volume ratio leads to more efficient adsorption of molecules together with local plasmonic enhancement effects [35,36]. Thus, systems consisting of a plasmonic nanostructure and graphene are referred to as plasmon–graphene hybrids [37]. On the other hand, interactions of molecules with aromatic systems via π-stacking is strongly promoted by the sp^2-hybridized carbon atoms arranged in a honeycomb structure [M]. In this study a sensor for diethyl phthalate as model analyte was developed. It is known that this type of plasticizers adsorbs on polystyrene resins by multiple adsorbent–adsorbate interactions such as hydrogen bonding and π-stacking [38], which makes them an ideal analyte for the evaluation of the graphene-modified gold surfaces in SPR.

Nanostructured surfaces are promising in enhancing [M] the signals in surface-sensitive techniques. The excitation of localized surface plasmons are known to improve Raman signals on structured metal surfaces significantly, and often utilized in sensing systems. A Web of Science survey revealed more than 1600 publications on the concept of surface-enhanced Raman scattering (SERS) in the year 2015 alone. In contrast, in the same year only 25 publications report on the enhancement of SPR signals by introducing nanostructured surfaces. One reason can be attributed to the different size of the sensing spots used in these two prominent techniques. Commercial SPR devices usually illuminate spots in the range of several square millimeters. This is about $3 \cdot 10^7$-times

larger than the area in Raman microscopy using a 100× objective. This comes with the need to fabricate regular nanostructures in large lateral dimensions, while also ideally delivering fast and reproducible substrates. These requirements are easily met in nanosphere lithography as sphere size and monolayer formation allow for facile nanohole array design and systematic variation of its properties.

3.3 Results and Discussion

A nanohole array modified SPR chip was fabricated according to the method described by Masson *et al.* [39,40]. Drop casting of the polystyrene particles [M] on a clean glass slide leads to a densely packed monolayer on the substrate (Figure 3.3). The sphere mask consists of ordered areas of several square millimeters covering more than the optical spot size of the SPR device (0.23 cm^2) [M]. Highly ordered monolayers are mandatory to obtain a periodic and defined structuring of the substrates [M], as described for signal enhancement in wavelength-dependent SPR studies [41].
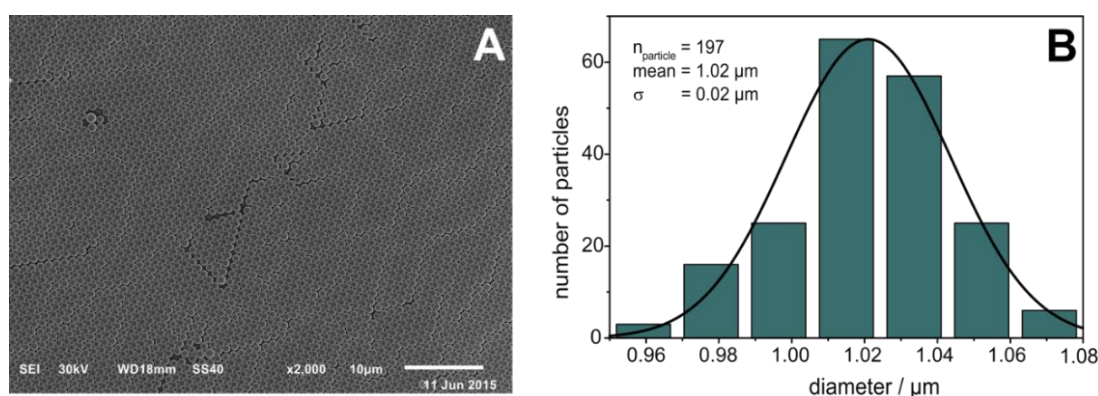
Figure 3.3 │ SEM image (A) of a densely packed monolayer of polystyrene particles with a diameter of 1.02 µm. Substrates were covered by ~45 nm Au with a ~3 nm Ti adhesion layer. Scale bar is 10 µm. (B) The respective particle size distribution fitted with a Gaussian function [M].

The diameter and periodicity of the nanoholes strongly influences he plasmonic excitation and the sensitivity [42]. With hole sizes smaller than the wavelength of incident light [M], a large variety of optical properties such as filtering of wavelength and enhanced transmission of light through the holes occurs [43]. Understanding the principles of the optical properties of the arrays with a hole diameter smaller than the wavelength of light [M] has been in the focus of research in the last years [44,45]. In one example, the influence of the nanohole diameter at a fixed periodicity on the transmission

spectra was investigated. With decreasing hole diameter the SPR wavelength shifts to shorter wavelengths and hence changes the optical properties [46]. Yet, much is still unknown and further understanding of the potential in sensing applications of substrates with both surface plasmon modes can be achieved by comparison of their analytical properties. Thus, different diameter-to-periodicity ratios (D/P) for a specific analytical application were studied, as the optimal plasmonic properties, *e.g.*, penetration depth of the plasmonic field and sensitivity depend on the excitation method [41].

In order to vary the D/P (Figure 3.4) of the nanostructured substrate, the spheres were changed in size without altering their position on top of the glass slide by plasma etching. The periodicity (*P*) is not affected by this process, as the particles remain at their initial positions [M]. Spheres were etched from 0.82 to 0.36 µm with a small standard deviation of a maximum of ±0.05 µm (particle-size distribution shown in Figure 3.5).
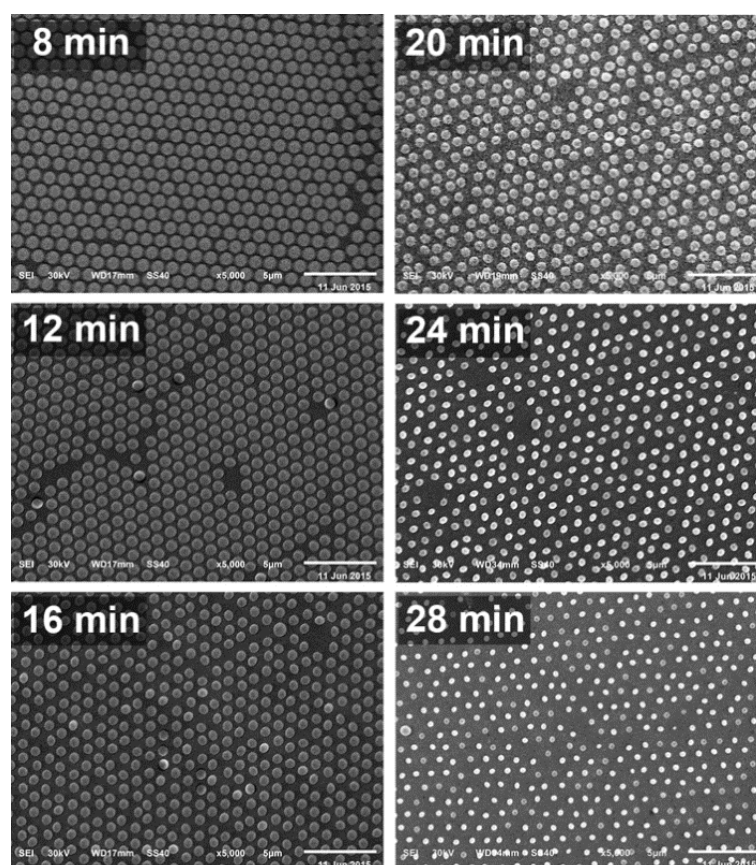
Figure 3.4│ SEM images of the sphere masks etched by oxygen plasma at 18 W with different times (8–28 min). A decrease in the diameter of the polystyrene particles with an increase of the etching time can be seen. The periodicity is not affected by the etching process as the spheres remain at their initial position. Substrates were covered by ~45 nm Au with a ~3 nm Ti adhesion layer after the etching process. All scale bars are 5 µm [M].
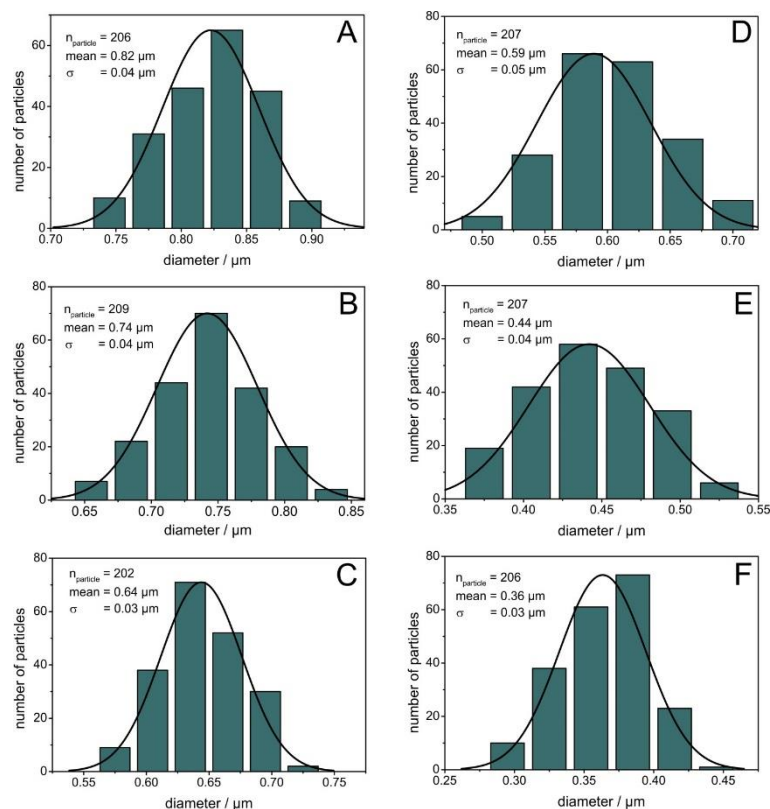
Figure 3.5│ The respective size distribution analysis of the particles is from the SEM images (compare Figure 3). A Gaussian function was used for fitting. Substrates were covered by ~45 nm Au with a ~3 nm Ti adhesion layer. A decrease in the diameter of the polystyrene particles with an increase of the etching time from 8 min (A) to 28 min (F) can be seen [M].

The hexagonal arrangement of the closed-packed monolayer is still visible after oxygen plasma treatment [M]. By varying the etching time, a linear relationship to the particle diameter was determined (Figure 3.6) [M]. Hence, desirable hole diameters and consequently desirable *D/P* can be fabricated easily by adjusting the etching time.

The sphere mask was then covered by a thin film of gold with a thickness of ~45 nm. This thickness is identically to commercial SPR slides with a continuous gold film and was chosen for providing optimal results in angle-dependent SPR devices using 650 nm excitation [47,48]. In a final step the substrates were sonicated in ethanol to remove the PS spheres [M]. Figure 3.7 shows an SEM image of a glass chip covered by the thin gold film structured as a nanohole array with a *D/P* ratio of 0.80, high regularity and sharp borders.
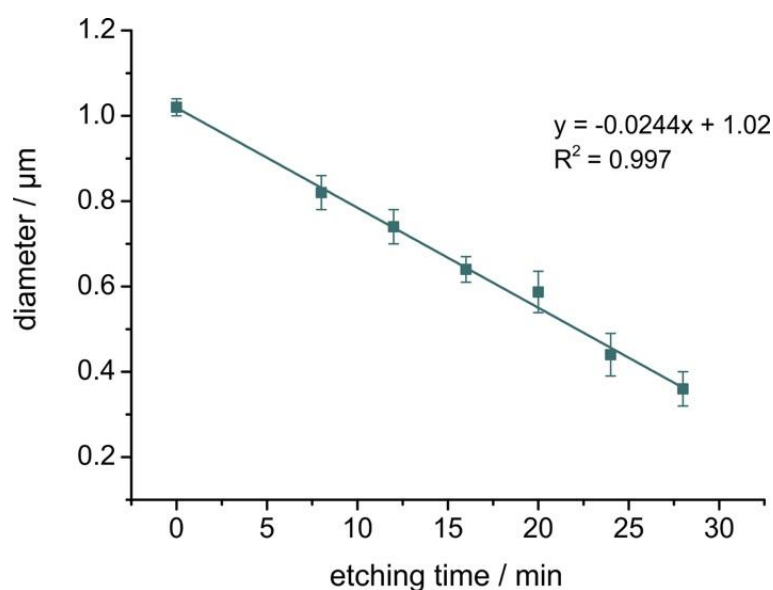
Figure 3.6│ Time dependence of the particle diameter reduction. Particles have a starting diameter of 1.02 µm. Etching is performed using reactive ion etching with oxygen plasma. Standard deviation is taken from the respective size distribution of the SEM image analysis [M].
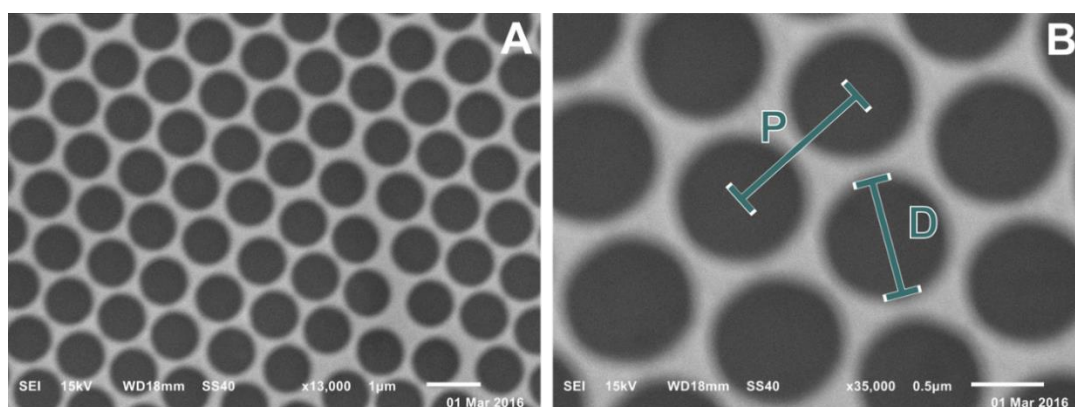
Figure 3.7│ SEM image of a nanohole array with a hole diameter of 0.82 ± 0.04 µm. Spheres were etched for 8 min. Substrates were covered by ~45 nm Au with a ~3 nm Ti adhesion layer. Particles were removed by sonication in ethanol. Scale bars are 1 µm (A) and 0.5 µm (B).

For the fabrication of the plasmon–graphene hybrids, the nanostructured substrates were functionalized with rGO via spin coating. The resulting two-dimensional graphene nanomaterial was characterized using Raman microscopy (Figure 3.8). Reduced graphene oxide is identified by the three distinct Raman bands at 1345 cm^{-1} (D-Peak), 1603 cm^{-1} (G-Peak), and 2682 cm^{-1} (2D-Peak) (Figure 5B) [49]. The presence of multilayers is indicated by the low intensity of the 2D-peak at 2690 cm^{-1} [50]. Raman maps showing the intensity of the D-, G- and the 2D-peaks over an area of 13 × 13 µm

demonstrate a full coverage of the nanohole array with rGO. Deviations in the Raman intensity can be ascribed to inhomogeneous multilayers, which is due to the spin coating process.
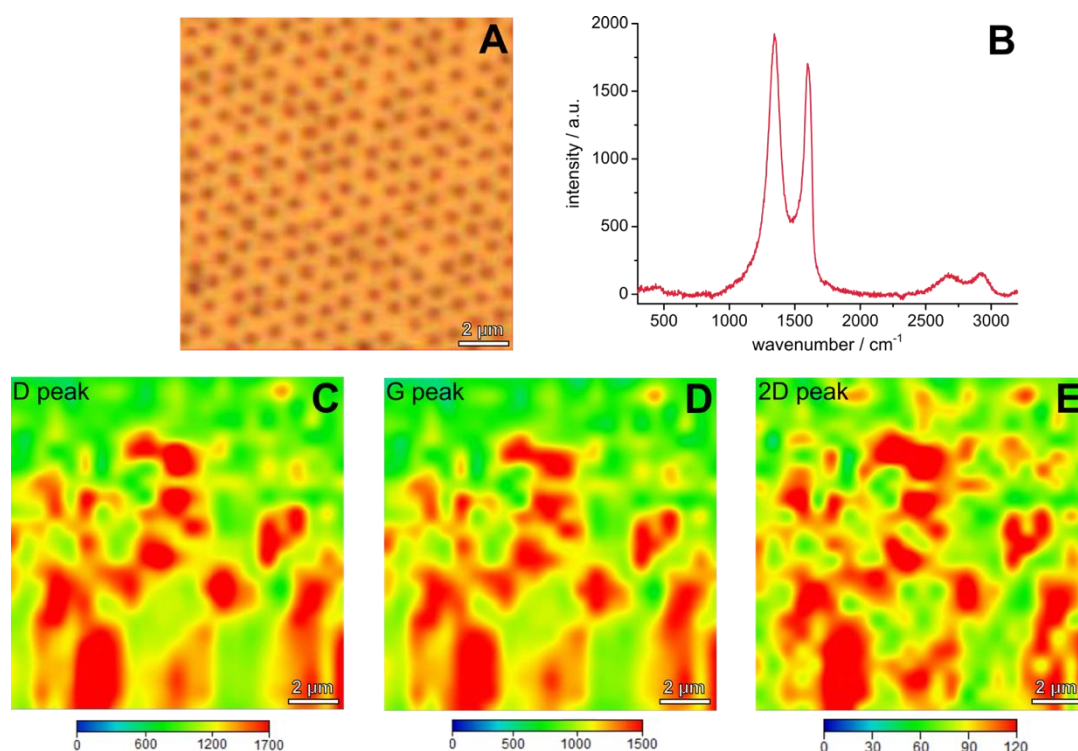
Figure 3.8 Microscopic image (A), exemplary Raman spectrum (B) and Raman maps (C–E) of the sensor slide consisting of rGO on a nanohole array with a *D/P* ratio of 0.43. The maps show the Raman intensity of the D-peak at 1345 cm^{-1} (C), the G-peak at 1603 cm^{-1} (D) and the 2D-peak at 2682 cm^{-1} (E) on the area shown in the microscopic image (A).

The presence of localized surface plasmons was demonstrated by analyzing the resonance curves before and after functionalization with rGO (Table 3.1) [M]. Normally, it is expected that a decrease of the amount of gold is accompanied by a decrease in the sensitivity. However, the results display a contrary trend, which in turn indicates the excitation of localized surface plasmons arising from the nanostructures on the substrate and interactions with the rGO [51]. In fact, it was found that, in general, all nanohole arrays regardless of their *D/P* ratios demonstrated a higher shift in the resonance angle of 250–380% compared to a continuous gold film. Somewhat surprisingly the improvement in surface sensitivity achieved for different *D/P* ratios of 0.35 to 0.58 is almost of the same order. The SPR response is affected by the presence of different plasmonic properties and accordingly strongly influenced by the dimensions of the nanostructures. Possible explanations for the findings are variations in the plasmonic

band structure, leading to different excitation wavelengths and penetration depths. It has been reported that the periodicity only slightly impacts the shape of curve for smaller *D/P* ratios (<0.5) and is similar (low values for the full width at half maximum (FWHM)) to a continuous gold film, whereas for larger *D/P* ratios (above 0.5) the curve is broadened [52]. Here, i.e., for wavelength-dependent SPR, the shape of the SPR curve was investigated as a function of the *D/P* ratio. It was found that nanohole arrays with *D/P* ratios of 0.35 and 0.43 display FWHM values of 3.5° and 4.0°, which are similar to that of a continuous gold film with 3.5°. Starting with a *D/P* ratio of 0.58 the FWHM is increasing (4.9°). For higher *D/P* ratio values from 0.63 to 0.80 high FWHM values of 5.9° to 6.4° are observed. As a less steep rise of the curve results in a lower sensitivity and as with decreasing *D/P* ratio a sharper curve and hence a higher sensitivity can be observed, the three *D/P* ratios of 0.58, 0.43 and 0.35 were chosen for additional studies.

Table 3.1│ Change in SPR resonance angle of nanohole arrays with different *D/P*-ratios compared to a continuous gold film. Each value represents the average value of three measurements. Errors indicate the standard deviation of these measurements [M].

	continuous film	D/P of nanohole array					
		0.80	0.73	0.63	0.58	0.43	0.35
$\Delta\theta_{SPR}$ / °	0.13 ± 0.08	0.5 ± 0.1	0.49 ± 0.03	0.6 ± 0.1	0.6 ± 0.2	0.5 ± 0.1	0.6 ± 0.2

To demonstrate the advantage of the plasmon–graphene hybrids within its sensing properties, the detection of diethyl phthalate as a plasticizer in water was investigated. The concentration-dependent signal change was studied with the best performing rGO-modified nanohole arrays, and compared to rGO-modified continuous gold films (Table 3.2). The binding of the analyte to rGO was studied by SPR measurements resulting in a saturation curve in good accordance to the Langmuir model (Equation 1):

$$\Delta s = \frac{c}{K + c} , \tag{1}$$

where Δs is the signal change, c is the DEP concentration and K represents the equilibrium dissociation constant.

Table 3.2│ Binding constants K_A for rGO-modified nanohole arrays with *D/P* ratios 0.58, 0.43 and 0.35 compared to a continuous rGO-modified gold film. Data were fitted with the Langmuir equation (Equation 1). Fitting parameters are shown in Table 3.3.

	continuous gold film	*D/P* of the nanohole array		
		0.35	0.43	0.58
K_A / $10^6 \cdot M^{-1}$	6 ± 1	5 ± 1	7 ± 0.9	5 ± 1

Table 3.3│ Fitting parameter for the interaction of DEP with rGO on various substrates. The Langmuir model was used.

substrate		*K* / µM	K_A / µM^{-1}	R^2
Continuous film		0.17 ± 0.03	6 ± 1	0.9693
Nanohole array with *D/P*	0.29	0.22 ± 0.05	5 ± 1	0.9149
	0.43	0.15 ± 0.02	7 ± 0.9	0.9847
	0.58	0.20 ± 0.04	5 ± 1	0.9585

All binding constants are almost identical, with the highest value for a *D/P* ratio of 0.43. This indicates a reproducible rGO layer deposition and no influence of the nanohole array structure on the interaction of DEP with rGO via π-stacking.

Based on these findings a nanohole array with a *D/P* ratio of 0.43 was applied as sensing substrate for the analysis of DEP in double distilled water. The signal change of this system with increasing DEP concentrations was determined and compared to a continuous gold film (Figure 3.9). For the nanohole array with a *D/P* of 0.43, saturation is almost reached at 5 µM (97% according to the Langmuir fit) and a roughly 12-fold enhancement of the maximum signal response compared to a continuous gold film is observed. Therefore, a 10-times better limit of detection (LOD) of ca. 20 nM is found when measuring with substrates with *D/P* = 0.43 compared to a continuous gold film (ca. 190 nM). The concentration covers the guideline values of the World Health Organization in fresh and drinking water for bis(2-ethylhexyl)phthalate (3–40 nM), the most widespread phthalate commonly used as reference for other phthalates [53,54]. The substrate provides therefore a very promising platform for detecting DEP in real water samples at low concentrations.
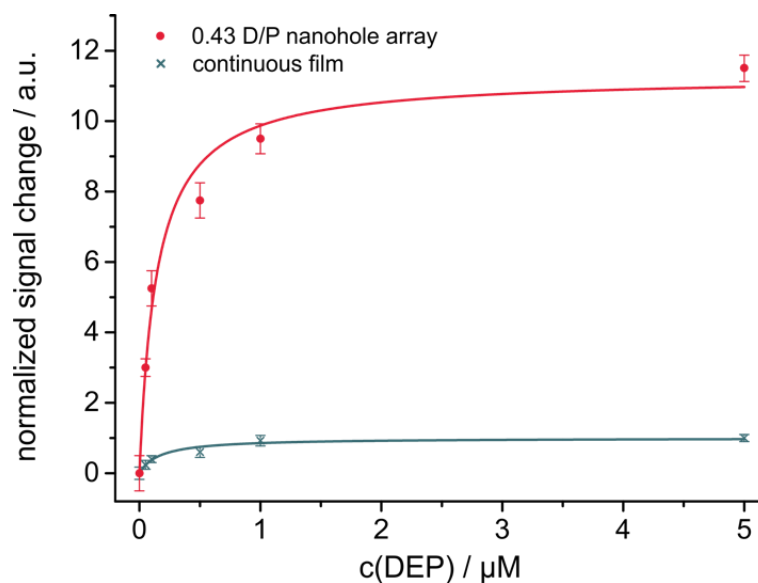
Figure 3.9 | Normalized signal change at a constant angle in response to binding of DEP to rGO-modified nanohole arrays (*D/P* = 0.43) covering a concentration range from 0.05 to 5 µM. For comparison the response of a continuous gold film modified with rGO is shown. Error bars indicate S/N. Data were fitted with the Langmuir equation (Equation 1).

The applicability of plasmon–graphene hybrids in commercial SPR devices measuring the angle dependence at a constant wavelength is demonstrated by the investigation of real water samples. For all real water samples higher signal changes were achieved when the nanohole arrays were functionalized with graphene shown exemplary with water from the river Danube (Figure 3.10A). By switching back to washing conditions, the original baseline was again obtained. That means that no specific binding between sample components and the graphene layer was formed. Thus, synergistic plasmonic effects caused by the interplay of the localized surface plasmons with the plasmonics of the overlaid carbon nanostructures lead to the significant signal enhancement. Secondly, when the water samples were spiked with the model analyte DEP, which will bind to graphene via π-stacking, the binding was stable even upon washing with the water sample without spiked DEP (Figure 3.10B). Extensive washing with double distilled water for several hours is needed to recover the sensor surface again (data not shown). Finally, two lake water (Lake Starnberg, Germany and Lake Garda, Italy), a sea water (Ionian Sea, Greece) and a river water (Danube, Germany) samples were spiked with 0.05 µM DEP. The obtained signal changes were compared to 0.05 µM DEP in double distilled water. In all cases this low concentration of the analyte was recovered with a satisfying

yield (Figure 3.10C). From these results one can conclude that SPR on nanohole array modified with rGO enables a label-free online system to monitor changes in concentrations of phthalates as an example for analytes with the ability of π-stacking. This clearly demonstrates the advantage of the interplay of the nanostructured gold layer with the carbon nanomaterial as neither rGO on continuous gold nor a nanohole array without rGO modification will lead to such sensitive signal changes.
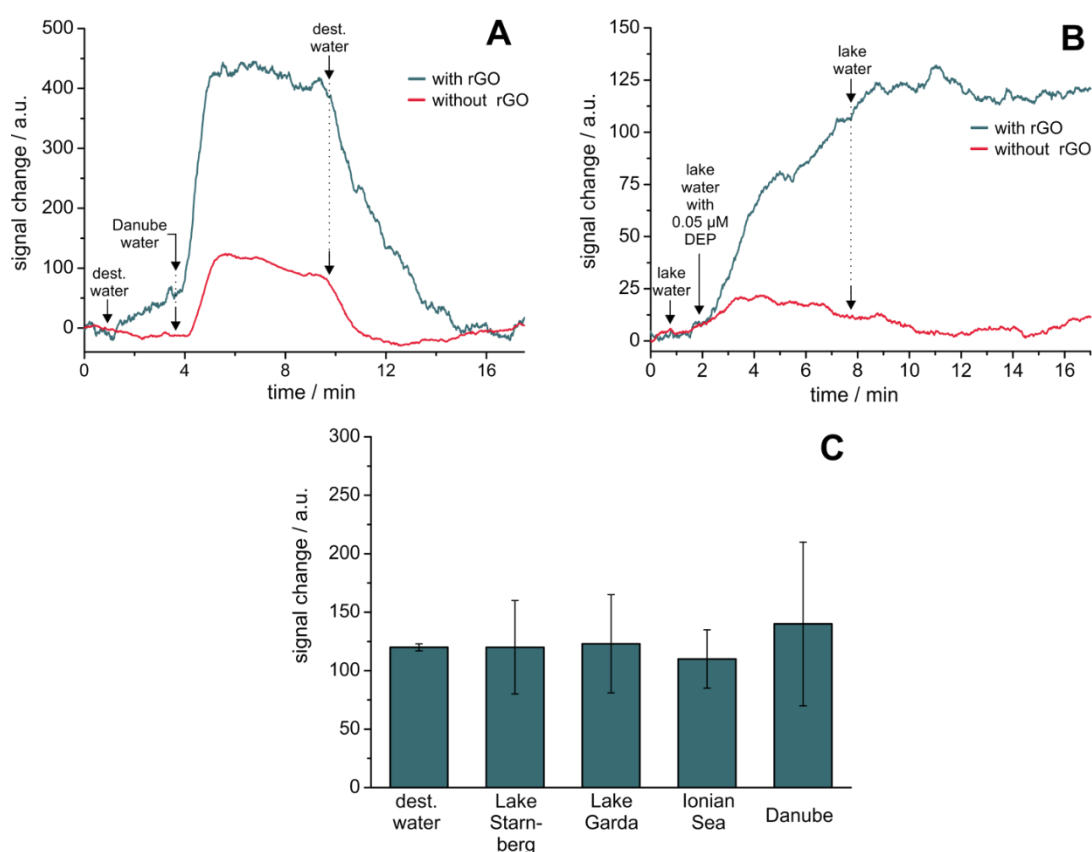
Figure 3.10 Exemplary signal traces at a constant angle for a nanohole array with D/P = 0.43 (A) with and without rGO receptor layers recorded for the addition of Danube water and recovery with the addition of distilled water, and (B) of Lake Starnberg water followed by the same water spiked with 0.05 µM DEP and subsequent washing with original Lake Starnberg water again. (C) Signal change for various water samples for a nanohole array (D/P = 0.43) with rGO. Samples were spiked with 0.05 µM DEP.

3.4 Conclusion

Nanosphere lithography was demonstrated to be a versatile technique for the fabrication of size-tailored nanohole arrays on a large scale for plasmonic enhancement in angular-dependent surface plasmon resonance with a constant wavelength setting. Plasmon–graphene hybrids were fabricated by spin-coating of the carbon nanomaterial on top of the substrates. This system was able to demonstrate a 10-fold lower limit of detection for small molecules than continuous gold films in a surface plasmon resonance affinity set-up. At the same time, very similar binding constants between the continuous gold film and various nanohole arrays emphasize that the nanostructured surface does not affect the interaction of DEP with rGO. The feasibility of the signal enhancement by localized plasmons was demonstrated for the detection of small molecules such as DEP in environmental water samples without pre-treatment. This enables the detection of even small molecules at low concentrations. Nevertheless, selectivity still needs to be improved. Specific receptors can be attached to the carbon nanomaterial or selective filters based on molecular imprinted polymer films can be applied. The combination of several semi-specific sensors to an artificial nose with chemometric analysis of a complex matrix will also offer a possible solution. Therefore, it is expected that hybrid materials consisting of nanostructured gold together with two-dimensional nanomaterials will be attractive in designing new sensor applications based on SPR transduction.

3.5 Experimental

3.5.1 Nanohole Array Fabrication

All substrates are based on glass slides (20×20 mm^2) of F1-Type with a refractive index of 1.61 (Mivitec GmbH, Sinzing, Germany). All glass slides were cleaned in piranha solution for 90 min and in a mixture of water, ammonia and hydrogen peroxide at a 5:1:1 (v/v/v) ratio for 60 min in an ultrasonication bath [M]. Between treatments the glass slides were rinsed with water and sonicated three times in water for 15 min. Each time the water was exchanged [M].

The fabrication of nanohole arrays consists of several steps [39,40, M]. First a sphere mask of a hexagonal, closed packed, two dimensional crystal of polymer particles needs to be formed [M] via self-assembly by a slow evaporation process. Subsequent etching of the particles [M] creates a void between neighboring particles, generating a non-close

packed ordered sphere monolayer. The obtained sphere mask acts as a pattern during gold deposition [M]. Varying the etching time results in different diameters of the spheres and respectively holes. Lift-off of the sphere mask is achieved by sonication in ethanol [M].

The sphere mask is gained by drop-coating of 40 µL of a water/ethanol solution 87:13 (v/v) containing 13 mg·mL^{-1} polystyrene particles on a clean and dry glass slide. The polystyrene particles have a diameter of 1.04 µm (SD = 0.04 µm, microparticles GmbH) [M]. Covering with a Petri dish allows a slow evaporation rate, resulting in a close-packed monolayer. The sphere masks were dried overnight. In order to create a nanohole array the diameter of the spheres need to be etched by reactive ion etching using oxygen plasma (Plasmalab 80 Plus, Oxford Instruments, Abingdon, United Kingdom) prior to metallization [M]. Different diameters of the polystyrene spheres were achieved by varying the etching time from 8 to 28 min at 18 W. On the etched sphere mask a thin layer of ca. 3 nm Ti was deposited before Au deposition (ca. 45 nm) [M]. The resulting arrays were analyzed using SEM. Finally, the PS spheres were removed from the surface by sonication in ethanol for 2 min [M].

3.5.2 Reduced Graphene Oxide

The rGO was synthesized starting from graphite following a modified Hummers method and a subsequent chemical reduction [55]. To cover the substrates with a uniform layer of reduced graphene oxide 200 µL of a 0.25 µg·mL^{-1} solution containing 1:1 (v/v) water and isopropanol was deposited in the middle on the surface and allowed to settle for 5 min [M]. The solvent with excess on graphene was removed by spin coating (Laurell Spin Coater WS-400-6NPP-LITE; Laurell Technologies Corporation, North Wales, Pennsylvania, USA) at 1000 rpm for 11 min and 2500 rpm for 1 min. After treatment the slides were rinsed with ethanol and dried with N_2 [M].

3.5.3 Surface Plasmon Resonance Spectroscopy

The SPR analysis was performed with a BioSuplar SPR instrument (Mivitec GmbH, Sinzing, Germany) using a F1-65 glass prism installed on a swivel carriage. The substrate is placed on the top face with index-matching fluid between the chip and the prism [M]. A flow cell with two channels is placed on the chip and samples were passed through the cell. The device operates with a laser illumination at 650 nm [M]. The bulk

sensitivity to refractive index (intensity per refractive index units (RIU)) was measured with aqueous sucrose solutions (1–8% w/w) covering a range of 1.33–1.35 RIU. For measurements the change in intensity of reflected light at a fixed angle was monitored [M]. SPR slides covered with a continuous gold film of 45 nm thickness were obtained from Mivitec GmbH [M]. Four environment water samples were taken from Lake Starnberg (Starnberg, Germany), Ionian Sea (Laganas, Greek), Lake Garda (Limone sul Garda, Italy) and River Danube (Regensburg, Germany) in sealed glass bottles and stored in the dark until measurement. No sample pre-treatment was applied. Interaction of the respective DEP solution was allowed for 6 min. To remove unbound DEP and ensure an adsorption-based signal change on the sensor surface, a 10 min washing step was performed after each DEP solution analysis.

3.5.4 Raman Microscopy Measurements

Raman microscopy measurements (DXR Raman microscope, Thermo Fisher Scientific GmbH, Dreieich, Germany) were performed at 532 nm laser excitation (10 mW) and with a 50 μm slit [M]. The spectra were acquired [M] for 1 s and averaged over ten measurements. The microscopic image and the Raman maps were taken at 100 times magnification with a MPlan N objective (100×/0.90 BD, Olympus SE & Co. KG, Hamburg, Germany).

Acknowledgements

3.6 References

[1]   Mousa A, Basheer C, Rahman Al-Arfaj A (2013) Determination of phthalate esters in bottled water using dispersive liquid-liquid microextraction coupled with GC-MS. J Sep Science 36:2003–2009.

[2]   Wu X, Hong H, Liu X, Guan W, Meng L, Ye Y, Ma Y (2013) Graphene-dispersive solid-phase extraction of phthalate acid esters from environmental water. Sci Total Environ 444:224–230.

[3]   Abdel daiem MM, Rivera-Utrilla J, Ocampo-Pérez R, Méndez-Díaz JD, Sánchez-Polo M (2012) Environmental impact of phthalic acid esters and their removal from water and sediments by different technologies—a review. J Environ Manage 109:164–178.

[4]   Liang P, Xu J, Li Q (2008) Application of dispersive liquid-liquid microextraction and high-performance liquid chromatography for the determination of three phthalate esters in water samples. Anal Chim Acta 609:53–58.

[5]   Cinelli G, Avino P, Notardonato I, Centola A, Russo MV (2013) Rapid analysis of six phthalate esters in wine by ultrasound-vortex-assisted dispersive liquid-liquid micro-extraction coupled with gas chromatography-flame ionization detector or gas chromatography-ion trap mass spectrometry. Anal Chim Acta 769:72–78.

[6]   Li N, Wang D, Zhou Y, Ma M, Li J, Wang Z (2010) Dibutyl phthalate contributes to the thyroid receptor antagonistic activity in drinking water processes. Environ Sci Technol 44:6863–6868.

[7]   Ye Q, Liu L, Chen Z, Hong L (2014) Analysis of phthalate acid esters in environmental water by magnetic graphene solid phase extraction coupled with gas chromatography-mass spectrometry. J Chromatogr A 1329:24–29.

[8]   Homola J (2008) Surface plasmon resonance sensors for detection of chemical and biological species. Chem Rev 108:462–493.

[9] Kabashin AV, Evans P, Pastkovsky S, Hendren W, Wurtz GA, Atkinson R, Pollard R, Podolskiy VA, Zayats AV (2009) Plasmonic nanorod metamaterials for biosensing. Nat Mater 8:867–871.

[10] Fenzl C, Hirsch T, Baeumner AJ (2016) Nanomaterials as versatile tools for signal amplification in (bio)analytical applications. Trends Analyt Chem 79:306–316.

[11] Fenzl C, Genslein C, Domonkos C, Edwards K, Hirsch T, Baeumner AJ (2016) Investigating non-specific binding to chemically engineered sensor surfaces using liposomes as models. Analyst 141:5265-5273.

[12] Shahjamali MM, Bosman M, Cao S, Huang X, Saadat S, Martinsson E, Aili D, Tay YY, Liedberg B, Loo SCJ, Zhang H, Boey F, Xue C (2012) Gold Coating of Silver Nanoprisms. Adv Funct Mater 22:849–854.

[13] Brolo AG (2012) Plasmonics for future biosensors. Nat Photonics 6:709–713.

[14] Tudos AJ, Schasfoort RBM (eds) (2008) Handbook of surface plasmon resonance. Cambridge: Royal Society of Chemistry 21:403.

[15] Willets KA, van Duyne RP (2007) Localized surface plasmon resonance spectroscopy and sensing. Annu Rev Phys Chem 58:267–297.

[16] Mayer KM, Hafner JH (2011) Localized surface plasmon resonance sensors. Chem Rev 111:3828–3857.

[17] Couture M, Zhao SS, Masson J (2013) Modern surface plasmon resonance for bioanalytics and biophysics. Phys Chem Chem Phys 15:11190–11216.

[18] Escobedo C (2013) On-chip nanohole array based sensing: a review. Lab chip 13:2445–2463.

[19] He L, Musick MD, Nicewarner SR, Salinas FG, Benkovic SJ, Natan MJ, Keating CD (2000) Colloidal Au-Enhanced Surface Plasmon Resonance for Ultrasensitive Detection of DNA Hybridization. J Am Chem Soc 122:9071–9077.

[20] Zhang J, Wang Y, Wong TI, Liu X, Zhou X, Liedberg B (2015) Electrofocusing-enhanced localized surface plasmon resonance biosensors. Nanoscale 7:17244–17248.

[21] Kelf TA, Sugawara Y, Cole RM, Baumberg JJ, Abdelsalam ME, Cintra S, Mahajan S, Russell AE, Bartlett PN (2006) Localized and delocalized plasmons in metallic nanovoids. Phys Rev B 74: 245415.

[22] Couture M, Ray KK, Poirier-Richard H, Crofton A, Masson J (2016) 96-Well Plasmonic Sensing with Nanohole Arrays. ACS Sens 1:287–294.

[23] Hideki M, Fukuda K (1995) Ordered metal nanohole arrays made by a two-step replication of honeycomb structures of anodic alumina. Science 268:1466-1468.

[24] Lesuffleur A, Im H, Lindquist NC, Oha S (2007) Periodic nanohole arrays with shape-enhanced plasmon resonance as real-time biosensors. Appl Phys Lett 90:243110.

[25] Whitney AV, Myers BD, van Duyne RP (2004) Sub-100 nm Triangular Nanopores Fabricated with the Reactive Ion Etching Variant of Nanosphere Lithography and Angle-Resolved Nanosphere Lithography. Nano Lett 4:1507–1511.

[26] Dintinger J, Robel I, Kamat PV, Genet C, Ebbesen TW (2006) Terahertz All-Optical Molecule- Plasmon Modulation. Adv Mater 18:1645–1648.

[27] Henzie J, Barton JE, Stender CL, Odom TW (2006) Large-area nanoscale patterning: chemistry meets fabrication. Acc Chem Res 39:249–257.

[28] Ji J, O'Connell JG, Carter DJD, Larson DN (2008) High-throughput nanohole array based system to monitor multiple binding events in real time. Anal Chem 80:2491–2498.

[29] Kim JH, Moyer PJ (2007) Laser-induced fluorescence within subwavelength metallic arrays of nanoholes indicating minimal dependence on hole periodicity. Appl Phys Lett 90:131111.

[30] Stewart ME, Anderton CR, Thompson LB, Maria J, Gray SK, Rogers JA, Nuzzo RG (2008) Nanostructured plasmonic sensors. Chem Rev 108:494–521.

[31] Huang C, Forste A, Walheim S, Schimmel T (2015) Polymer blend lithography for metal films: large-area patterning with over 1 billion holes/inch^2. Beilstein J Nanotechnol 6:1205–1211.

[32] Masson J, Murray-Methot M, Live LS (2010) Nanohole arrays in chemical analysis: manufacturing methods and applications. Analyst 135:1483–1489.

[33] Colson P, Henrist C, Cloots R (2013) Nanosphere Lithography: A Powerful Method for the Controlled Manufacturing of Nanomaterials. J Nanomater 2013:1–19.

[34] Correia-Ledo D, Gibson KF, Dhawan A, Couture M, Vo-Dinh T, Graham D, Masson J (2012) Assessing the Location of Surface Plasmons Over Nanotriangle and Nanohole Arrays of Different Size and Periodicity. Phys Chem C Nanomater Interfaces 116:6884–6892.

[35] Geim AK, Novoselov KS (2007) The rise of graphene. Nat Mat 6:183–191.

[36] Liu Y, Cheng R, Liao L, Zhou H, Bai J, Liu G, Liu L, Huang Y, Duan X (2011) Plasmon resonance enhanced multicolour photodetection by graphene. Nat Commun 2:579.

[37] Thackray BD, Thomas PA, Auton GH, Rodriguez FJ, Marshall OP, Kravets VG, Grigorenko AN (2015) Super-narrow, extremely high quality collective plasmon resonances at telecom wavelengths and their application in a hybrid graphene-plasmonic modulator. Nano Let 15:3519–3523.

[38] Zhang W, Xu Z, Pan B, Hong C, Jia K, Jiang P, Zhang Q, Pan B (2008) Equilibrium and heat of adsorption of diethyl phthalate on heterogeneous adsorbents. J Colloid Interface Sci 325:41–47.

[39] Couture M, Live LS, Dhawan A, Masson J (2012) EOT or Kretschmann configuration? Comparative study of the plasmonic modes in gold nanohole arrays. Analyst 137:4162–4170.

[40] Couture M, Liang Y, Poirier Richard H, Faid R, Peng W, Masson J (2013) Tuning the 3D plasmon field of nanohole arrays. Nanoscale 5:12399–12408.

[41] Genet C, Ebbesen TW (2007) Light in tiny holes. Nature 445:39–46.

[42] Kegel LL, Boyne D, Booksh KS (2014) Sensing with prism-based near-infrared surface plasmon resonance spectroscopy on nanohole array platforms. Anal Chem 86:3355–3364.

[43] Parsons J, Hendry E, Burrows CP, Auguié B, Sambles JR, Barnes WL (2009) Localized surface-plasmon resonances in periodic nondiffracting metallic nanoparticle and nanohole arrays. Phys Rev B 79: 073412.

[44] Lee K, Wang W, Wei P (2008) Comparisons of Surface Plasmon Sensitivities in Periodic Gold Nanostructures. Plasmonics 3:119–125.

[45] Ekgasit S, Thammacharoen C, Yu F, Knoll W (2005) Influence of the Metal Film Thickness on the Sensitivity of Surface Plasmon Resonance Biosensors. Appl Spectrosc 59:661–667.

[46] Homola J, Sinclair YS, Gauglitz G (1999) Surface plasmon resonance sensors: review. Sens Actuators B Chem 54:3–15.

[47] Ferrari AC, Meyer JC, Scardaci V, Casiraghi C, Lazzeri M, Mauri F, Piscanec S, Jiang D, Novoselov KS, Roth S, Geim AK (2006) Raman spectrum of graphene and graphene layers. Phys Rev Lett 97:187401.

[48] Backes C, Paton KR, Hanlon D, Yuan S, Katsnelson MI, Houston J, Smith RJ, McCloskey D, Donegan JF, Coleman JN (2016) Spectroscopic metrics allow in situ measurement of mean size and thickness of liquid-exfoliated few-layer graphene nanosheets. Nanoscale 8:4311–4323.

[49] Wu L, Chu HS, Koh WS, Li EP (2010) Highly sensitive graphene biosensors based on surface plasmon resonance. Opt Express 18:14395–14400.

[50] Live LS, Bolduc OR, Masson J (2010) Propagating surface plasmon resonance on microhole arrays. Anal Chem 82:3780–3787.

[51] Serodio P, Nogueira JMF (2006) Considerations on ultra-trace analysis of phthalates in drinking water. Water Res 40:2572–2582.

[52] Polo M, Llompart M, Garcia-Jares C, Cela R (2005) Multivariate optimization of a solid-phase microextraction method for the analysis of phthalate esters in environmental waters. J Chromatogr A 1072:63–72.

[53] Live LS, Masson J (2009) High Sensitivity of Plasmonic Microstructures near the Transition from Short-Range to Propagating Surface Plasmon. J Phys Chem C 113:10052–10060.

[54] Murray-Methot M, Menegazzo N, Masson J (2008) Analytical and physical optimization of nanohole-array sensors prepared by modified nanosphere lithography. Analyst 133:1714–1721.

[55] Zoepfl A, Lemberger M, Konig M, Ruhl G, Matysik F, Hirsch T (2014) Reduced graphene oxide and graphene composite materials for improved gas sensing at low temperature. Faraday Discuss 173:403–414.

Detection of small molecules with surface plasmon resonance by synergistic
plasmonic effects of nanostructured surfaces and graphene

64

4 Detection of Small Molecules with Surface Plasmon Resonance by Synergistic Plasmonic Effects of Nanostructured Surfaces and Graphene

4.1 Abstract

Surface plasmon resonance depends on the dielectric medium at the vicinity and makes it a quasi-universal detector. Therefore, and due to the label-free nature, SPR is a widely used sensing tool for real-time monitoring molecular interactions of various analytes. However, detection of highly diluted analytes and small molecules (< 400 Da) is still challenging. Gold nanohole arrays provide plasmonic hotspots with improved surface sensitivity and 2D carbon nanomaterials enable binding near the surface. Both effects together are promising in the development of SPR sensors for the efficient determination of small molecules. Graphene is known for efficient binding of molecules with delocalized aromatic π-systems. Additionally, the electromagnetic field is locally enhanced and modulated by the interaction of graphene photonics with the plasmonics of metal nanostructures. The advantages of chemical vapor deposition (CVD) graphene over reduced graphene oxide (rGO) is illustrated by a proof of concept study. In comparison to substrates consisting of a continuous film the surface sensitivity is enhanced for a nanohole arrays and further improved for CVD graphene functionalization in contrast to rGO. The feasibility of the sensor was demonstrated for the detection of adenine down to a concentration of 0.9 µM.

Detection of small molecules with surface plasmon resonance by synergistic plasmonic effects of nanostructured surfaces and graphene

65

Author contributions

Most of the experimental work was carried out by CG. PH and CG performed the RIE and the SEM analysis. EMK synthesized the graphene oxide. CG wrote the manuscript. The article was revised by CG, PH, EMK, RB, AJB and TH. TH is corresponding author.

Detection of small molecules with surface plasmon resonance by synergistic
plasmonic effects of nanostructured surfaces and graphene

66

4.2 Introduction

Surface plasmon resonance (SPR) is a well-established technique for analysis of biomolecular interactions of larger molecules, *e.g.* proteins, providing benefits like label-free real-time monitoring of binding events based on refractive index changes. However, the detection of small molecules is still challenging, due to the limited sensitivity [1,2]. Approaches based on nanostructures, such as nanohole arrays, with a field depth confined close to the surface can improve the sensitivity and amplify the signal [3]. Nanohole arrays offer great promise for various applications, due to the modulation of the plasmonic properties by changing the dimensions and periodicity of the nanostructures. Such variations affect the penetration depth of the evanescent field [4]. Consequential enhanced surface sensitivity of nanohole structured thin metallic films within bioanalytical detection has been reported. [5]

Recently, graphene, as the most prominent 2D-material, has gained interest in the use as receptor layer for sensing systems. A high surface-to-volume ratio, interaction of molecules via π-stacking, possible chemical modifications and the presence of intrinsic surface plasmons will boost the performance of surface plasmon resonance sensors [6,7]. Graphene can be derived by many ways from top-down exfoliation techniques starting from graphite or by bottom-up methods like chemical vapor deposition (CVD) on metal substrates [8]. The physical and chemical properties of the resulting 2D carbon nanomaterial differ a lot as one will obtain materials of different flake size and different number of layers [9]. Furthermore, all methods will introduce defects or impurities during the fabrication process. Due to the simple and inexpensive synthesis starting from graphite, reduced graphene oxide (rGO) is often used in development and in large scale applications of graphene based devices. It is described as graphene-like sheets with a certain number of defects, resulting from the remaining oxygen-containing groups [10]. CVD graphene is a high-quality monolayer readily accessible for the transfer on a receiver substrate [11]. In this study reduced graphene oxide, fabricated by chemical exfoliation as a top-down approach was compared to graphene obtained from a CVD process on a copper substrate. Raman microscopy can be utilized for characterization of different graphene types and the homogeneity of the transfer method based on representative peaks. The feasibility of nanohole arrays with rGO for the detection of small molecules like plasticizers has been reported, recently [12]. Enhanced sensitivity of graphene-modified nanohole arrays in the detection of the nucleobase adenine, a building block of DNA and a model for small molecules, is demonstrated.

Detection of small molecules with surface plasmon resonance by synergistic plasmonic effects of nanostructured surfaces and graphene

67

4.3 Results and Discussion

Nanohole arrays are fabricated by a modified nanosphere lithography. In a first step a hexagonal closed packed monolayer of monodisperse polystyrene particles is assembled on a glass slide. The particles are etched by plasma treatment to diameters of the desired hole size. Deposition of gold, followed by sonication to remove the particles, creates structures described by a periodic arrangement of nanoholes [4]. For characterization of nanohole arrays and their plasmonic properties the diameter to periodicity ratio (D/P), described by the size of the holes and the distance between the center of two holes, is the most important parameter. The plasmonic properties, which strongly influence the sensitivity and penetration depth of the plasmonic field, depend on the application and need to be optimized. Hole diameters smaller than the excitation wavelength have been reported to enhance the surface sensitivity and applied within (bio)analytical sensing [13]. From former studies the best enhancement in the surface sensitivity was determined for D/P ratios from 0.6 to 0.35 [12]. Therefore, a nanohole array with a 0.35 D/P ratio was used as sensing substrate. Here, a hole diameter of 0.37 μm and a periodicity of 1.04 μm was chosen (Figure 4.1). Regular periodic areas of nanohole arrays of several square millimeter in size are obtained. This is important as the area of interest which is investigated by the laser spot of most commercial available SPR devices covers the same range.
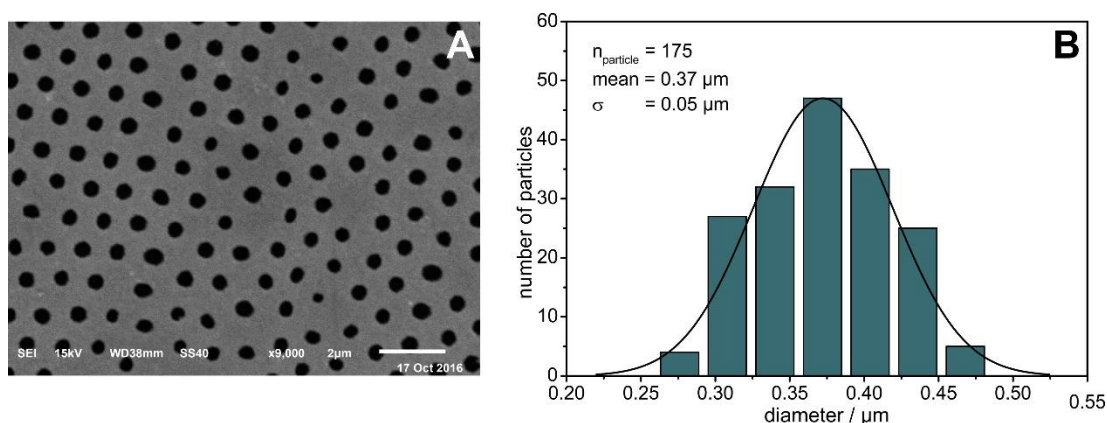
Figure 4.1│ (A) SEM images of a nanohole array with 0.35 D/P ratio. Polystyrene particles had a starting diameter of 1.04 μm and were etched by oxygen plasma at 18 W for 28 min. The periodicity is not affected by the etching process as the spheres remain at their initial position. Substrates were covered by ~45 nm Au with a ~3 nm Ti adhesion layer after the etching process. Scale bar is 2 μm. (B) The respective size distribution histogram of the hole diameter obtained from SEM images describes a Gaussian profile which can be seen by the fitting.

Detection of small molecules with surface plasmon resonance by synergistic plasmonic effects of nanostructured surfaces and graphene

68

By spin-coating of an aqueous dispersions of rGO substrates are modified with a thin film of the 2D carbon nanomaterial. However, it is difficult to apply a defined number of layers over large areas with good reproducibility. A controllable modification method of a homogenous film is important for the plasmonic enhancement. Therefore, CVD graphene is an alternative approach for functionalization. It contains less structural defects and the number of graphene layers can be controlled [6]. The functionalized substrates were analyzed using Raman microscopy (Figure 4.2).
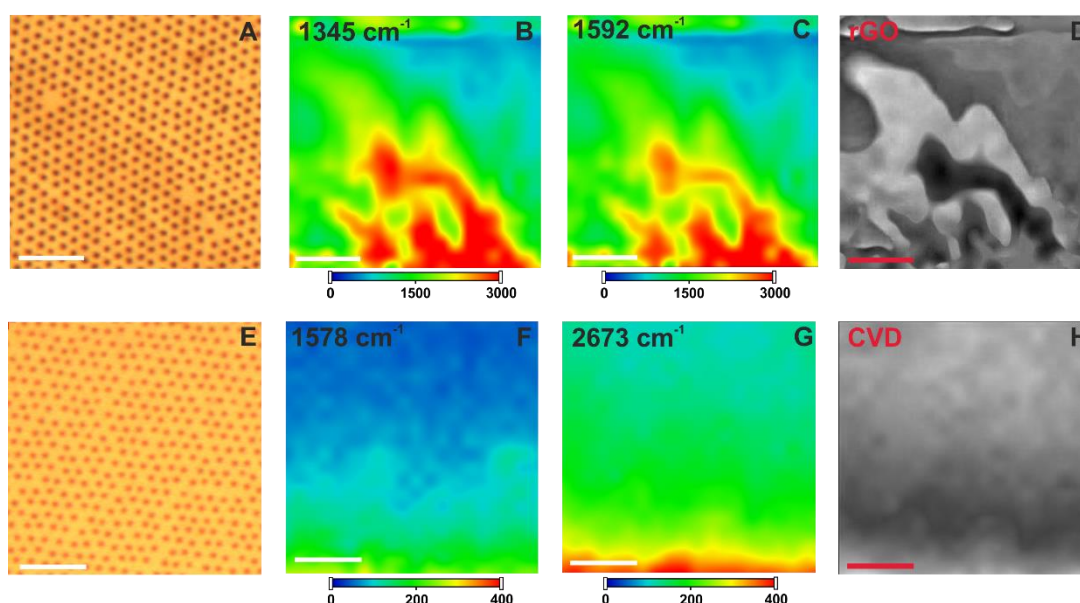
Figure 4.2│ Microscopic image of a nanohole array with a D/P ratio of 0.35 modified with rGO (A) and CVD graphene (E). The upper maps show the Raman intensity of the D-peak at 1345 cm^{-1} (B) and the G-peak at 1592 cm^{-1} (C) on the area shown in the microscopic image (A) and the lower maps show the Raman intensity of the G-peak at 1578 cm^{-1}(F) and the 2D-peak at 2673 cm^{-1} (G) on the area shown in the microscopic image (E). Scale bars are 5 µm. Image (D) represents the division of two maps with the same intensity scale of the D- and G Peak from rGO and the image (H) results from the division of two maps with the same intensity scale of the 2D- and G Peak from CVD graphene. Maps were recorded on the respective microscopic images.

In general, the peak intensities are significantly higher for rGO and reflect larger fluctuations compared to CVD graphene (Figure 4.2 B, C, F and G). Drifts in the intensities over the large area can be attributed to a drift the in focal plane due to extreme long measurement times or chamfer and unevenness of the glass slide. For rGO the I_D/I_G ratio and for CVD graphene the I_{2D}/I_G ratio should be constant, if a homogenous layer is present. By division of the color information of two intensity maps of characteristic peaks, an image is generated presenting qualitative information of the film homogeneity. A

Detection of small molecules with surface plasmon resonance by synergistic plasmonic effects of nanostructured surfaces and graphene

69

continuous color of the resulting images indicates a constant ratio and hence no variations in the layer thickness or number of defects. Intense fluctuations and sharp edges in the colors for the rGO image (Figure 4.2 D), can be ascribed to the formation of multilayers with stacks. A more homogenous layer with a low number of layers of CVD graphene is indicated by minor and smooth changes in the color intensity (Figure 4.2 H).

The plasmonic enhancement of nanohole arrays functionalized with graphene is demonstrated by Raman spectra of graphene measured on a continuous film and a nanohole array with 0.35 D/P ratio (Figure 4.3). Higher peak intensities (~3-times for CVD graphene and ~12-times for rGO) are found on a nanohole arrays compared to a continuous film. The difference in the enhancement of rGO and CVD is attributed to different modification methods. Spin-coating of rGO yields areas with multilayer and larger variations, whereas wet transfer of CVD graphene results in a more homogenous film and monolayers.
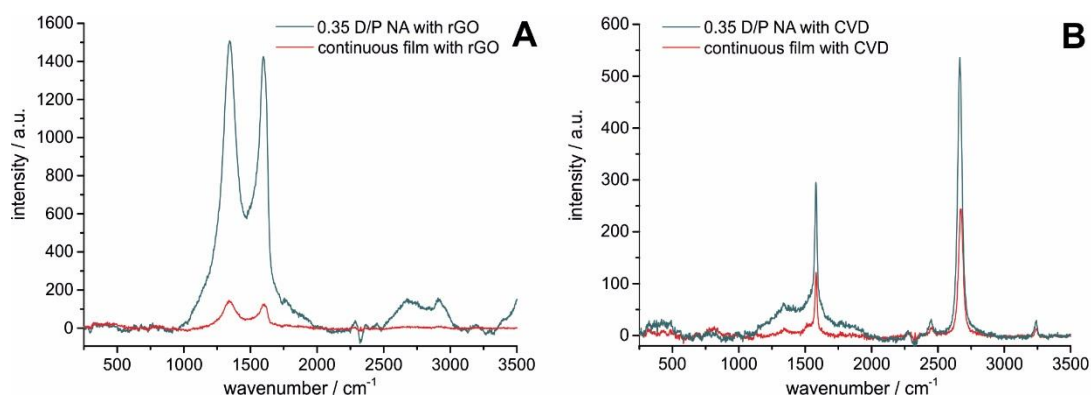
Figure 4.3 Raman spectrum of rGO (A) and CVD graphene (B), averages over 10 measurement spots, taken on a continuous gold film and a nanohole array of 0.35 D/P ratio. All experimental settings for acquiring the spectra were kept constant.

Different graphene types are characterized by analyzing the significant peak intensities of the Raman spectrum. The ratio of the D-Peak (~1350 cm^{-1}) to G-Peak (~1585 cm^{-1}), referred to as I_D/I_G, provides information about the flake size and the presence of defects. The D-Peak results mainly form graphene edges and is not present in monolayer graphene. Shape and intensity of the 2D-Peak (~2700 cm^{-1}) changes with the number of layers and appears as a single narrow peak for monolayer graphene with around double the intensity of the G-Peak [9,14]. The I_D/I_G ratio was found to be 0.21 ± 0.05 and 1.05 ± 0.04 for CVD graphene and rGO, respectively. In comparison, the intensity of the 2D-peak and the G-peak (I_{2D}/I_G) was determined as 1.8 ± 0.1 for CVD and 0.11 ± 0.01 for rGO (Figure 4.3 A and B). Results indicate the successful transfer of CVD graphene onto

Detection of small molecules with surface plasmon resonance by synergistic plasmonic effects of nanostructured surfaces and graphene

70

the substrates, due to the presence of a small single 2D-peak with around double the intensity of the G-peak and a I_D/I_G ratio in the range of 0.05 to 0.3, which is typical for CVD-derived monolayer samples [15]. Spectra of rGO show the typical features: broad peaks and most importantly a I_D/I_G ratio slightly higher than 1 [16].

Surface sensitivity was analyzed by the change in the SPR resonance angle before and after the modification with graphene (Table 4.1). The presence of localized surface plasmons of the nanoholes is indicated by a higher shift in the resonance angle compared to a continuous film and hence results in an enhancement in the surface sensitivity. For functionalization of a continuous gold film a 440% increase in angular change was observed for CVD graphene compared to rGO. An improvement of the surface sensitivity for a nanohole array with a 0.35 D/P ratio as receiver substrate is displayed by an 80% higher shift in the resonance angle.

Table 4.1 | Change in SPR resonance angle and the bulk sensitivity of graphene modified nanohole arrays with a D/P-ratio of 0.35 D/P compared to a continuous gold films. Each value represents the average of three measurements. Errors indicate the standard deviation of these measurements. (*Values were taken from Genslein *et al.* [12]

	surface sensitivity $\Delta\theta_{SPR}$ / deg		bulk sensitivity $\Delta RU/\Delta RIU \cdot 10^4$	
	continuous film	NA with 0.35 D/P	continuous film	NA with 0.35 D/P
rGO	0.13 ± 0.08*	0.6 ± 0.2*	12.8 ± 0.2	5.7 ± 0.1
CVD graphene	0.7 ± 0.1	1.1 ± 0.1	11.2 ± 0.09	4.6 ± 0.02

A simulation of the SPR response for the modification with CVD with the experiment parameters revealed an angle change of 0.47 for a monolayer of graphene and 0.94 for a bilayer [17,18]. The determined value for a continuous film is around the average of both, implying the presence of mono- and bilayers. An increase in the surface sensitivity for a nanohole array modified with CVD compared to a continuous film is assigned to the presence of localized surface plasmons. Accompanying with the higher surface sensitivity, a lower bulk sensitivity (change in refractive intensity (RU) per refractive index units (RIU)) for nanohole arrays is found, which supports the assumption of a localized plasmonic effect. Propagation surface plasmons are characterized by a longer decay length of the plasmonic field and hence a higher bulk sensitivity. Lower bulk sensitivity

Detection of small molecules with surface plasmon resonance by synergistic
plasmonic effects of nanostructured surfaces and graphene

71

arises from a shorter penetration depth as an effect of localized surface plasmons. Intrinsic surface plasmons of graphene are alerted by the number of layers or doping [7]. Differences in the interaction of the both graphene types with the nanohole arrays result in variations in the enhanced electromagnetic field at the nanostructures, due to the different plasmonic properties of CVD and rGO.

The capabilities of nanohole arrays modified with graphene within specific sensing applications is illustrated in Figure 4.4 presenting the SPR signal changes of the graphene modified nanohole substrates upon binding of adenine. The concentration-depended signal change was determined with the Kretchmann configuration at a constant angle.
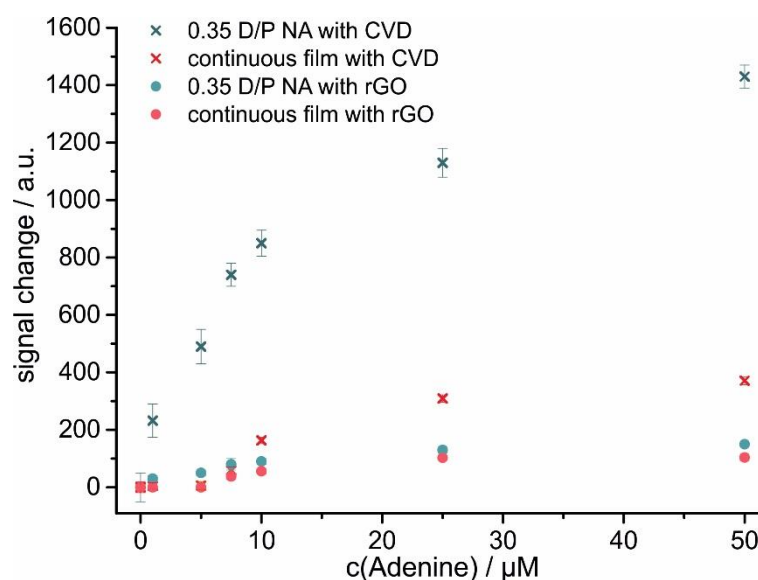
Figure 4.4│ Signal change at a constant angle upon binding of adenine to rGO- and CVD-modified nanohole arrays (D/P = 0.35) covering a concentration range from 1 to 50 µM. For comparison, the response of a continuous gold film modified with rGO and CVD is shown. Error bars have been calculated from the signal-to-noise ratio.

For substrates with CVD graphene a ~290% increase in the maximal signal response is found for a nanohole array in contrast to a continuous film. The higher surface sensitivity for substrates modified with CVD graphene is demonstrated by the ~850% signal enhancement for a nanohole array with a 0.35 D/P ratio with CVD graphene compared to rGO. The limit of detection (LOD) for continuous films modified with rGO or CVD graphene are both ~6 µM. A 3-times better LOD for the nanohole array with rGO of ~2 µM and a 7-timer better LOD of ~0.9 µM for a nanohole array with CVD compared to a continuous film modified with the respective graphene type. The binding of adenine to

Detection of small molecules with surface plasmon resonance by synergistic plasmonic effects of nanostructured surfaces and graphene

72

graphene is based on π-stacking and van der Waals interactions. Other purines will show similar behavior [19].

To evaluate the performance of substrates modified with CVD graphene in a complex matrix, the concentration of the purine bases of thermally denatured DNA was determined for a graphene modified nanohole array with a 0.35 D/P ratio Therefore, a purine content of 60% for a nanohole array was determined. Values are in good agreement with literature (~ 54%) [20,21]. In contrast to a graphene modified continuous gold film the nanohole array showed enhanced sensitivity, which enabled a successful determination of the purine content at 10-times lower analyte concertation (0.12 µg·mL^{-1})

4.4 Conclusion

SPR substrates baes on graphene modified nanohole arrays were fabricated. Compared to rGO, CVD graphene results in more homogenous and reproducible graphene films. Within SPR measurements the highest surface sensitivity was determined for nanohole arrays modified with CVD graphene. A 7-fold lower LOD for the detection of adenine was found for this system, demonstrating the feasibility for the signal enhancement by localized surface plasmons in the detection of small molecules. The applicability was shown by the determination of the purine bases in thermally denatured DNA. For further studies the selectivity of the system should be improved. Here, 1-Pyrenebutyric acid can be attached to the 2D carbon nanomaterial via π-stacking and subsequently modified by a receptor, leading to a universal approach for selective (bio)assays.

4.5 Experimental

4.5.1 Nanohole Array Fabrication

Glass slides (20 × 20 mm^2) of F1-Type with a refractive index of 1.61 (Mivitec GmbH, Sinzing, Germany) were used and cleaned in piranha solution for 90 min and subsequently sonicated for 60 minutes in a mixture of water, ammonia and hydrogen peroxide at a 5:1:1 (v/v/v) ratio. All SPR substrates were prepared according to the protocol described in Genslein et al [12]. Briefly, first a sphere mask of a hexagonal, closed packed polystyrene particles is formed via self-assembly by a slow evaporation process. A solution of 40 µL of a water/ethanol solution 87:13 (v/v) containing

Detection of small molecules with surface plasmon resonance by synergistic plasmonic effects of nanostructured surfaces and graphene

73

13 mg·mL^{-1} polystyrene particles were drop-coated on the cleaned glass slides. Subsequent etching of the particles creates a void between neighboring particles. The particle assembly acts as sphere mask for the gold deposition on the glass. A gold film of 45 nm thickness was deposited on a approx. 3 nm thin titanium adhesion layer. Particle diameter and respectively hole diameter was prepared by etching for 28 min at 18 W with reactive ion etching using oxygen plasma. Lift-off of the sphere mask is achieved by sonication in ethanol. The polystyrene particles have a diameter of 1.04 μm (SD = 0.04 μm, Microparticles GmbH). The resulting arrays were analyzed using SEM.

4.5.2 Substrate Modification

Substrates were functionalised with rGO and CVD graphene. The modification with rGO has been recently described [12]. Briefly, rGO was synthesized by a modified Hummers method and a subsequent chemical reduction. To cover the substrates with a uniform layer, 200 μL of a 0.25 μg·mL^{-1} reduced graphene oxide solution containing 1:1 (v/v) water and isopropanol was deposited on the substrate surface and the solvent excess was removed by spin coating. For modification with CVD graphene a wet transfer method was used [22]. A 10 mm x 10 mm monolayer of graphene on a copper substrate with a PMMA coating (Graphenea, San Sebastián, Spain) was placed on a 400 μM aqueous FeCl$_3$ solution. After complete etching of the copper, the film was thoroughly washed with water and transferred on the desired substrate. In order to remove residue water and to smoothen the film, substrates were shortly placed on a hotplate. By immersing the substrate in acetone for 15 min the PMMA layer was dissolved. After intensive rinsing with EtOH the modified substrates were dried overnight.

4.5.3 Surface Plasmon Resonance Spectroscopy

A BioSuplar SPR instrument (Mivitec GmbH, Sinzing, Germany) with a F1-65 glass prism installed on a swivel carriage was applied for SPR analysis. The substrates are placed on the prism with an index-matching fluid in between. For excitation of SP a 650 nm laser is implemented. Samples were passed through a two-channel flow cell integrated on top of the substrates. The bulk sensitivity, defined as the intensity of reflected light per refractive index units (RIU), was measured with aqueous sucrose solutions (1–4% w/w) covering a range of 1.33–1.34 RIU. SPR slides covered with a continuous gold film of 45 nm thickness were obtained from Mivitec GmbH. During measurements, the angle of incidence was constant and the change in intensity was monitored. Adenine binding to

Detection of small molecules with surface plasmon resonance by synergistic plasmonic effects of nanostructured surfaces and graphene

74

the modified substrates was studied by covering a concentration range of 1 to 50 µM in water. For real sample application, a 12 mg·mL^{-1} aqueous solution of DNA from herring sperm (Sodium salt, Sigma) containing 1 mM HCl was heated for 15 min at 100 °C. After a fast cooling in an ice bath, the DNA solution was diluted to the desired concentrations with water. Respective adenine/herring DNA solutions were introduced to the system for 6 min. After each solution, a 10 min washing step was carried out, in order to remove unbound adenine/herring DNA, ensuring signal change based on absorption.

4.5.4 Raman Microscopy Measurements

A 532 nm laser excitation (10 mW) and a 50 µm slit was used for Raman microscopy measurements (DXR Raman microscope, Thermo Fisher Scientific GmbH, Dreieich, Germany). The spectra were acquired for 1 s and averaged over ten measurements. For Raman maps and microscopic images a 100 times magnification with a MPlan N objective (100×/0.90 BD, Olympus SE & Co. KG, Hamburg, Germany) was applied.

Acknowledgements

4.6 References

[1]   Eng L, Nygren-Babol L, Hanning A (2016) Label-enhanced surface plasmon resonance applied to label-free interaction analysis of small molecules and fragments. Anal Biochem 510:79–87.

[2]   Homola J (2003) Present and future of surface plasmon resonance biosensors. Anal Bioanal Chem 377:528–539.

[3]   Masson J (2017) Surface plasmon resonance clinical biosensors for medical diagnostics. ACS Sens 2:16-30.

[4]   Couture M, Liang Y, Poirier Richard H, Faid R, Peng W, Masson J (2013) Tuning the 3D plasmon field of nanohole arrays. Nanoscale 5:12399–12408.

Detection of small molecules with surface plasmon resonance by synergistic
plasmonic effects of nanostructured surfaces and graphene

75

[5]   Couture M, Ray KK, Poirier-Richard H, Crofton A, Masson J (2016) 96-Well
       Plasmonic Sensing with Nanohole Arrays. ACS Sens 1:287–294.

[6]   Szunerits S, Maalouli N, Wijaya E, Vilcot J, Boukherroub R (2013) Recent
       advances in the development of graphene-based surface plasmon resonance
       (SPR) interfaces. Anal Bioanal Chem 405:1435–1443.

[7]   Grigorenko AN, Polini M, Novoselov KS (2012) Graphene plasmonics. Nat
       Photonics 6:749–758.

[8]   Edwards RS, Coleman KS (2013) Graphene synthesis: relationship to applications.
       Nanoscale 5:38–51.

[9]   Backes C, Paton KR, Hanlon D, Yuan S, Katsnelson MI, Houston J, Smith RJ,
       McCloskey D, Donegan JF, Coleman JN (2016) Spectroscopic metrics allow in situ
       measurement of mean size and thickness of liquid-exfoliated few-layer graphene
       nanosheets. Nanoscale 8:4311–4323.

[10] Gomez-Navarro C, Meyer JC, Sundaram RS, Chuvilin A, Kurasch S, Burghard M,
       Kern K, Kaiser U (2010) Atomic structure of reduced graphene oxide. Nano Lett
       10:1144–1148.

[11] Mattevi C, Kim H, Chhowalla M (2011) A review of chemical vapour deposition of
       graphene on copper. J Mater Chem 21:3324–3334.

[12] Genslein C, Hausler P, Kirchner E, Bierl R, Baeumner AJ, Hirsch T (2016)
       Graphene-enhanced plasmonic nanohole arrays for environmental sensing in
       aqueous samples. Beilstein J Nanotechnol 7:1564–1573.

[13] Genet C, Ebbesen TW (2007) Light in tiny holes. Nature 445:39–46.

[14] Ferrari AC, Meyer JC, Scardaci V, Casiraghi C, Lazzeri M, Mauri F, Piscanec S,
       Jiang D, Novoselov KS, Roth S, Geim AK (2006) Raman spectrum of graphene
       and graphene layers. Phys Rev Lett 97:187401.

[15] Malard LM, Pimenta MA, Dresselhaus G, Dresselhaus MS (2009) Raman
       spectroscopy in graphene. PhysRep 473:51–87.

[16] Moon IK, Lee J, Ruoff RS, Lee H (2010) Reduced graphene oxide by chemical
       graphitization. Nat Commun 1:73.

[17] Weber JW, Calado VE, van de Sanden MCM (2010) Optical constants of graphene
       measured by spectroscopic ellipsometry. Appl Phys Lett 97: 091904.

[18] Rakić AD, Djurišić AB, Elazar JM, Majewski ML (1998) Optical properties of
       metallic films for vertical-cavity optoelectronic devices. Appl Opt 37:5271–5283.

Detection of small molecules with surface plasmon resonance by synergistic plasmonic effects of nanostructured surfaces and graphene

76

[19] Varghese N, Mogera U, Govindaraj A, Das A, Maiti PK, Sood AK, Rao CNR (2009) Binding of DNA nucleobases and nucleosides with graphene. Chemphyschem 10:206–210.

[20] Huang K, Niu D, Sun J, Han C, Wu Z, Li Y, Xiong X (2011) Novel electrochemical sensor based on functionalized graphene for simultaneous determination of adenine and guanine in DNA. Colloids Surf B Biointerfaces 82:543–549.

[21] Wang P, Wu H, Dai Z, Zou X (2011) Simultaneous detection of guanine, adenine, thymine and cytosine at choline monolayer supported multiwalled carbon nanotubes film. Biosens Bioelectron 26:3339–3345.

[22] Suk JW, Kitt A, Magnuson CW, Hao Y, Ahmed S, An J, Swan AK, Goldberg BB, Ruoff RS (2011) Transfer of CVD-grown monolayer graphene onto arbitrary substrates. ACS Nano 5:6916–6924.

Plasmonic Enhancement of NIR to UV Upconversion by a Nanoengineered
Interface Consisting of NaYF₄:Yb,Tm Nanoparticles and a Gold Nanotriangle
Array for Optical Detection of Vitamin B12 in Serum

77

5 Plasmonic Enhancement of NIR to UV Upconversion by a Nanoengineered Interface Consisting of NaYF$_4$:Yb,Tm Nanoparticles and a Gold Nanotriangle Array for Optical Detection of Vitamin B12 in Serum

5.1 Abstract

determination of vitamin B12 via simple luminescence readout in serum without any pretreatment. The interplay of Tm^{3+}-doped $NaYF_4$ nanoparticles (UCNPs) and a gold nanotriangle array prepared by a nanosphere lithography on a glass slide is responsible for an efficient NIR to UV upconversion. Hot spots of the gold assembly generate a local electromagnetic field enhancement, favoring the 4-photon upconversion process at low power excitation of approx. 13 $W \cdot cm^{-2}$. An improvement of about six-times of the intensity for the emission peaking at 345 nm is achieved. The nanoengineered interface has been applied in a proof-of-concept sensor for vitamin B12 in serum, which is known as a marker for the potential risk of cancer, Alzheimer disease or during pregnancy for neurological abnormalities in newborn babies. An outstanding limit of detection of 0.6 $\pm$ 0.2 nM can be achieved by a simple intensity-based optical readout, consuming only 200 µL of a sample, which qualifies easy miniaturization for point-of-care diagnostics. Additionally, this label-free approach can be used for long-term monitoring because of the high photostability of the upconversion nanoparticles.

Plasmonic Enhancement of NIR to UV Upconversion by a Nanoengineered
Interface Consisting of NaYF₄:Yb,Tm Nanoparticles and a Gold Nanotriangle
Array for Optical Detection of Vitamin B12 in Serum

78
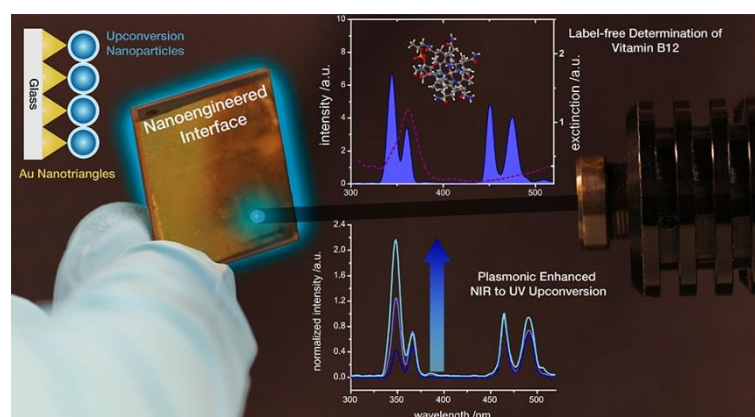
Figure 5.1 Graphical abstract of the nanoengineered interface system.

This chapter has been submitted.

Wiesholler Lisa Marie*, Genslein Christa*, Schroter Alexandra, Hirsch Thomas.
Submitted to Analytical Chemistry.

Author contributions:

LMW and CG contributed equally. Most of the experimental work was carried out by LMW and CG. LMW and AS synthesized the UCNPs. CG fabricated the nanotriangle arrays. CG and AS constructed the nanoengineered interface. LMW, CG and AS performed luminescence measurements of the substrates. LMW carried out the vitamin B12 measurements and the cross-sensitivity study. LMW and CG wrote the manuscript. The article was revised by LMW, CG, AS and TH. TH is corresponding author.

Plasmonic Enhancement of NIR to UV Upconversion by a Nanoengineered
Interface Consisting of NaYF₄:Yb,Tm Nanoparticles and a Gold Nanotriangle
Array for Optical Detection of Vitamin B12 in Serum

79

5.2 Introduction

An increasing demand of sensors, especially in the field of health care and point-of-care diagnostics [1] motivates researchers to develop new concepts to overcome limitations of elaborative detection principles [2]. Online monitoring is highly desired in production lines in environment control, or in diagnostics, as it does not require periodic sampling and maximizes the information which provides efficiency, safety and health [3]. Label-free approaches, especially those which monitor intrinsic features of an analyte, *e.g.* its absorption characteristics are most suitable for long-time usage [4]. Miniaturization and energy efficiency are also key players in the sensor development as they enable an easy integration in many systems. The tremendous progress in nanotechnology established a lot of new nanomaterials with outstanding properties, helping to advance sensor technologies. Upconversion nanoparticles (UCNPs) are one of these materials, as they efficiently convert NIR light to an UV/VIS emission [5]. In particular the good biocompatibility of the UCNPs and the reduction of the background fluorescence [6] make them attractive for applications like biological sensing [7-9] and bioimaging [6,10]. Despite the progress in the last years, for some applications the quantum efficiency of these nanoparticles, which is attributed to the general low absorption coefficient of Ln^{3+} ions, caused by the Laporte–forbidden 4f-4f-transitions, is still not sufficient [11,12]. Haase *et al.* have reported on the synthesis of erbium-doped core-shell nanoparticles of 45 nm in size, which exhibit almost the same brightness as bulk material [13]. For biological applications UCNPs doped with thulium are of interest as they are capable to emit at 345 nm and 360 nm, realized by a four-photon process [14]. These emissions require usually a high laser power. Researchers develop many strategies [15] for enhancing the upconversion luminescence,[16] like optimizing the concentrations of the lanthanide ions, [17] modulating the shape and phase of the particles,[18] designing composite materials [19] Spectral management in UCNPs can enhance a particular emission peak by redistribution of the excitation energy [20]. Another promising strategy is the assembly of the particles onto solid supports [21] like the combination of the UCNPs with metallic nanostructured surfaces. Here, the key point is the occurrence of surface plasmons, appearing in the presence of conducting materials, defined as oscillations at the interface between a material with free electrons (*e.g.* gold) and a dielectric material [22]. Interaction of surface plasmons with UCNPs have been reported to enhance the upconversion efficiency [23,24]. These short-ranging, high-frequent electromagnetic resonances of electrons are changing the electromagnetic field (EMF)

Plasmonic Enhancement of NIR to UV Upconversion by a Nanoengineered
Interface Consisting of NaYF$_4$:Yb,Tm Nanoparticles and a Gold Nanotriangle
Array for Optical Detection of Vitamin B12 in Serum

80

in close proximity to upconversion nanoparticles [24]. The interplay of UCNPs and metallic nanostructured surfaces is influenced by the plasmonic properties of the material and the geometrical structures such as shape and size [25]. Localized surface plasmons (LSPs) are favored for emission enhancement. They are characterized by a confined EMF rather than propagating surface plasmons on a continuous metal film [26]. The optical phenomenon is generated by a light wave trapped at a structure smaller than its wavelength, called hot spots [27]. Light interactions are strongly enhanced at the edges of such structures and the energy is focused to a close vicinity at the metallic surface [28]. For sensor applications regular arrangements of these nanostructures need to be fabricated in large dimensions with sufficient reproducibility. Nanosphere lithography, based on the self-assembly of nanoparticles, covers these requirements. The use of different sphere sizes allows for facile hot spot design, in particular nanotriangle arrays [29]. In this work a gold nanotriangle array is merged with UCNPs to result in a nanoengineered interface, with the advantages of high UV luminescence and label-free online monitoring. The increased upconversion emission in the UV was selected for sensing the vitamin B12 (vitB12) concentration in serum. Recent studies have shown that vitB12 in blood serum is a marker for Altzheimer disease [30] and low vitB12 content in serum during pregnancy enhances the risk of neurological abnormalities in new born babies [31]. Both attractive scenarios for point-of-care diagnostics.

5.3 Materials and Methods

5.3.1 Chemicals and Characterization Methods

Lanthanide chloride hexahydrates (> 99.9%) were purchased from Sigma Aldrich and Treibacher Industrie AG. Oleic acid and 1-octadecene (both technical grade, 90%) were obtained from Alfa Aesar. Nitrosonium tertrafluoroborate (95%) was purchased from Sigma Aldrich. All other chemicals were of analytical grade and obtained from Sigma Aldrich, Merck or Acros. All chemicals were used as received without further purification.

The size of the nanoparticles was determined by transmission electron microscopy (TEM) with a 120 kV Philips CM12 microscope (www.fei.com) on carbon coated copper grids (400 mesh) from Plano (www.plano-em.de). A small volume (10 µL) of particles dispersed in cyclohexane (1 mg·mL^{-1}) was dropped on the grid and the solvent was

Plasmonic Enhancement of NIR to UV Upconversion by a Nanoengineered
Interface Consisting of NaYF₄:Yb,Tm Nanoparticles and a Gold Nanotriangle
Array for Optical Detection of Vitamin B12 in Serum

81

allowed to evaporate. The elemental composition was verified by using a flame-EOP (end on plasma) inductively coupled plasma optical emission spectrometer (ICP-OES) from Spectro (www.spectro.com). Dynamic light scattering (DLS) was performed with a Malvern Zetasizer Nano ZS (www.malvern.com) to characterize the particle-size-distribution in dispersions. Disposable semi-micro poly(methyl methacrylate) cuvettes were used and the temperature was hold at a constant level of 20 °C. To analyze the crystal structure, X-ray powder diffraction patterns (XRD) with a resolution of 0.005° (2θ) were collected using a STOE STADI P diffractometer (www.stoe.com) equipped with a Dectris Mython 1K detector (www.dectris.com). Monochromatic Cu Kα_1 radiation (λ = 1.54056 Å) was used. Extinction spectra of the functionalized glass slides were recorded with a portable high performance near-infrared (NIR) spectrometer with high-throughput Czerny-Turner optics and a fanless TEC-cooled InGaAs image sensor (www.broadcom.com). A halogen lamp dealt as light source. The beam was shaped by a combination of plano convex lenses and a positive meniscus lens. Spectra were averaged over 100 measurements with an integration time of 0.75 s. Luminescence measurements were carried out with an Aminco Bowman Series 2 luminescence spectrometer of Thermo Electron Corporation (www.corporate.thermofisher.com) equipped with a continuous wave (cw) 980 nm laser module (200 mV) from Picotronic (www.picotronic.com) for excitation. Absorbance measurements of the vitB12 solutions were obtained with a Varian Cary 50 spectrophotometer (www.agilent.com).

5.3.2 Synthesis and Surface Modification of Upconversion Nanoparticles

The synthesis of hexagonal phase, oleate-capped UCNPs with sizes of 26 nm was in accordance to the method reported by Wilhelm *et al.* [32].

Synthesis of Hexagonal NaYF₄:25%Yb,0.3%Tm

A total of 5 mmol rare earth trichlorides of Y^{3+}, Yb^{3+} and Tm^{3+} with the corresponding molar doping ratios as desired in the nanoparticle were dissolved in 40 mL methanol and transferred into a three necked round bottom flask under nitrogen flow. A mixture of 8 mL oleic acid and 15 mL 1-octadecene per 1 mmol of rare earth salts was added to the solution. The suspension was heated to 160 °C and vacuum was applied for 30 min to form a clear solution. The solution was cooled to room temperature and 0.148 g (4.0 mmol) NH₄F and 0.1 g (2.5 mmol) NaOH dissolved in 20 mL methanol were added per 1 mmol of rare earth salts. The suspension was kept at 120 °C for 30 min and then heated to reflux (approx. 325 °C). The progress of the reaction was monitored with a

Plasmonic Enhancement of NIR to UV Upconversion by a Nanoengineered
Interface Consisting of NaYF$_4$:Yb,Tm Nanoparticles and a Gold Nanotriangle
Array for Optical Detection of Vitamin B12 in Serum

82

980 nm CW laser module. 10 min from the time on, when upconversion luminescence can be observed for the first time, the reaction mixture was cooled to room temperature. The particles were precipitated by the addition of ethanol in excess and collected by centrifugation at 1,000 g for 5 min. The precipitate was washed twice with chloroform/ethanol (1:10, v/v) and 3-times with cyclohexane/acetone (1:10, v/v) by repeated redispersion-precipitation-centrifugation cycles. Finally, the particles were dispersed in cyclohexane, centrifuged at 1,000 g for 3 min to remove aggregates, and the supernatant was collected and stored at 4 °C.

5.3.3 Surface Modification of NaYF$_4$:25%Yb,0.3%Tm

The ligand exchange strategy with tetrafluoroborate is based on the method described by Dong *et al.* [33]. In a two-phase system consisting of equal volumes of cyclohexane and DMF the nanoparticles were dispersed. NOBF$_4$ (1 mg per 1 mg UCNPs) was added and the dispersion was stirred and slightly heated (~40 °C) for 10 min. During this time the oleate capped hydrophobic UCNPs were transferred from the cyclohexane phase into the DMF phase. The process can be easily monitored by control of the upconversion luminescence via excitation with a 980 nm cw laser module (200 mW). Surface modification is complete when only the DMF phase shows upconversion luminescence. The clear upper cyclohexane phase was discarded, and the particles were precipitated by excess of chloroform. The suspension is centrifuged at 1,000 g for 5 min. The jellylike precipitate is washed twice with chloroform. Finally, the BF$_4$-stabilized particles are dispersed in DMF, and aggregates were removed by centrifugation at 1,000 g for 3 min. Polyacrylic acid (MW 2100) was dissolved in water (2 mg·mL 1) and added to the BF^{4-}-stabilized nanoparticles dispersed in DMF. The solution was stirred and also kept at a moderate temperature of 40 °C for 15 min. Afterwards the dispersion was centrifuged (13,600 g for 20 min) and washed twice for 20 min with water (13,600 g). The supernatants were finally collected after centrifugation at 1,000 g for 3 min.

5.3.4 Functionalization of Glass Slides

All substrates are based on glass slides (20 x 20 mm²) of F1 type with a refractive index of 1.61 (Mivitec GmbH, Sinzing, Germany). Glass slides were cleaned in a piranha solution (3:1 (v/v) mixture of conc. H$_2$SO$_4$ and 30% (w/w) H$_2$O$_2$) for 90 minutes and in a mixture of water, ammonia and hydrogen peroxide with a 5:1:1 (v/v/v) ratio for 60 min.

Plasmonic Enhancement of NIR to UV Upconversion by a Nanoengineered
Interface Consisting of NaYF$_4$:Yb,Tm Nanoparticles and a Gold Nanotriangle
Array for Optical Detection of Vitamin B12 in Serum

83

Triangle arrays were prepared according to a modified protocol described by Genslein *et al* [34]. In brief, polystyrene particles were dispersed in a water/ethanol solution with a ratio of 87:13 (v/v), with a concentration of 13 mg·mL^{-1}. A sphere mask of particles with a diameter of 1.04 ± 0.04 µm was formed on the glass substrates by drop-coating of 40 µL of particle dispersion. After evaporation of the solvent, the sphere mask was covered by a film of ~5 nm titanium and ~50 nm gold. The metal films were deposited by electron-beam vapor deposition consisting of a Leybold Univex 450 vacuum pump (www.leyboldproducts.de), a Ferro-Tec EVM-8 e-beam gun (www.ferrotec.com) and an Inficon oscillating quartz (www.inficon.com) device. In the last step the polystyrene spheres were lift-off from the surface by sonication in ethanol for 2 min, yielding triangle nanoarrays. Glass slides covered with a continuous gold film of ~50 nm thickness on a 5 nm adhesion layer of chromium were obtained from Mivitec GmbH. Scanning electron microscopy (SEM) was used for characterization (JSM-6510 SEM-device, JEOL GmbH, Eching, Germany) with a voltage of 15 and 30 kV

5.3.5 Preparation and Characterization of a Particle Layer via Self-Assembly

For monolayer formation on a continuous gold film and on the nanotriangle array 1-mercaptohexadecane and for a glass slide hexadecyltrimethoxysilane was used. First, the gold was modified with an alkanethiol self-assembled monolayer (SAM). The gold modified glass slides (either with a continuous gold film or with a gold nanotriangle assembly) were washed with ethanol and dried with nitrogen. The monolayer on substrates with a continuous gold film or a triangle array was formed by immersion in a solution of 1-mercaptohexadecane in ethanol (200 µg·mL^{-1}) overnight. For the SAM formation on a glass slide a solution of hexadecyltrimethoxysilane in ethanol (200 µg·mL^{-1}) was used. After washing with ethanol, 200 µL of oleate capped NaYF$_4$:Yb,Tm nanoparticles in cyclohexane (22 mg·mL^{-1}) were deposited on the gold substrate. The solvent was evaporated at ambient air, and the slide subsequently washed with cyclohexane. To achieve a complete coverage of the substrates by particles, the NaYF$_4$:Yb,Tm-solution was dropped on the surface for four times, after each deposition the substrate was washed thoroughly with cyclohexane. For characterization SEM (SUPRA 55VP ZEISS, Carl Zeiss AG, Oberkochen, Germany) at a voltage of 8 kV was used.

Plasmonic Enhancement of NIR to UV Upconversion by a Nanoengineered
Interface Consisting of NaYF$_4$:Yb,Tm Nanoparticles and a Gold Nanotriangle
Array for Optical Detection of Vitamin B12 in Serum

84

5.3.6 Measurement of Vitamin B12

A homemade measure-ment cell was used for detection. On the nanoengineered interface a PDMS gasket was mounted and sealed with a glass slide. The cell holds a total volume of 200 µL of the analyte solutions and was fixed in the spectrometer. A 980 nm laser (200 mW, cw) illuminates the nanoengineered interface via the glass cell. The upconversion luminescence was detected in a reflectometric configuration with a con-stant angle, to avoid any excitation light at the detector.

5.4 Results and Discussion

5.4.1 Substrate Fabrication and Functionalization with NaYF$_4$:Yb,Tm Upconversion Nanoparticles

The nanoengineered interface is formed by an assembly of a nanostructured gold array with UCNPs on top as outlined in Figure 5.2. An interaction of the plasmonic features of the gold with the UCNPs is expected to enhance the luminescence properties of the anti-stokes emission of the nanoparticle [35]. The structured gold on the glass was fabricated by nanosphere lithography [36].

This method offers outstanding and convenient possibilities in terms of a) the variability in the dimensions and periodicity of the metallic nanostructures, b) its fast and precise patterning of large-scaled surfaces in the cm^2 regime, and c) the easy and cheap fabrication, which does not need any expensive instrumentation. In a first step an ethanolic solution consisting of polystyrene spheres (PSS) of a diameter of 1.0 µm was drop-casted on a clean glass slide (Figure 5.3).

Plasmonic Enhancement of NIR to UV Upconversion by a Nanoengineered
Interface Consisting of NaYF₄:Yb,Tm Nanoparticles and a Gold Nanotriangle
Array for Optical Detection of Vitamin B12 in Serum

85
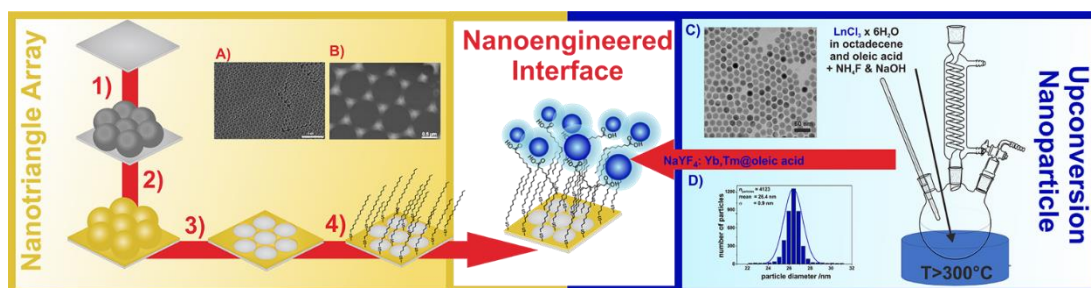
Figure 5.2 Schema of the fabrication of the nanoengineered interface. The left part illustrates the assembly and functionalization of the nanotriangle array. Starting with a glass slide, on which polystyrene spheres were drop coated (1) and then gold is deposited by evaporation (2). After the slide was sonicated to remove the polystyrene spheres (3) and a nanotriangle array was obtained. This array was further functionalized with a self-assembled monolayer of a thiol for coupling of the particles (4). The SEM image in (A) shows the polystyrene mask with gold on top and in (B) the resulting nanotriangle array. On the right the synthesis of the NaYF₄:25%Yb,0.3%Tm UCNPs by a bottom-up method is displayed. TEM images in (C) and the corresponding size distribution (D) reveal monodisperse particles of about 26 nm in diameter. In the middle the two nanoengineered interface is displayed by the self-assembly of the UCNPs on the surface functionalized gold nanotriangle array.
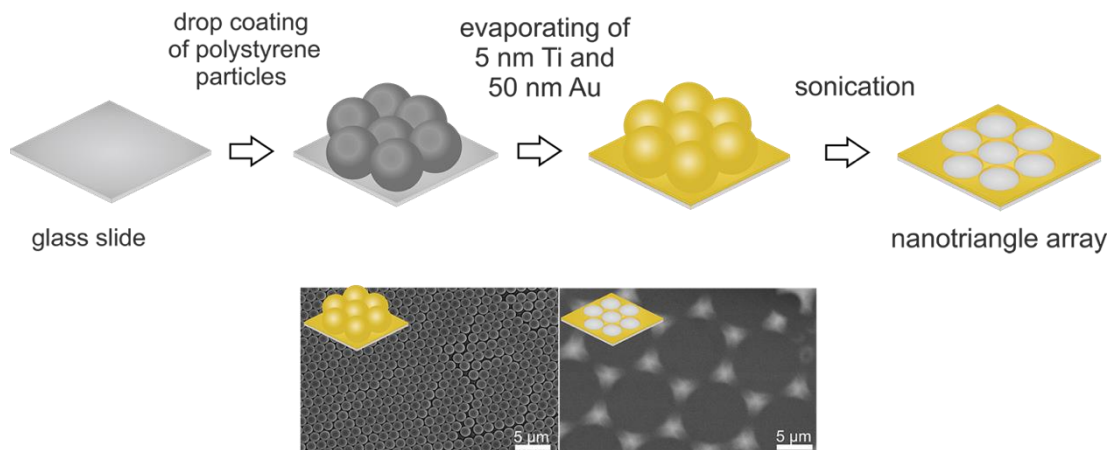
Figure 5.3 Outline of the fabrication steps to form a triangle array with a modified nanosphere lithography technique. Polystyrene particles of ~1 µm in diameter were used for mask formation gold (~50 nm) was deposited on a ~5 nm Ti adhesion layer by thermal vacuum deposition. In a last step the particles were removed by sonication in a water bath. The scanning electron microscope (SEM) images of the polystyrene sphere mask (left) and the triangle array (right) show the highly ordered hexagonal arrangement of the polystyrene spheres after the deposition of the gold layer and resulting array of the nanotriangles with a center to center distance of 1 µm and a gold nanotriangle area of 0.04 µm².

Plasmonic Enhancement of NIR to UV Upconversion by a Nanoengineered
Interface Consisting of NaYF$_4$:Yb,Tm Nanoparticles and a Gold Nanotriangle
Array for Optical Detection of Vitamin B12 in Serum

86

The concentration of the spheres is set to allow the formation of a self-assembled, hexagonal closed packed monolayer arrangement. After slow evaporation of the solvent, an adhesive layer of ~5 nm titanium followed by ~50 nm gold is evaporated on top of the assembly. In a last step the particles are removed by sonication for two minutes. The PSS act as mask which define the area where the gold film is deposited on the glass. Scanning electron microscopy confirmed the hexagonal arrangement of the PSS as well as the formation of the gold nanotriangle array (Figure 5.3). An area on the glass slide of only 9% is covered by the gold (Figure 5.4 and calculation presented in the following), which concentrates the electro-magnetic field (EMF) generated by free electrons in the metal in so-called hot spots at the corners of the triangle. By changing the diameter of the PSS, the density, and the size of the gold nanotriangles can be easily adjusted. Therefore, it is expected that the plasmonic features, especially the EMF enhancement, can be tuned.
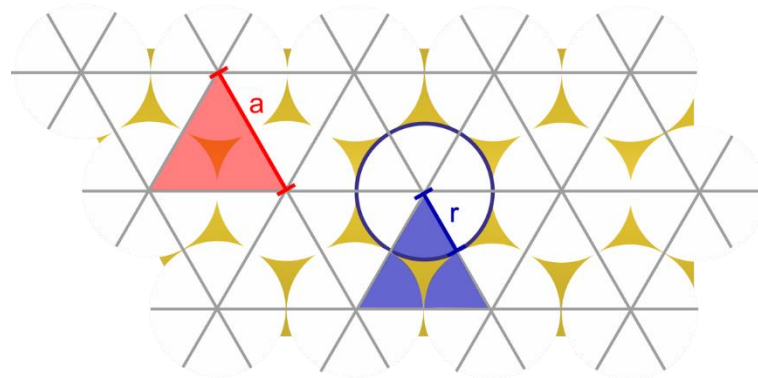
Figure 5.4│ Scheme of the hexagonal arrangement of the polystyrene sphere mask and the gold nanotriangle array.

Calculation of the area covered by gold the nanotriangle array:

$$a = 2 \cdot r = 1 \, \mu m$$

$$A(Triangle\ Array) = A(Triangle, red) - 3 \cdot A(Circular\ Segement, blue)$$

$$A(Triangle, red) = \frac{a^2 \cdot \sqrt{3}}{4} = 0.43 \, \mu m^2$$

$$3 \cdot A(Circular\ Segement, blue) = \frac{\pi \cdot r^2}{2} = 0.39 \, \mu m^2$$

$$Surface\ Coverage = \frac{A(Triangle, red) - 3 \cdot A(Circular\ Segment, blue)}{A(Triangle, red)}$$

$$= \frac{0.43 \, \mu m^2 - 0.39 \, \mu m^2}{0.43 \, \mu m^2} = 9.3 \cdot 10^{-2}$$

Plasmonic Enhancement of NIR to UV Upconversion by a Nanoengineered
Interface Consisting of NaYF₄:Yb,Tm Nanoparticles and a Gold Nanotriangle
Array for Optical Detection of Vitamin B12 in Serum

87

Upconversion nanoparticles of the composition NaYF$_4$:25%Yb,0.3%Tm with oleic acid as capping ligand were prepared via a bottom up synthesis by a well-established method [32].Ytterbium ions act as sensitizer excitable at 980 nm and which transfer the energy in a multi-photon process sequentially to the Tm^{3+}-ions. Upon relaxation anti-Stokes emissions of narrow bandwidth at 800 nm, 475 nm, 450 nm, 360 nm and 345 nm can be recorded [37]. In dispersion, at low power irradiation, the emissions at higher energy become less bright compared to those at longer wavelengths.
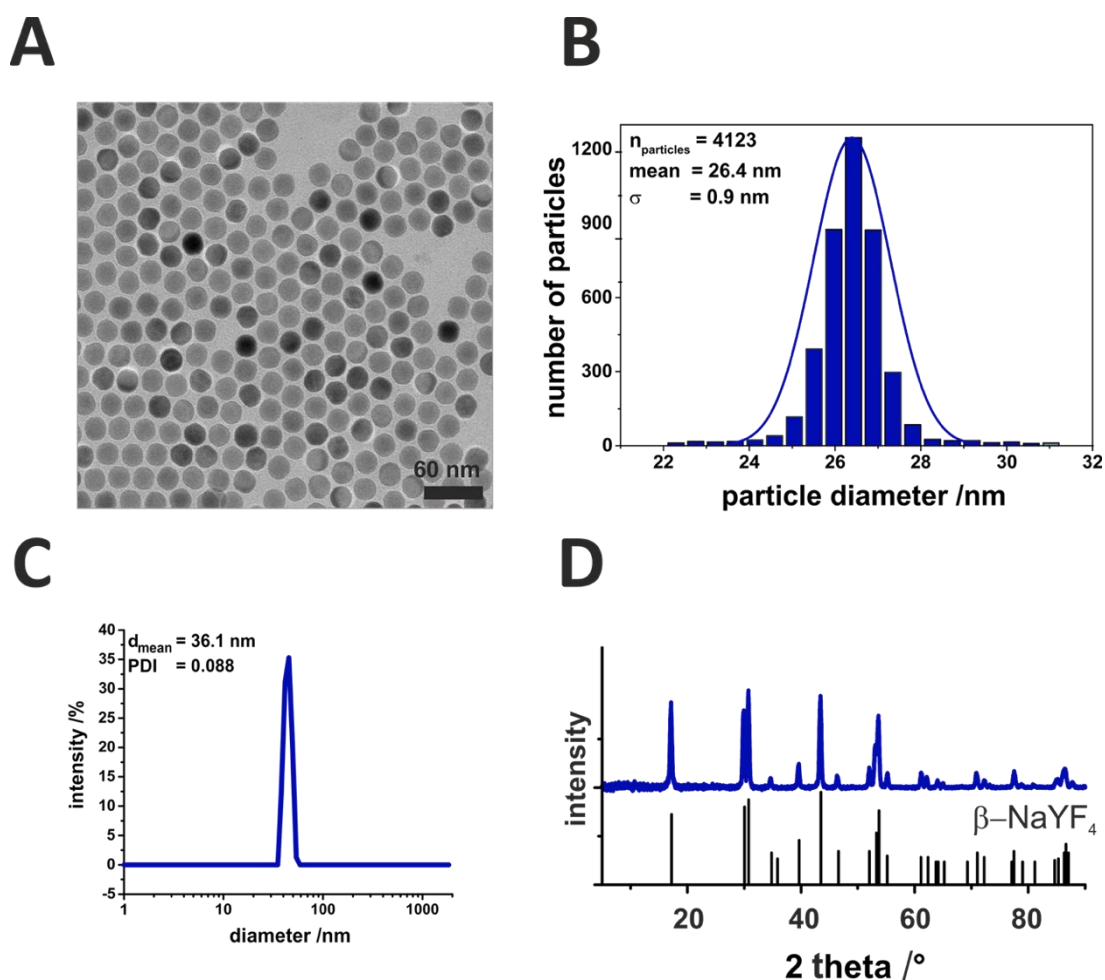
Figure 5.5 TEM-image (A) and corresponding size distribution (B) of NaYF$_4$:Yb,Tm particles. The diameter averaged from 4,123 particles is 26.4 ± 0.9 nm. The monodispersity of the particles was confirmed by a solvodynamic diameter of 33 nm with a polydispersity index of 0.086, measured by dynamic light scattering of the particle dispersion in cyclohexane (3 mg·L^{-1}) (C). No agglomeration of the particles in dispersion can be observed. The diffraction pattern (blue) reveals a hexagonal crystal phase as the reflexes of the nanocrystals match the standard reference pattern of β-NaYF$_4$ (ICDD PDF #16-334) (black) (D).

Plasmonic Enhancement of NIR to UV Upconversion by a Nanoengineered
Interface Consisting of NaYF₄:Yb,Tm Nanoparticles and a Gold Nanotriangle
Array for Optical Detection of Vitamin B12 in Serum

88

The emission intensity and the quantum efficiency depend not only on the excitation power density but also on the size and the crystallinity. A favorable low phonon energy of about 350 cm^{-1} of $NaYF_4$ was the reason to choose this material as host [38]. Monodisperse particles with a diameter of 26 ± 0.9 nm estimated from TEM-images (Figure 5.5 A&B) were synthesized with pure hexagonal crystallinity as demonstrated by XRD measurements (Figure 5.5 D). Such a crystal structure is known for its one order of magnitude brighter upconversion luminescence compared to the cubic form [39]. No tendency for agglomeration in cyclohexane was found and verified by dynamic light scattering (Figure 5.5 C). ICP-OES measurements were performed to determine the exact composition and concentration of the UCNPs (Table 5.1). The content of Yb^{3+} ($25\% \pm 0.2\%$, w/w) and Tm^{3+} ($0.4\% \pm 0.1\%$ w/w) is in good accordance to the ratio of the rare earth chlorides used during the synthesis. Finally, the nanoengineered interfaces is obtained by the linkage of the UCNPs to the gold nanotriangle array by self-assembly.

Table 5.1 | The composition of the UCNPs was verified by ICP-OES measurements. The content of each rare earth ion in the particles is in accordance to the theoretical calculated amount of rare earth salts used in for the synthesis of $NaYF_4$:25%Yb,0.3%Tm.

Ion	Y^{3+}	Yb^{3+}	Tm^{3+}	Diameter
Mole percentage	74.6 ± 0.2 %	25 ± 0.2 %	0.4 ± 0.1 %	26 ± 0.9 nm

The glass slides with the nanotriangle array were immersed overnight in an ethanolic solution of a long-chained alkanethiol ($HS-(CH_2)_{15}-CH_3$) in order to form a self-assembled monolayer on gold which is needed to warrant a stable binding of the UCNPs via intercalation of the long-chained oleate capping ligands. After subsequently dropping of a total amount of 800 µL of a dispersion of the oleate capped UCNPs in cyclohexane (22 mg·mL^{-1}) onto the glass slide with the thiol-modified gold nanotriangle array, a stable arrangement of the particles on the surface was achieved. Even after several washing steps a blue upconversion of the nanoengineered interface can be seen upon 980 nm excitation which proves the stable binding of the UCNPs, covering the whole surface. This was confirmed by SEM-studies (Figure 5.6) showing stacks of particles caused by van-der-Waals and hydrophobic interactions on top of the modified glass slide.

Plasmonic Enhancement of NIR to UV Upconversion by a Nanoengineered
Interface Consisting of NaYF₄:Yb,Tm Nanoparticles and a Gold Nanotriangle
Array for Optical Detection of Vitamin B12 in Serum

89
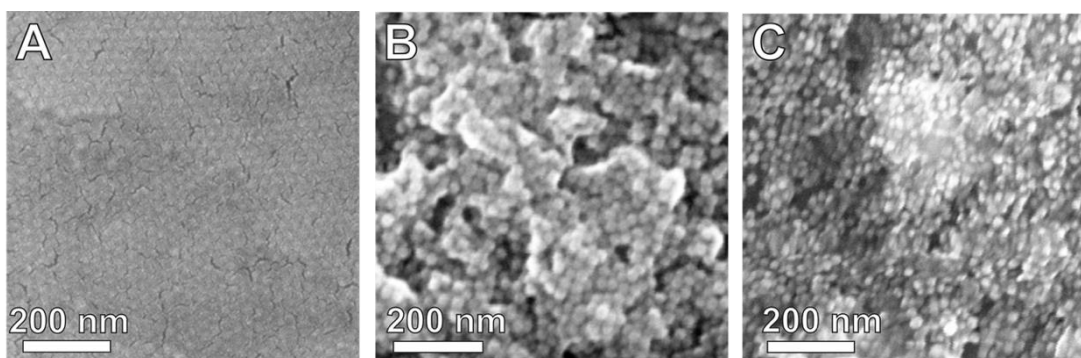
Figure 5.6 | SEM images of the three substrates: blank substrate (glass slide) (A), a continuous gold film (B) and a nanoengineered interface (triangle array) (C) functionalized with NaYF₄:25%Yb, 0.3%Tm particles.

5.4.2 Luminescence Properties

NaYF₄:Yb,Tm nanoparticles were assembled on three different types of glass slides: a) a blank slide, b) modified with a continuous gold film and c) modified with a gold nanotriangle array. The thickness of the gold was identically on both types. The enhancement of the NIR to UV upconversion caused by the gold and especially by the nanotriangle array can be seen from the normalization of the spectra to the 450 nm emission (Figure 5.7).
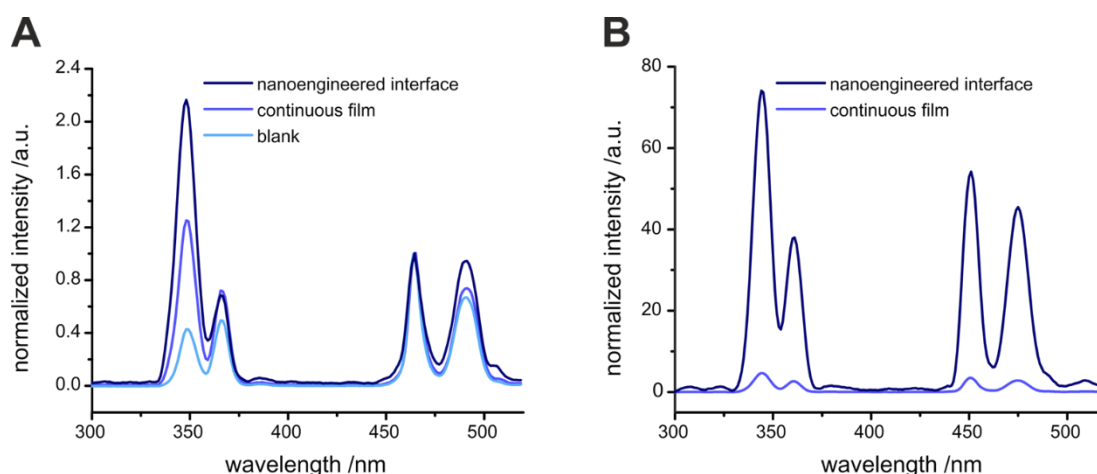
Figure 5.7 | Luminescence spectra of UCNPs attached on a blank substrate (glass slide, light blue), a continuous gold film (blue) and a nanoengineered interface (gold triangle array, dark blue). The spectra in (**A**) were normalized to the 450 nm emission and in (**B**) they were normalized on the gold area. Nanoparticles were excited by a 980 nm laser module (200 mW, cw).

Plasmonic Enhancement of NIR to UV Upconversion by a Nanoengineered
Interface Consisting of NaYF$_4$:Yb,Tm Nanoparticles and a Gold Nanotriangle
Array for Optical Detection of Vitamin B12 in Serum

90

For the emission at 344 nm and 360 nm a peak inversion can be observed when gold is in close proximity to the UCNPs. The peak ratio of $I_{344\,nm}$/$I_{360\,nm}$ of 0.8 in case of a blank glass substrate changes to 1.7 for the continuous gold film and up to 3.2 for the nanotriangle array. On both gold surfaces plasmonic features are responsible for the higher efficiency of the $^1I_6$ to $^3H_6$ transition. The EMF is supposed to interact with the UCNPs to improve the up-conversion efficiency as demonstrated by a peak inversion in the UV. Li Min Jin *et al.* reported recently that the four-photon-process of the upconversion luminescence becomes more likely compared to the three-photon process when increasing the excitation power density, which will result in peak ratios >1.39. Under low power excitation of approximately 13 W·cm^{-2}, as it was used throughout these studies, the probability of the $^1I_6$ to $^3H_6$ transition for particles is very unlikely. This is demonstrated by a spectrum of the dispersion of these particles in cyclohexane, with a peak ratio $I_{344\,nm}$/$I_{360\,nm}$ of about 0.8 (Figure 5.7 A) which is very similar to the ratio measured for the UCNP-modified glass slide. An explanation for the extraordinary enhancement might be given by the hot spots, generating localized surface plasmons (LSP) at nano dimensions, in contrast to the propagating surface plasmons on a continuous gold film [41]. The EMF at the hot spots will confine the excitation power density and therefore the brightness of the 345 nm peak will be enhanced. In the study of Li Min Jin *et al.* the excitation power dependent change of the emission peak ratio was shown for larger NaYF$_4$:Yb,Tm@NaYF$_4$ nanorods with a length of ~46 nm and a width of ~25 nm. The highest value they report for $I_{344\,nm}$/$I_{360\,nm}$ was ~1.5, recorded at an excitation power density of ~60 W·cm^{-2}. This clearly shows that a massive enhancement of the small UCNPs of 26 nm diameter on the nanoengineered surfaces at low excitation power density of ~13 W·cm^{-2} takes place. Unfortunately, with the equipment in our lab we were not able to perform an excitation power dependent study. As a control experiment, extinction measurements with the three different types of substrates were carried out. For nanotriangle arrays the gold area is significantly lower as for a continuous gold film, therefore a lower absorbance at 980 nm is expected. This is not the case, as the extinction is increased in a similar way for both gold surfaces, indicating the presence of an additional plasmonic effect (Figure 5.8). Furthermore, luminescence measurements with increased distance between gold and UCNPs, realized by depositing the UCNPs on the opposite side to the nanotriangle array onto a glass slide of ~1 mm thickness, showed no enhancement of the NIR to UV upconversion, confirming the effect of the plasmonic features on the UCNPs (Figure 5.9). In Figure 5.6 B the spectra were normalized by the respective gold area. In such case a ~16 times higher upconversion

Plasmonic Enhancement of NIR to UV Upconversion by a Nanoengineered
Interface Consisting of NaYF4:Yb,Tm Nanoparticles and a Gold Nanotriangle
Array for Optical Detection of Vitamin B12 in Serum

91

efficiency for the emission in the UV was found for the nanoengineered interface compared to the continuous gold film.
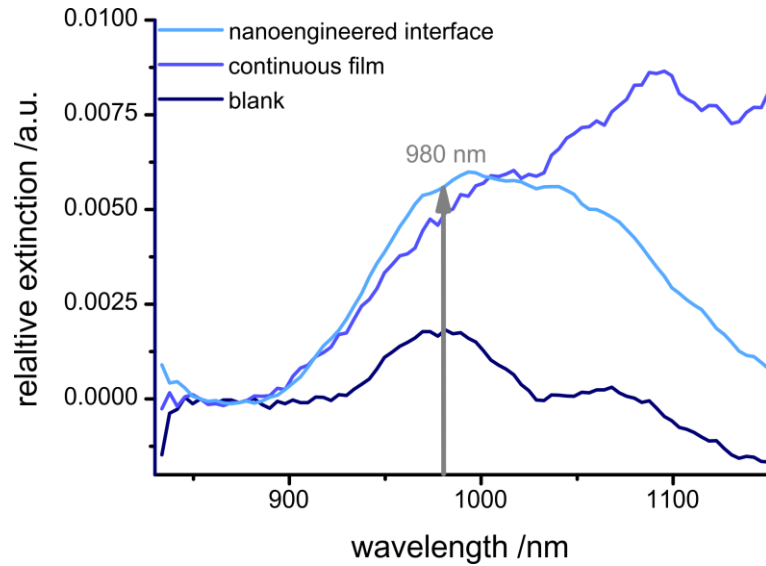
Figure 5.8│ Extinction spectra of the UCNPs on a glass slide (blank), a continuous gold film and a gold nanotriangle array (nanoengineered interface). Spectra were normalized for illustration of the peak variation and the excitation wavelength of 980 nm of the UCNPs is shown. Substrates were covered by ~50 nm Au with a ~5 nm Ti adhesion layer.
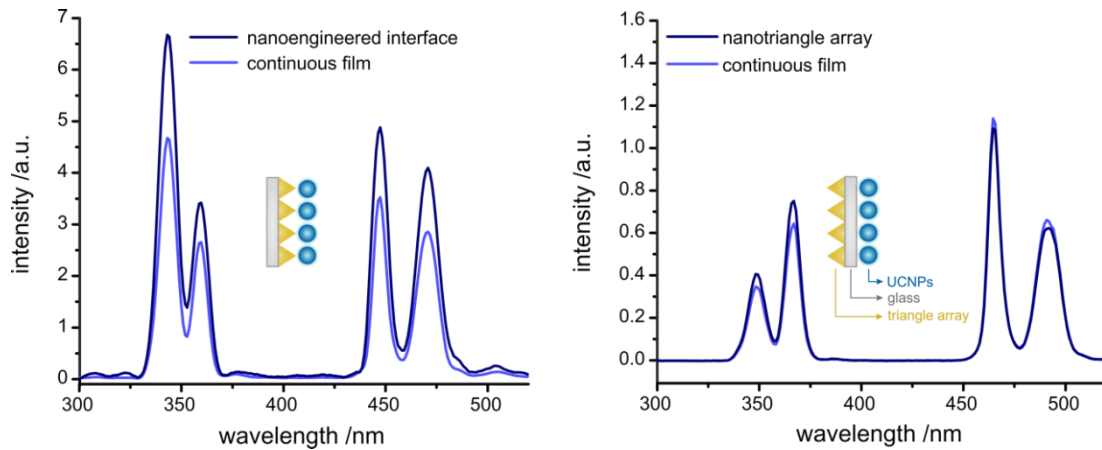
Figure 5.9│ Luminescence spectra of the NaYF4:25%Yb^{3+},0.3%Tm^{3+} particles assembled on a continuous gold film and a gold nanotriangle array upon 980 nm excitation at approx. 13 W·cm^{-2}. On the left side UCNPs were placed on the gold, on the right side UCNPs were attached to the glass with the gold on the other side as symbolized by the schema in the inserts. The spectra were not normalized to any peak. The inversion of the intensity ratio of the two emission peaks in the UV range as well as the increased emission intensity for both peaks shows the impact of the gold to the NIR to UV upconversion for the nanoengineered interface.

Plasmonic Enhancement of NIR to UV Upconversion by a Nanoengineered
Interface Consisting of NaYF$_4$:Yb,Tm Nanoparticles and a Gold Nanotriangle
Array for Optical Detection of Vitamin B12 in Serum

92

5.4.3 Luminescence Detection of Vitamin B12 at Nanoengineered Interfaces

The outstanding enhancement of the UV emission of the UCNPs by the nanoengineered inter-face enables a novel kind of sensing application based on luminescence measurements. One of the biggest advantages can be attributed by the fact that the UV-region of the electromagnetic spectrum gets accessible for simple label-free, intensity-based readout of changes in analyte concentration caused by reabsorption processes. This is attributed to the excitation in the NIR which will minimize background caused by fluorescence of organic molecules, proteins, or tissue. Vitamin B12, as model analyte, exhibits an absorption peak at 361 nm overlapping the anti-Stokes emission of the $^1I_6$ to $^3H_6$ and $^1D_2$ to $^3H_6$ transitions, peaking at 345 nm and 360 nm (Figure 5.10). Therefore, it is expected that the luminescence of the UCNPs in the UV will decrease in presence of vitB12. The determination of vitB12 by the same principle but in a classical cuvette assay with dispersed particles highlights the capabilities of the nanoengineered interface. Here the same UCNPs have been used with the exception that the ligand oleate was replaced by polyacrylic acid via a ligand exchange protocol [42].
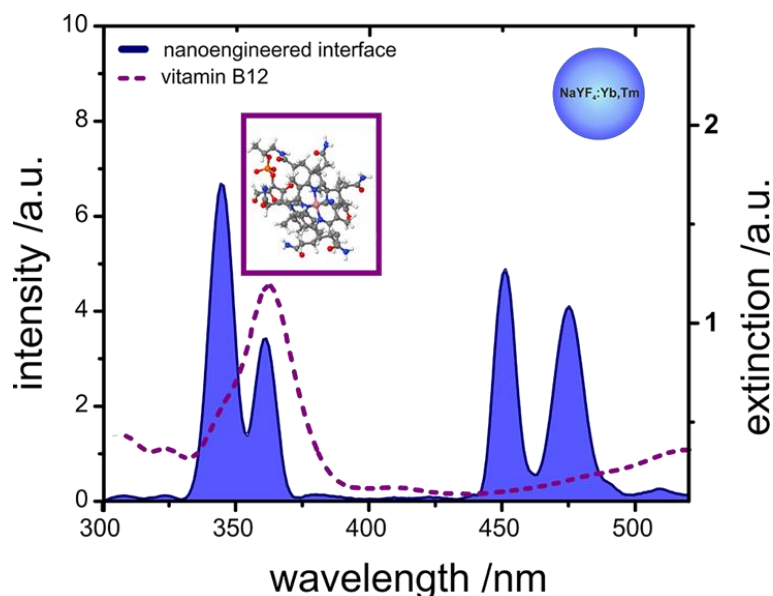
Figure 5.10 | The upconversion luminescence of a nanoengineered interface (blue) showing a spectral overlap with the absorbance of vitB12 (purple).

Plasmonic Enhancement of NIR to UV Upconversion by a Nanoengineered
Interface Consisting of NaYF₄:Yb,Tm Nanoparticles and a Gold Nanotriangle
Array for Optical Detection of Vitamin B12 in Serum

93

For the determination of vitB12 using the nanoengineered interface a homemade measurement cell consisting of two glass slides, one modified with the nanoengineered interface, separated by a ~3 mm thin PDMS gasket, holding a total volume of 200 μL of the analyte, was used. Figure 5.11A compares the spectra for the different vitB12 concentrations. With increasing the concentration of vitB12 from ~3 nM to ~630 nM the luminescence of the UCNPs in the cuvette is almost not affected. Therefore, this method cannot be used with low power NIR laser excitation in a complex media and high-power excitation at 980 nm suffers from the drawback that aqueous samples will be heated due to a local absorption maximum of water at this wavelength [43].
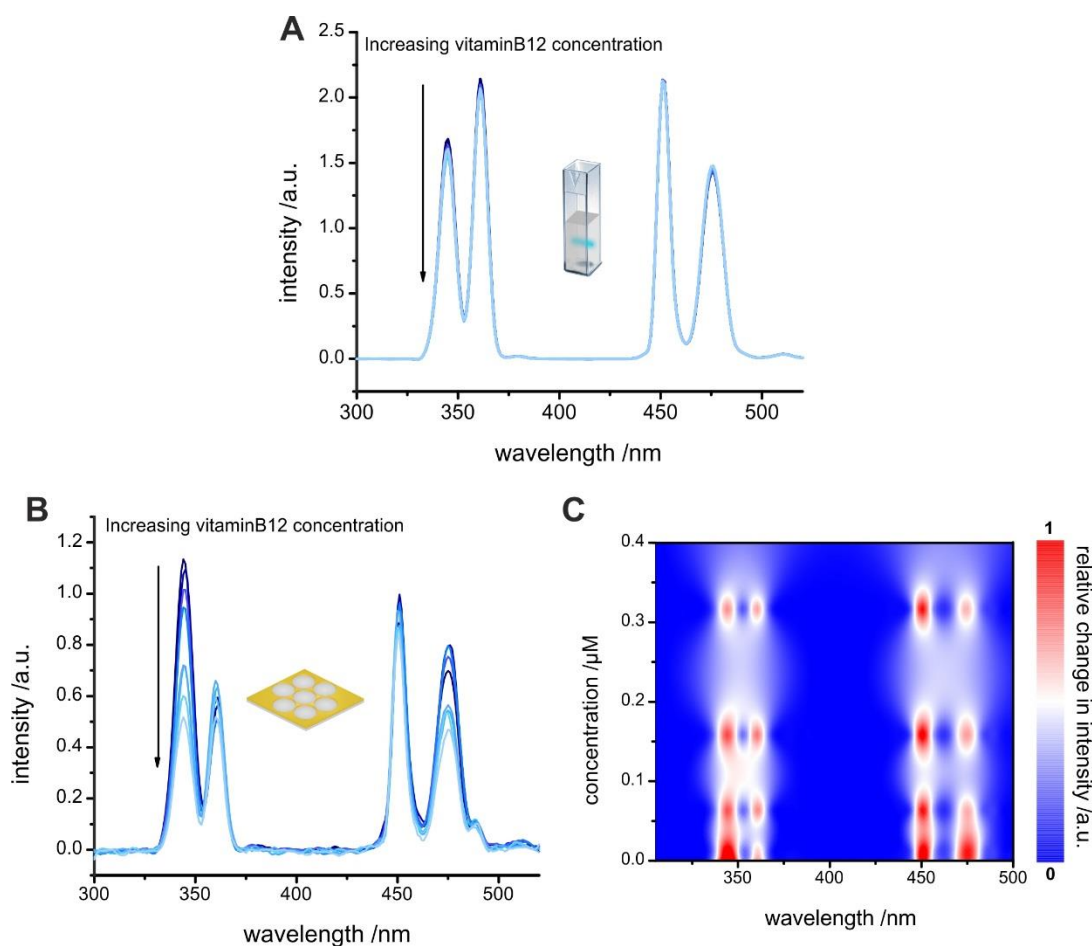
Figure 5.11│ Luminescence spectra of NaYF₄:Yb,Tm@PAA particles in aqueous solution (10 mg·mL⁻¹) (A) and luminescence spectra of NaYF₄:Yb,Tm@oleate particles attached on a gold triangle array (nanoengineered interface) (B) in presence of an increasing amount of vitB12 ranging from 3 nM to 634 nM. In (C) the relative change of the emission spectra of the nanoengineered interface as a function of the vitB12 concentration is depicted as a color map. All spectra were excited by a 980 nm laser module at ~13 W·cm⁻²

Plasmonic Enhancement of NIR to UV Upconversion by a Nanoengineered
Interface Consisting of NaYF$_4$:Yb,Tm Nanoparticles and a Gold Nanotriangle
Array for Optical Detection of Vitamin B12 in Serum

94

In contrast, the NIR to UV upconverted luminescence of the nanoengineered interface leads to a strong decrease of the signal in the UV (Figure 5.11 B) for small analyte concentrations and low excitation power density. All upconversion peaks in the UV and blue region of the spectrum are influenced in their intensity by the vitB12 concentration. For evaluation of the highest peak change a 2D-color map of the relative change in the luminescence intensity in the spectral range from 300 nm to 500 nm upon the increase in the vitB12 concentration is shown (Figure 5.11 C). For the emissions at 360 nm and 450 nm nearly no change in the relative intensity is observed. The peak at 475 nm decreases at low concentrations similar to the one at 345 nm, but for the later one the dynamic range is larger. From Figure 5.10 it can be seen that there is no significant spectral overlap for the peak at 450 nm, therefore one explanation of the decrease may be attributed to the fact that the excited states in UCNPs might not be fully independent as they both get fed by energy transfer from Yb^{3+} ions. Another possible explanation might be that the gold interacts also with the deactivation pathway of the excited states of Tm^{3+}(Figure 5.12).
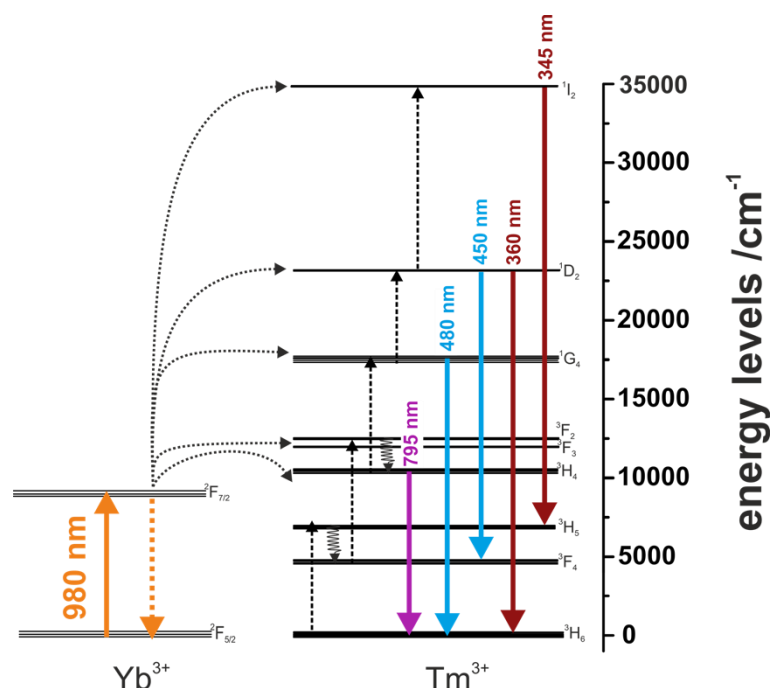
Figure 5.12 Energy levels of Tm^{3+} and Yb^{3+} showing the transitions for 980 nm excitation of Yb^{3+} and the sequential energy transfer to Tm^{3+} to populate the states $^1I_2$, $^1D_2$, $^1G_4$ and $^3H_5$, resulting in emissions at 345 nm, 360 nm, 450 nm, 480 nm and 785 nm. Non-radiative transitions are colored in black.

Plasmonic Enhancement of NIR to UV Upconversion by a Nanoengineered
Interface Consisting of NaYF$_4$:Yb,Tm Nanoparticles and a Gold Nanotriangle
Array for Optical Detection of Vitamin B12 in Serum

95

Both postulations will be investigated in a future study describing the detailed photo-physics of such nanoengineered interfaces. As a consequence, it is suggested to use the wavelength of 400 nm as a reference signal as it shows no dependence on the vitB12 concentration (Figure 5.11 C). Serum spiked with vitB12 at concentrations from 3 nM to 634 nM, without the need of any pretreatment and the low consumption of sample volume (200 µL), demonstrates the performance of the nanoengineered interface in sensing by the plasmonic enhancement of the NIR to UV upconversion. Two methods for data evaluation were compared.

From the spectral overlap of the analyte with both upconversion emissions in the UV also the change in the peak area, integrated from 334 nm to 395 nm was monitored as a function of the vitB12 concentration. This result was compared to the change in the ratio $I_{345\,nm}$ to $I_{400\,nm}$ (Figure 5.13 A). Both methods of data evaluation correlate very well as can be seen by almost identical sensitivities. A limit of detection (LOD) of 1.3 ± 0.4 nM (peak area change) and 0.6 ± 0.2 nM (peak intensity change) was calculated (S/N = 3). The method comprises also by good selectivity towards molecules, commonly presented in the serum and expected to affect the luminescence measurements. No cross-sensitivity was found for retinol, ascorbic acid, folic acid and pyridoxin hydrochloride (Figure 5.13 B).
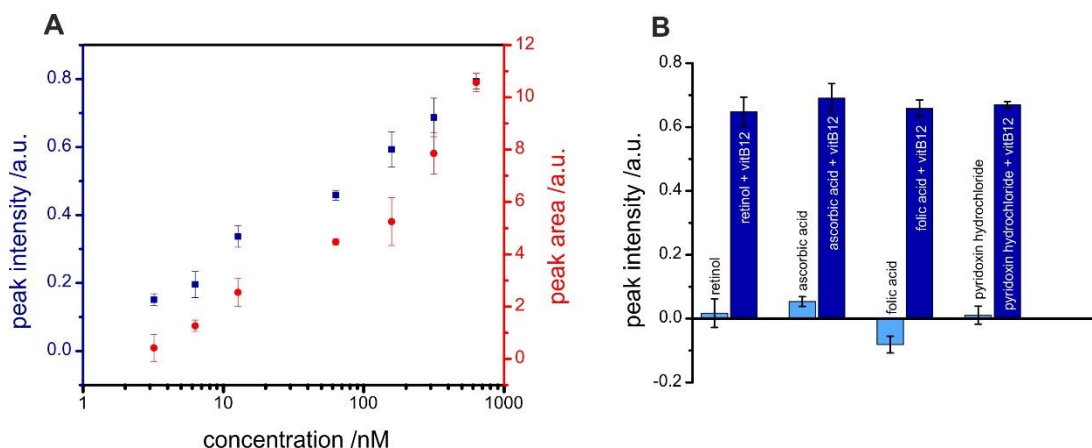
Figure 5.13 (A) Calibration plots of the upconversion luminescence for peak intensity (blue) at 345 nm or peak area (red) integrated from 334 nm to 395 nm in serum, spiked with different amounts of vitB12. The luminescence spectra for both methods were normalized to the luminescence intensity recorded at 400 nm. Excitation was performed by a 980 nm laser module of ~13 W·cm^{-2} power density. (B) The cross sensitivity was evaluated by the peak inten-sity readout at 345 nm at concentrations of 634 nM of all molecules. The light blue bars represent the change of the intensity of the possible interfering substance and the dark blue bars show the impact of these substances to the vitB12 determination.

Plasmonic Enhancement of NIR to UV Upconversion by a Nanoengineered
Interface Consisting of NaYF₄:Yb,Tm Nanoparticles and a Gold Nanotriangle
Array for Optical Detection of Vitamin B12 in Serum

96

The LOD for vitB12 determination with the nanoengineered interface is approximately two orders of magnitude lower than for established analytical techniques like HPLC, Raman spectroscopy, fluorescence and surface plasmon resonance (Table 5.2). Immunoassays and mass spectrometry demonstrate the lowest LOD, with a remarkably value of 0.063 fM for mass spectrometry. Those techniques suffer from costly instruments, numerous processing steps and lengthy assay times. A microbiological assay already requires 25 hours exposure time, which is needed to be performed for the detection of vitB12 by HPLC [44].

Table 5.2│ Comparison of different techniques for the determination of vitB12 in real samples by their limit of detection (LOD).

Technique	LOD / nM	Sample volume / μL	Assay time	Pre-treatment	Comments	References
Mass spectrometry	$0.63\cdot10^{-8}$	n.r.[1]	5 days	Yes	cost intensive	[47]
Immunoassays	0.001	50 - 100	20 h	Yes	laborious	[48]
Chemi-luminescence	0.016	30 - 50	3.6-6 s	Yes	not label free	[45]
Microbiological detection	0.13	50 – 100	20 h	Yes	growth rate is also influenced by antibiotics	[49]
Nanoengineered interface	0.6	200	1 min	No	-	this work
HPLC	51	20	5 min	Yes	No online monitoring	[50]
Surface plasmon resonance	63	n.r.	5 min	Yes	poor specificity	[51]
Raman spectroscopy	70	2.500	7 h	Yes	interfered by proteins	[44]
Fluorescence	100	2.000	7 h	No	high background due to UV excitation	[52]

1) n.r. = not reported

Plasmonic Enhancement of NIR to UV Upconversion by a Nanoengineered
Interface Consisting of NaYF$_4$:Yb,Tm Nanoparticles and a Gold Nanotriangle
Array for Optical Detection of Vitamin B12 in Serum

97

Here, the nanoengineered interface with assay times of a few minutes and a LOD sufficient for biosensor applications is beneficial. The most important fact, which emphasizes the capabilities of our system is the label-free nature. Chemiluminescence (CL) and radioimmunoassay enable a similar LOD but depend on labeling and high trained operators. The detection of vitB12 via CL relies on the presence of Co^{2+}. Without a label discrimination between free and unbound cobalt is not possible [45,46].

In contrast, the method presented in this work can also be used for online monitoring as it does not require any label or sample pretreatment. Due to the low power excitation, cheap, small laser modules combined with microfluidics and a standard spectrometer in the size of a match box can be used. Both making this approach attractive for sensing applications. In contrast to surface plasmon resonance the nanoengineered interface can be assembled on all optical transparent materials and no need of high refractive index glass for coupling of surface plasmons is required.

5.5 Conclusions

In conclusion, an enhancement strategy of the NIR to UV upconversion of NaYF$_4$:Yb,Tm by the construction of an nanoengineered interface consisting of a glass slide modified by gold nanotriangle arrays with UCNPs on top is presented. It is demonstrated that such an assembly enhances the emission peak at 344 nm upon excitation at 980 nm by an excitation power density of only 13 W·cm^{-2} by a factor of ~6. Such a low power excitation makes this concept highly attractive for sensing application based on luminescence detection in the UV region, especially in bio-logical samples as the NIR excitation avoids autofluores-cence. This proof of concept can be used for an early readout of vitB12 in serum where upregulated concentrations indicate breast and liver cancer in early stage [53,54]. These results indicate that nanoengineered interfaces based on UCNPs deposited on nanotriangles arrays are promising for label free online monitoring of biomolecules.

Plasmonic Enhancement of NIR to UV Upconversion by a Nanoengineered
Interface Consisting of NaYF$_4$:Yb,Tm Nanoparticles and a Gold Nanotriangle
Array for Optical Detection of Vitamin B12 in Serum

98

Acknowledgements

5.6 References

[1]   Nayak S, Blumenfeld NR, Laksanasopin T, Sia SK (2017) Point-of-Care Diagnostics: Recent Developments in a Connected Age. Anal Chem 89:102–123.

[2]   Griss R, Schena A, Reymond L, Patiny L, Werner D, Tinberg CE, Baker D, Johnsson K (2014) Bioluminescent sensor proteins for point-of-care therapeutic drug monitoring. Nature Chem Biol 10:598–603.

[3]   Fan R, Ebrahimi M, Quitmann H, Aden M, Czermak P (2016) An Innovative Optical Sensor for the Online Monitoring and Control of Biomass Concentration in a Membrane Bioreactor System for Lactic Acid Production. Sensors 16.

[4]   Tu L, Li X, Bian S, Yu Y, Li J, Huang L, Liu P, Wu Q, Wang W (2017) Label-free and real-time monitoring of single cell attachment on template-stripped plasmonic nano-holes. Sci Rep 7:11020.

[5]   Hinamoto T, Takashina H, Sugimoto H, Fujii M (2017) Controlling Surface Plasmon Resonance of Metal Nanocap for Upconversion Enhancement. J Phys Chem C 121:8077–8083.

[6]   Wang F, Banerjee D, Liu Y, Chen X, Liu X (2010) Upconversion nanoparticles in biological labeling, imaging, and therapy. Analyst 135:1839–1854.

[7]   Wang F, Liu X (2009) Recent advances in the chemistry of lanthanide-doped upconversion nanocrystals. Chem Soc Rev 38:976–989.

[8]   Gao R, Hao C, Xu L, Xu C, Kuang H (2018) Spiny Nanorod and Upconversion Nanoparticle Satellite Assemblies for Ultrasensitive Detection of Messenger RNA in Living Cells. Anal Chem 90:5414–5421.

Plasmonic Enhancement of NIR to UV Upconversion by a Nanoengineered
Interface Consisting of NaYF$_4$:Yb,Tm Nanoparticles and a Gold Nanotriangle
Array for Optical Detection of Vitamin B12 in Serum

99

[9]   Buchner M, Ngoensawat U, Schenck M, Fenzl C, Wongkaew N, Matlock-
        Colangelo L, Hirsch T, Duerkop A, Baeumner AJ (2017) Embedded nanolamps in
        electrospun nanofibers enabling online monitoring and ratiometric measurements.
        J Mater Chem C 5:9712–9720.

[10]   Mader HS, Kele P, Saleh SM, Wolfbeis OS (2010) Upconverting luminescent
        nanoparticles for use in bioconjugation and bioimaging. Curr Opin Chem Biol
        14:582–596.

[11]   Feng AL, You ML, Tian L, Singamaneni S, Liu M, Duan Z, Lu TJ, Xu F, Lin M
        (2015) Distance-dependent plasmon-enhanced fluorescence of upconversion
        nanoparticles using polyelectrolyte multilayers as tunable spacers. Sci Rep 5:7779.

[12]   Luu Q, Hor A, Fisher J, Anderson RB, Liu S, Luk T, Paudel HP, Farrokh Baroughi
        M, May PS, Smith S (2014) Two-Color Surface Plasmon Polariton Enhanced
        Upconversion in NaYF$_4$:Yb:Tm Nanoparticles on Au Nanopillar Arrays. J Phys
        Chem C 118:3251–3257.

[13]   Homann C, Krukewitt L, Frenzel F, Grauel B, Würth C, Resch-Genger U, Haase M
        (2018) NaYF$_4$:Yb,Er/NaYF$_4$ Core/Shell Nanocrystals with High Upconversion
        Luminescence Quantum Yield. Angew Chem 57:8765–8769.

[14]   Suyver JF, Grimm J, van Veen MK, Biner D, Krämer KW, Güdel HU (2006)
        Upconversion spectroscopy and properties of NaYF$_4$ doped with and/or. J Lumin
        117:1–12.

[15]   Wiesholler LM, Hirsch T (2018) Strategies for the design of bright upconversion
        nanoparticles for bioanalytical applications. Opt Mat 80:253–264.

[16]   Lu D, Mao C, Cho SK, Ahn S, Park W (2016) Experimental demonstration of
        plasmon enhanced energy transfer rate in NaYF$_4$:Yb^{3+},Er^{3+} upconversion
        nanoparticles. Sci Rep 6:18894.

[17]   Chen G, Ohulchanskyy TY, Kumar R, Agren H, Prasad PN (2010) Ultrasmall
        monodisperse NaYF$_4$:Yb^{3+}/Tm^{3+} nanocrystals with enhanced near-infrared to near-
        infrared upconversion photoluminescence. ACS Nano 4:3163–3168.

[18]   Lin M, Zhao Y, Liu M, Qiu M, Dong Y, Duan Z, Li YH, Pingguan-Murphy B, Lu TJ,
        Xu F (2014) Synthesis of upconversion NaYF$_4$:Yb^{3+},Er^{3+} particles with enhanced
        luminescent intensity through control of morphology and phase. J. Mater Chem C
        2:3671–3676.

[19]   Qiu Z, Shu J, Tang D (2018) Near-Infrared-to-Ultraviolet Light-Mediated
        Photoelectrochemical Aptasensing Platform for Cancer Biomarker Based on Core-
        Shell NaYF$_4$:Yb,Tm@TiO$_2$ Upconversion Microrods. Anal Chem 90:1021–1028.

Plasmonic Enhancement of NIR to UV Upconversion by a Nanoengineered
Interface Consisting of NaYF₄:Yb,Tm Nanoparticles and a Gold Nanotriangle
Array for Optical Detection of Vitamin B12 in Serum

100

[20] Wang Y, Zheng K, Song S, Fan D, Zhang H, Liu X (2018) Remote manipulation of upconversion luminescence. Chem Soc Rev.

[21] Yi G, Chow G (2007) Water-Soluble NaYF₄:Yb,Er(Tm)/NaYF₄ /Polymer Core/Shell/Shell Nanoparticles with Significant Enhancement of Upconversion Fluorescence. Chem Mater 19:341–343.

[22] Brolo AG (2012) Plasmonics for future biosensors. Nat Photon 6:709–713.

[23] Saboktakin M, Ye X, Oh SJ, Hong S, Fafarman AT, Chettiar UK, Engheta N, Murray CB, Kagan CR (2012) Metal-enhanced upconversion luminescence tunable through metal nanoparticle-nanophosphor separation. ACS Nano 6:8758–8766.

[24] Di Wu M, García-Etxarri A, Salleo A, Dionne JA (2014) Plasmon-Enhanced Upconversion. J Phys Chem Lett 5:4020–4031.

[25] Xiong K, Emilsson G, Dahlin AB (2016) Biosensing using plasmonic nanohole arrays with small, homogenous and tunable aperture diameters. Analyst 141:3803–3810.

[26] Aćimović SS, Šípová H, Emilsson G, Dahlin AB, Antosiewicz TJ, Käll M (2017) Superior LSPR substrates based on electromagnetic decoupling for on-a-chip high-throughput label-free biosensing. Light Sci Appl 6:e17042.

[27] Petryayeva E, Krull UJ (2011) Localized surface plasmon resonance: nanostructures, bioassays and biosensing--a review. Anal Chimica Acta 706:8–24.

[28] Fang Y, Jiao Y, Xiong K, Ogier R, Yang Z, Gao S, Dahlin AB, Käll M (2015) Plasmon Enhanced Internal Photoemission in Antenna-Spacer-Mirror Based Au/TiO₂ Nanostructures. Nano Lett 15:4059–4065.

[29] Masson J, Murray-Méthot M, Live LS (2010) Nanohole arrays in chemical analysis: manufacturing methods and applications. Analyst 135:1483–1489.

[30] Clarke R, Smith AD, Jobst KA, Refsum H, Sutton L, Ueland PM (1998) Folate, Vitamin B12, and Serum Total Homocysteine Levels in Confirmed Alzheimer Disease. Arch Neuroy 55:1449–1455.

[31] Guerra-Shinohara EM, Paiva AA, Rondó PH, Yamasa-ki K, Terzi CA, D'Almeida V (2002) Relationship between total homocysteine and folate levels in pregnant women and their newborn babies according to maternal serum levels of vitamin B12. BJOG 109:784–791.

Plasmonic Enhancement of NIR to UV Upconversion by a Nanoengineered
Interface Consisting of NaYF$_4$:Yb,Tm Nanoparticles and a Gold Nanotriangle
Array for Optical Detection of Vitamin B12 in Serum

101

[32] Wilhelm S, Kaiser M, Würth C, Heiland J, Carrillo-Carrion C, Muhr V, Wolfbeis OS, Parak WJ, Resch-Genger U, Hirsch T (2015) Water dispersible upconverting nanoparticles: effects of surface modification on their luminescence and colloidal stability. Nanoscale 7:1403–1410.

[33] Dong A, Ye X, Chen J, Kang Y, Gordon T, Kikkawa JM, Murray CB (2011) A generalized ligand-exchange strategy enabling sequential surface functionalization of colloidal nanocrystals. J Am Chem Soc 133:998–1006.

[34] Genslein C, Hausler P, Kirchner E, Bierl R, Baeumner AJ, Hirsch T (2017) Detection of small molecules with surface plasmon resonance by synergistic plasmonic effects of nanostructured surfaces and graphene. SPIE BiOS. 10080:100800F-100800F-7

[35] Paudel HP, Zhong L, Bayat K, Baroughi MF, Smith S, Lin C, Jiang C, Berry MT, May PS (2011) Enhancement of Near-Infrared-to-Visible Upconversion Luminescence Using Engineered Plasmonic Gold Surfaces. J Phys Chem C 115:19028–19036.

[36] Correia-Ledo D, Gibson KF, Dhawan A, Couture M, Vo-Dinh T, Graham D, Masson J (2012) Assessing the Location of Surface Plasmons Over Nanotriangle and Nanohole Arrays of Different Size and Periodicity. J Phys Chem. C Nanomater. Interfaces 116:6884–6892.

[37] Kumar R, Nyk M, Ohulchanskyy TY, Flask CA, Prasad PN (2009) Combined Optical and MR Bioimaging Using Rare Earth Ion Doped NaYF$_4$ Nanocrystals. Adv Funct Mater 19:853–859.

[38] Haase M, Schäfer H (2011) Upconverting nanoparticles. Angew Chem50:5808–5829.

[39] Xu CT, Zhan Q, Liu H, Somesfalean G, Qian J, He S, Andersson-Engels S (2013) Upconverting nanoparticles for pre-clinical diffuse optical imaging, microscopy and sensing: Current trends and future challenges. Laser Photon Rev 7:663–697.

[40] Jin LM, Chen X, Siu CK, Wang F, Yu SF (2017) Enhancing Multiphoton Upconversion from NaYF$_4$:Yb/Tm@NaYF$_4$ Core-Shell Nanoparticles via the Use of Laser Cavity. ACS Nano 11:843–849.

[41] Jackman JA, Rahim Ferhan A, Cho N (2017) Nanoplasmonic sensors for biointerfacial science. Chem Soc Rev 46:3615–3660.

[42] Naccache R, Vetrone F, Mahalingam V, Cuccia LA, Capobianco JA (2009) Controlled Synthesis and Water Dispersibility of Hexagonal Phase NaGdF$_4$:Ho^{3+}/Yb^{3+} Nanoparticles. Chem Mater 21:717–723.

Plasmonic Enhancement of NIR to UV Upconversion by a Nanoengineered
Interface Consisting of NaYF₄:Yb,Tm Nanoparticles and a Gold Nanotriangle
Array for Optical Detection of Vitamin B12 in Serum

102

[43] Li Y, Tang J, Pan D, Sun L, Chen C, Liu Y, Wang Y, Shi S, Yan C (2016) A Versatile Imaging and Therapeutic Platform Based on Dual-Band Luminescent Lanthanide Nanoparticles toward Tumor Metastasis Inhibition. ACS Nano 10:2766–2773.

[44] Radu AI, Kuellmer M, Giese B, Huebner U, Weber K, Cialla-May D, Popp J (2016) Surface-enhanced Raman spectroscopy (SERS) in food analytics: Detection of vitamins B2 and B12 in cereals. Talanta 160:289–297.

[45] Lok KS, Abdul Muttalib, Siti Zubaidah binte, Lee PPF, Kwok YC, Nguyen N (2012) Rapid determination of vitamin B12 concentration with a chemiluminescence lab on a chip. Lab Chip 12:2353–2361.

[46] Ovalle M, Arroyo E, Stoytcheva M, Zlatev R, Enriquez L, Olivas A (2015) An amperometric microbial biosensor for the determination of vitamin B 12. Anal Methods 7:8185–8189.

[47] Carkeet C, Dueker SR, Lango J, Buchholz BA, Miller JW, Green R, Hammock DB, Roth RJ, Anderson JP (2006) Human vitamin B12 absorption measurement by accelerator mass spectrometry using specifically labeled ^{14}C-cobalamin. Proc Natl Acad Sci 103:5694-5699

[48] Selva Kumar LS, Thakur MS (2011) Competitive immunoassay for analysis of vitamin B(12). Anal Biochem 418:238–246.

[49] Kelleher BP, Broin SD (1991) Microbiological assay for vitamin B12 performed in 96-well microtiter plates. J Clin Pathol 44:592–595.

[50] Heudi O, Fontannaz P (2005) Determination of vitamin B5 in human urine by high-performance liquid chromatography coupled with mass spectrometry. J Sep Sci 28:669–672.

[51] Cannon MJ, Myszka DG, Bagnato JD, Alpers DH, West FG, Grissom CB (2002) Equilibrium and kinetic analyses of the interactions between vitamin B(12) binding proteins and cobalamins by surface plasmon resonance. Anal Biochem 305:1–9.

[52] Gholami J, Manteghian M, Badiei A, Javanbakht M, Ueda H (2015) Label free Detection of Vitamin B12 Based on Fluorescence Quenching of Graphene Oxide Nanolayer. Fullerenes, Nanotubes and Carbon Nanostruc 23:878–884.

[53] Arendt JFB, Pedersen L, Nexo E, Sørensen HT (2013) Elevated plasma vitamin B12 levels as a marker for cancer: a population-based cohort study. Journal of the National Cancer Institute 105:1799–1805. doi: 10.1093/jnci/djt315

Plasmonic Enhancement of NIR to UV Upconversion by a Nanoengineered
Interface Consisting of NaYF$_4$:Yb,Tm Nanoparticles and a Gold Nanotriangle
Array for Optical Detection of Vitamin B12 in Serum

103

[54] Matejcic M, Batlle J de, Ricci C, Biessy C, Perrier F, Huybrechts I, Weiderpass E, Boutron-Ruault MC, Cadeau C, His M, Cox DG, Boeing H, Fortner RT, Kaaks R, Lagiou P, Trichopoulou A, Benetou V, Tumino R, Panico S, Sieri S, Palli D, Ricceri F, Bueno-de-Mesquita HBA, Skeie G, Amiano P, Sánchez MJ, Chirlaque MD, Barricarte A, Quirós JR, Buckland G, van Gils CH, Peeters PH, Key TJ, Riboli E, Gylling B, Zeleniuch-Jacquotte A, Gunter MJ, Romieu I, Chajès V (2017) Biomarkers of folate and vitamin B12 and breast cancer risk: report from the EPIC cohort. Int Journal Cancer 140:1246–1259.

6 Conclusions and Future Perspectives

Nanostructured surfaces have emerged in the field of nanotechnology as a plasmonic sensing platform with unique optical properties and applied for a large range of transducing techniques [1]. The confined and strong electromagnetic field (EMF) combined with a shorter penetration depth of localized surface plasmons (LSP), present at the nanostructures, reduces the sensitive layer of the evanescent field in close proximity to the dielectric medium. Analytes attached to the surface consequently cover a larger fraction of evanescent field and lead to the higher signal changes [2]. This is somehow similar Förster resonance energy transfer (FRET) utilized in fluorescence-based sensors, showing a comparable distance dependent sensitivity. This non-radiative energy transfer only occurs if two light-sensitive molecules are very close, usually within less than 10 nm [3].

The higher surface sensitivity, together with the advantage of low sample volumes in the µL range make nanostructured surface a powerful tool in label free detection for single-shot devices as well as for continuous online monitoring in complex media. However, on the way of nanostructured surfaces to widespread applications as sensors still several limitations and challenges need to be addressed, which will be discussed in this chapter as well as future trends for improved design and performance.

6.1 Fabrication of Nanostructured Surfaces

Important aspects for fabrication of nanostructured surfaces are flexibility, time consumption and scalability [4]. The represented results indicate that self-assembly techniques are highly advantageous for the design of sensors. Substrates can be quickly patterned over large areas (in the range of cm) and high throughput is enabled, overcoming the limitations of conventional lithography. Such bottom-up approaches rely on the arrangement of nanoparticles or co-polymers forming the shape of the structures influenced by parameters like type of solvents, evaporation time or mixing ratio [5]. The ease of manipulation of the shape and dimensions combined with large-area coverage makes them highly suitable for sensor applications in contrast to the rigid and lengthy conventional lithographic techniques. For prototyping and for fabrication that require a maximum control in terms of precision and resolution [6], techniques such as electron

beam lithography (EBL) and focused ion beam (FIB) milling are still the best solution [7]. In the case one needs to detect or image single molecules these lithographic techniques are still recommended as high regularity and high reproducibility will provide higher resolution and higher sensitivity [8]. For most applications, as shown for surface plasmon resonance spectroscopy (SPR) and plasmon-enhanced upconversion (PEU) applications, self-assembly techniques are sufficient. They allow for large scale fabrication with a high flexibility of the nanostructured surface and a sufficient resolution with a few defects due to formation process and its parameters [9]. Limitless structural variety in the nanometer range can be generated by self-assembly techniques like block copolymers [10] or colloidal nanocrystals [11] as nanostructure building blocks. In addition, the opportunities to transfer these nanostructured motives by pattern transfer printing [12], covalent bonding-assisted nanotransfer [13] or solvent assisted nanotransfer printing [14], extends their use to almost any substrate of choice, even complex hybrid materials which cannot resist high temperature, vacuum or certain solvents, needed for lithographic fabrication. Although for accessing new types of structures, sizes and a better understanding and control of influencing parameters like solvent, temperature and concentration of the components is still needed [12,15]. For transducing techniques utilizing hot spots, like surface enhanced Raman scattering (SERS) on nanostructured surfaces the number of spots and hence the sensing capabilities are limited to the surface area of the substrate. Concepts for increasing the number of hot spots by the use of stacks of nanostructures are currently developed. The group of Y. S. Jung used the self-assembly of block copolymers and solvent-assisted nano-transfer printing for the fabrication of different nanostructured stacks. Multistacked nanowires increased the sensing performance of SERS with a maximum enhancement factor (EF) of 4.1×107 for two-layer silver (Ag) nanorods on a continuous Ag film with regard to a continuous Ag film [5]. The additional hot spots contribute to the performance as well as plasmonic coupling between the layers. Limiting factor is the maximum penetration depth of the incident light into the substrate and from which Raman-scattered photons can get out to be collected by the detector. Nano-assemblies fabricated by stacks of gold allows for size miniaturization and hole densification. For such systems a four times larger shift in the resonance peaks in comparison to a continuous gold film was reported for changes in refractive index [14]. Nevertheless, it should be mentioned that these improvements come with more and complex fabrication steps. This makes the development of such systems somehow elaborative, but for an established system all fabrication steps can be easily integrated in a production line.

At the moment one can observe a trend in literature to investigate different fabrication methods for different nanostructures. The large variety of present nanostructures consist of many different objects, most prominently nanostars [16] or nanotriangles [17]. Often the research focusses on structural changes of the specific design to gain specific plasmonic properties enabling signal enhancements [18]. The lack of systematic studies of the impact of one nanostructure with different sizes, periodicity and materials for sensing makes the assessment an ultimate structure and dimension very difficult so far.

6.2 Concepts for Sensing

Properties arising from the nanostructured surfaces lead to improved sensor designs. Various characteristics of the light interacting with the plasmonics of the nanostructure such as intensity, phase and wavelength can be measured, and their change subsequently translated to an analyte concentration. Therefore, a variety of techniques such as transmission, fluorescence, SPR and surface enhanced Raman scattering (SERS) take benefit from the localized plasmons, resulting in a boost of the sensing capabilities. It should be mentioned, that not all surface sensitive optical spectroscopy techniques can be improved by nanostructured substrates. Infrared attenuated total reflection (ATR) Spectroscopy depends on a diamond waveguide attached to an optical coupling element. Plamonic nanostructures attached to the surface provide enhanced spectral signatures in the infrared (IR) regime [19]. However, the plasmon frequencies of metals are fixed after structuring and limit the detection of multiple IR bands across a broad spectral range and the penetration depth of ATR configuration appears to be within a few micrometers [20]. Another very popular surface sensitive technique is reflectometric interference spectroscopy, which is based on white light beam inference with a glass transducer coated with a recognition layer, resulting in an interference patterns that shift with analyte binding. This method concentrates on changes in optical thickness and is sensitive within 100 nm, leading to an intrinsic high surface sensitivity [21] and does not require the use of nanostructured surfaces.

The higher surface sensitivity was demonstrated in this thesis by the combination of nanohole arrays (NAs) as a nanostructured surface and graphene as a 2D nanomaterial. Analyzing the shift in the resonance angle with SPR for the assembly of reduced graphene (rGO) on NAs, a 250-380% higher effect was found compared to a continuous gold film. In this system the combination of graphene plasmonic modes interacting with

the plasmonic properties of the nanostructures in addition with an atomically thin receptor layer minimally extending into the EMF is decisive. For analytical application the resolution of refractive index changes induced by small biomolecules binding or absorbing in close distance to the surface is the key issue. In this context, the nanoengineered system was able to decrease the limit of detection by one order of magnitude for diethyl phthalate in sea water without any pretreatment compared to a continuous gold film. A homogenous surface coverage and functionalization is a fundamental requirement for all sensor designs. The increased sensitivity of the nanostructured surfaces, especially in combination with single molecule detection, generates the need to meet even higher standards [22]. The enhanced sensing performances for homogenous and highly regular receptor layers was demonstrated in this work with a comparative study of reduced graphene oxide and chemical vapor deposition (CVD) graphene on NAs with same nanodimensions. In this proof-of-concept studies the capabilities of label-free plasmonic sensors and the importance of a thin and uniform receptor layer in close proximity to the nanostructured surface are confirmed. The system and findings can be advantageous to other transducers that require LSP.

For pushing graphene and other to 2D-matrials forward as receptor layers, better understanding of the optical and electrochemical (such as surface area and conductivity) properties by spectroscopic methods is important. Variations in the properties result from the fabrication process, which introduces defects and sheet size correlation [23]. Another parameter is selectivity, which is not intrinsically present in such materials. Approaches combining nanosheet generation and functionalization in parallel, like electrochemical exfoliation, become advantageous as the number of fabrication steps is reduced [24]. For better characterization of the functionalized 2D-material surface and their interaction with biomolecules atomic force microscopy and scanning tunneling microcopy analysis can be helpful.

For PEU and SERS edges and corners of nanostructures, so-called hot spots, create the largest local EMF enhancement and therefore represent the area of the highest signal increase. Light is focused to the hot spots, which serve as nanoantennas [25]. Upconversion nanoparticles (UCNPs) can benefit from the attachment to nanostructured surfaces. A self-assembled monolayer (SAM) on the gold triangle arrays (TA) is a simple and effective method for binding of the oleic acid modified particles via van der Waals interaction. The luminescence of UCNPs in the UV is enhanced by a factor of about six on TA compared to a continuous film and an optical sensor for vitamin B12 with a limit

of detection of 0.6 nM was constructed. This approach overcomes the limits in transmission spectroscopy of reduced sensitivity by light scattering in the UV region of the electromagnetic spectrum. A further development of the system can be conducted with introducing selectivity by attaching an aptamer to the surface of the UCNPs, leading to better sensitivity for point of care diagnostics [26]. Since such intensity-based read-out systems strongly depend on the excitation power density of the laser and the UCNP concentration, investigation of the FRET is an alternative option. Applications utilizing FRET take profit from plasmonic features, as demonstrated for gold nanoparticles (AuNPs) conjugated with aptamers and UCNPs functionalized with corresponding complementary DNA. The coupling with LSP extends the energy transfer rate and the distance of "classic" allowed dye-to-dye FRET pairs to ~20 nm, resulting in a low limit of detection (LOD) of 3 cfu·mL^{-1} for *E. coli* and a large linear relationship in the detection range of 5-10^6 cfu·mL^{-1} [27]. Locally enhanced fields created at hot spots can be beneficial for SERS. In a short extent the plasmonic enhancement for NAs compared to a continuous gold film with the deposition of different graphene types on the surface was illustrated with a ~3-times and ~12-times higher Raman signal for CVD graphene and rGO, respectively. Raman spectroscopy was applied in this thesis only for characterization of different graphene types and the homogeneity of the transfer method and not as transducer for sensor design. It has already been shown that plasmonic feature are capable for improving in vivo diagnostics, multimodal imaging [28] and allow for label-free nanometer-resolution [29] based on SERS. In this context a remarkable super-resolution chemical imaging and localization within 10 nm is achieved with dynamic illumination technique on NAs [18]. A nanoengineered surface consisting of a TA and graphene can be utilized for SERS due to signal enhancement, resulting from the coupling of the LSP present at hot spots and graphene plasmonics. With Raman markers like 5-ethynyl-2´-deoxyuridine (EdU), which are taken up by the cell and show a signal in the "silent" cell region due to the presence of alkynes (C≡C), the high potential of Raman spectroscopy for cell analysis was verified [30]. Adapting this principle to the nanoengineered surface with an increased surface sensitivity and considering the biocompatibility of graphene [31], the analysis of cells with this system can improve imaging of cells and studying processes at the cell membrane. Long term monitoring can be performed, which is often a problem within fluorescence imaging due to photobleaching of the fluorophore. Additionally, with higher signals the laser power can be reduced, or the laser wavelength can be increased. Raman scattering is proportion to the laser wavelength (Λ) with Λ^{-4} and thus a longer wavelength results in a reduced

scattering. Therefore, a longer wavelength than 532 nm is often not used although it decreases interrupting fluorescence. If the signal is increased the sensitive is still high for a longer wavelength with the advantages of fluorescence reduction.

Transmission spectroscopy is a simple, widely known and applied technique. Limitations are broad absorption peaks, the low sensitivity and high sample volume arising from Beer's law [32,33]. Nanostructured surfaces can be operated in a such collinear optical configuration. The resulting effects can significantly improve transmission spectroscopy. NAs are a prominent plasmonic system, that is feasible for interrogation in such a setup [34]. Sharp extraordinary optical transmission (EOT) resonance is present on periodic NAs, arising from grating effects and interplay of coherently interfering resonant interactions [35]. For investigation of the transmission spectra of NA in the near infrared region (NIR) a self-made setup was designed (Fig. 6.1 B). A halogen lamp dealt as light source and portable high performance near-infrared (NIR) spectrometer of the size of a credit card with high-throughput Czerny-Turner optics with a fanless TEC-cooled InGaAs image sensor was used for detection. Optimized illumination of the NA and light collection was achieved by a combination of plano convex lenses and a positive meniscus lens, that ensures a short focal length without introducing significant spherical aberration. A holder for the nanostructured surfaces was designed and mounted on a motorized goniometer for angular changes. Preliminary results display a few sharp peaks sensitive to changes in the bulk refractive index in the investigated wavelength range (Fig. 6.1 A). The occurring sharp peaks in the spectra for EOT can be assigned with the Bloch-wave SPP equation [36] (Fig. 6.1 D). Only peaks resulting from the gold-dielectric are sensitive for refractive index unit (RIU) changes. The peak at around 1400 nm is assigned to the glass-gold interface and therefore not effected by the RIU. For the peak and dip of ~1200 nm the highest sensitivity was found. A large dynamic range was determined for EOT and compared to SPR (Fig. 6.1 C). The fit of the linear signal change upon refractive index change is slightly better in terms of the error for SPR. Even if the linear regression over such a large RIU range does not have the same precision for EOT compared to SPR, the sensitivity can be better, because wavelength changes can be monitored with higher precision than changes in angular positions. Changes in the µRIU range are of analytical interest. Using NA with SPR that means a mechanical movement of 3.4 angular seconds and for EOT a wavelength change of 0.008 nm needs to be monitored. The desired angular resolution can be hardly achieved with stepper motors. Bulky gear system need to be sued for such high resolution. The same seems to be the case for the spectrometer used in this study. It generates a resolution of 4 nm by a

512 pixel sensor. A 500 times improvement of the resolution is needed to discriminate to 0.008 nm, meaning 256,000 pixel. Considering that sensors with 1.3 megapixels are available with similar chip size and minimization of the spectral range, for instance to the second biological window, allows to use all 1.3 megapixel for maximized wavelength resolution, the differentiation of µRIU with EOT seems feasible in near future. The development speed of miniaturized camera chips in smartphones [37] indicates that EOT has a very promising future and could outperform the SPR resolution in the future.
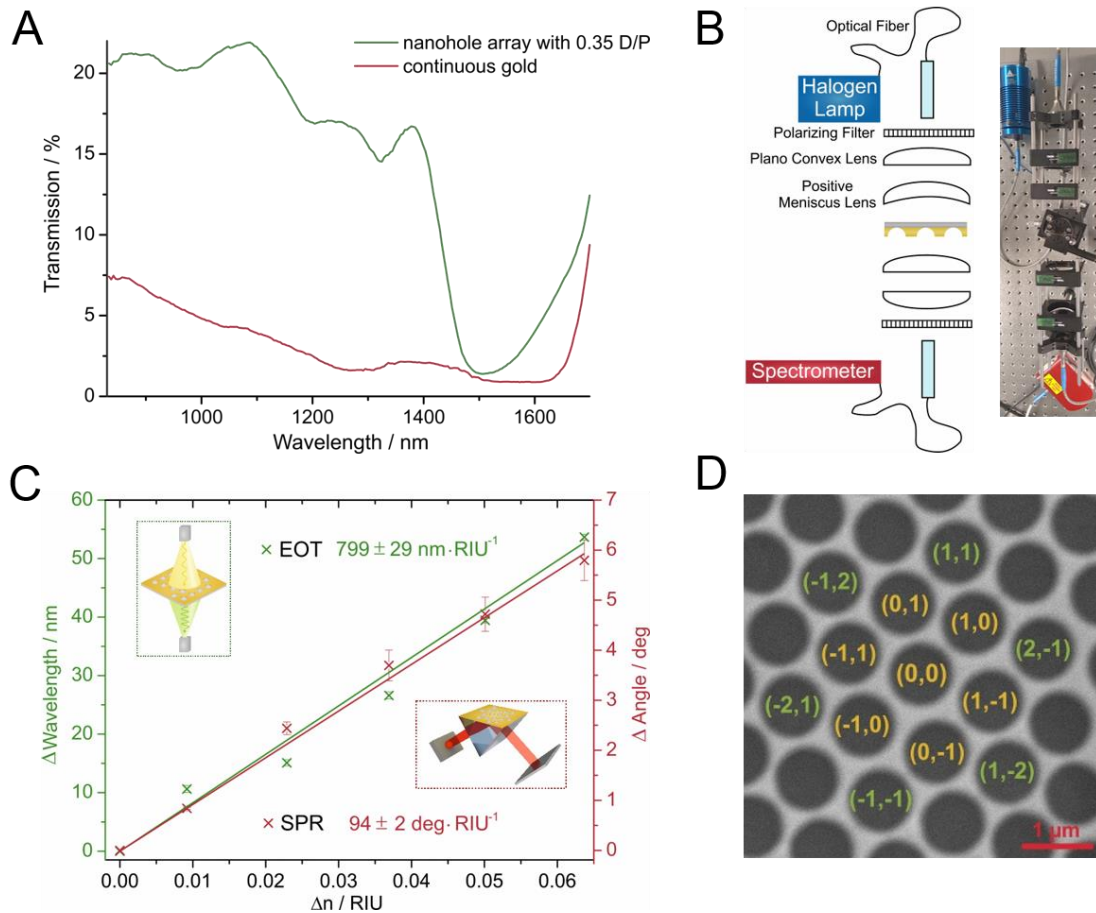

Figure 6.1 (A) Transmission spectra of a continuous gold film and a nanohole arrays (NA) with a D/P ratio of 0.35. As a reference a blank glass slide was used. The interrogation time is 0.75 s and the spectra are averaged over 100 measurements. (B) Schema of the transmission spectroscopy setup aside with a photo showing the laboratory system. (C) Comparison of the plasmonic shift upon refractive index change for SPR indicated as the angular shift and respectively the wavelength shift for EOT. (D) Exemplary SEM image of a NA. Scale bar is 1 µm and indicated are the different plasmonic bands which can be assigned.

The key messages of the comparison of SPR and EOT are: a) both techniques cover a large range of RIU with linear signal change, b) EOT set-up is simpler and cheaper and c) EOT might have a better dynamic range and higher sensitivity. Notably, in SPR normally the intensity changes at constant angle is measured, which has an even higher sensitivity. These values are very difficult to compare as they strongly depend on the power of the incident light and they are only valid under certain conditions. For EOT also intensity-based measurements are possible. High power light-emitting diodes (LEDs) with a power of up to 60 mW (at the relevant wavelength in the NIR) will be beneficial compared to 640 nm laser diodes in the 10 mW used in SPR. Additionally, the simple experimental excitation setup of EOT allows for miniaturizing compared to the SPR, which has to fulfil the coupling conditions.

The advantages of nanostructured surfaces in the UV/IVs range have been proven with UCNPs. Shifting the spectral range to the NIR comes with the following attractive features for future sensor design: Reduced phototoxicity and photobleaching, minimized scattering and absorption, and reduced background fluorescence [38].

The next challenge, which needs to be addressed is selectivity. Recently researchers are more and more working on concepts for introducing selectivity without losing the label-free nature of the LSP. A wider scope of nanostructured surfaces with impressive opportunities for spectroscopy has been depicted by H. Altug *et al.* in 2018. With the technique of a 2D pixelated dielectric metasurface neither a spectrometry nor frequency scanning or moving mechanical parts are required (Fig 6.2 C) [39]. The system only depends on a nanostructured surface, a beam splitter and an objective. Metasurfaces are artificial optical media consisting of subwavelength metallic and dielectric building blocks, characterized by optical phenomena not present in naturally occurring materials [40]. The metasurface consists of multiple arrays with sub elliptical structure (Fig 6.2 A and B). Ultrasharp resonances of the metasurface can be tuned to a discrete frequency and results in a molecular signature that can read out separately by multiple spectral points (Fig 6.2 D). Molecular absorption features can be read-out at various structural points. An absorption map similar to a barcode, that can be used for imaging is the result. Molecular fingerprint of a large range of biomolecules can detected with high sensitivity using this mid-infrared imaging system [39]. The findings will pave the way for other compact and high-performance multiplexing imaging applications of nanostructured surfaces without the need of bulky instruments.
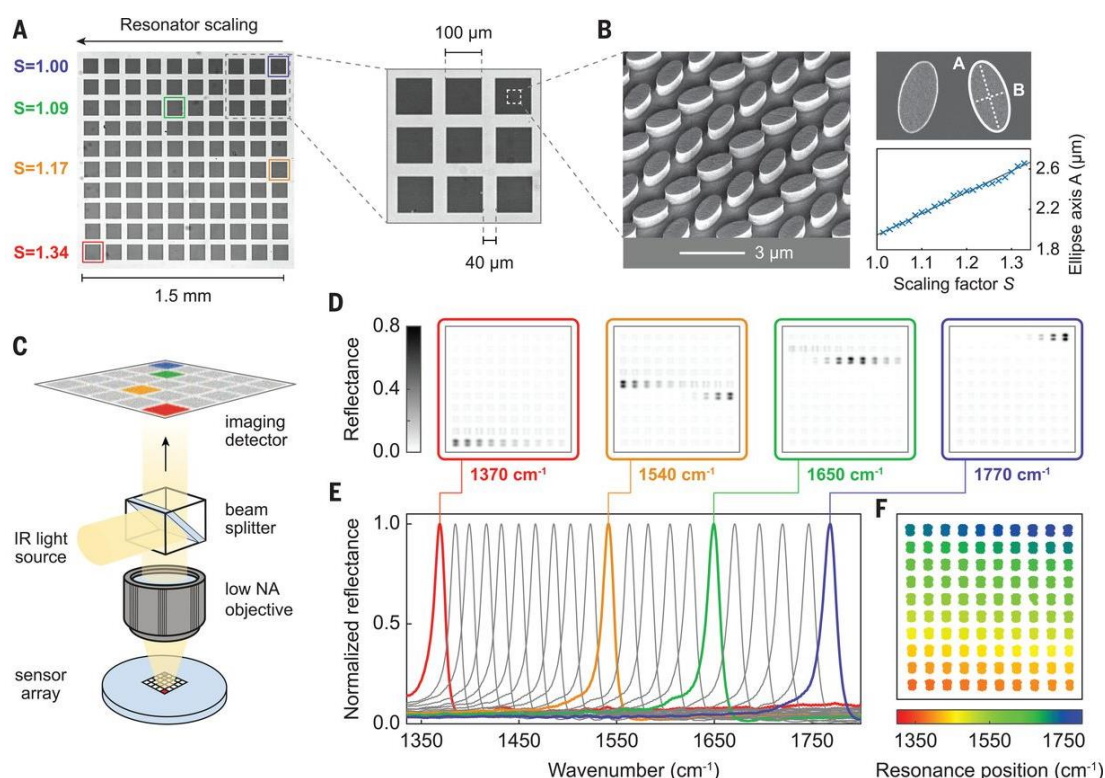
Figure 6.2 Experimental setup and detection with pixelated metasurfaces. (A) Optical images of the fabricated 100-pixel metasurface. (B) SEM image of the ellipse structure and the featured size. (C) Schematic of the imaging-based on the mid-IR microscopy system with metasurface arrays (D) Reflectance images of four recorded specific wavenumbers of the pixelated metasurface in the mid-IR spectral range. (E) Normalized reflectance spectra for 21 of the 100 metapixels. The colored curves of the resonance positions correspond to the respective reflectance images in (D). (F) Image of all metapixels at extracted resonance positions. Picture adapted with permission from Ref [39] © (2018) The American Association for the Advancement of Science.

The label-free, multiplexing and esay-read out ability of nanostructured surfaces with various transducers is convenient for the design of sensor networks. The aim is to continuously monitor changes in real-time with high sensitivity and multiple sensor combinations. In contrast to label-free approaches, the requirement of labels for selective detection has the drawback of the recovery of the recognition united, leading to only short-time usage. The reduced selectivity of label-free approaches will be more than compensated by the network of multiple arrays on one sensor and with other sensors. By data acquisition, data fusion and correlation for long terms the sensor network progresses and "learns" to interpreted and translates signal patterns into user friendly results [41]. This concept is known as machine learning and has become a pervasive attempt to improve modern life *e.g.* license plate-reading algorithms based on digital

camera images for tracking [42]. Smartphones, smart homes, and smart cars are emerging technologies in which analytical chemistry becomes an integral part by incorporating sensors for *e.g.* temperature sensors or health monitoring. Distributed sensors communicating with networked analytical labs will provide information which drives automated and leads to applications including health care, industrial processes and environmental monitoring. [43]. In the last years, sensor networks combined with machine learning have been used for environment monitoring such as temperature, humidity and gas concentration [44]. Nanostructured surfaces will contribute in the future to this field as a highly sensitive and tunable platform for the design of sensor arrays with multiple transducing techniques. Nanoengineered surfaces in combination with machine learning can improve fabrication process, quality control and detection of counterfeits. The ambitious goal of the implementation of nanostructured surfaces is the increase of safety in all matters, leading to higher standards of living and improvements in daily life.

6.3 References

[1]   Estevez M, Otte MA, Sepulveda B, Lechuga LM (2014) Trends and challenges of refractometric nanoplasmonic biosensors: a review. Anal Chim Acta 806:55–73.

[2]   Piliarik M, Kvasnička P, Galler N, Krenn JR, Homola J (2011) Local refractive index sensitivity of plasmonic nanoparticles. Opt Express 19:9213–9220.

[3]   Hildebrandt N, Spillmann CM, Algar WR, Pons T, Stewart MH, Oh E, Susumu K, Díaz SA, Delehanty JB, Medintz IL (2017) Energy Transfer with Semiconductor Quantum Dot Bioconjugates: A Versatile Platform for Biosensing, Energy Harvesting, and Other Developing Applications. Chem Rev 117:536–711.

[4]   Lee SH, Lindquist NC, Wittenberg NJ, Jordan LR, Oh S (2012) Real-time full-spectral imaging and affinity measurements from 50 microfluidic channels using nanohole surface plasmon resonance. Lab Chip 12:3882–3890.

[5]   Jeong JW, Arnob MMP, Baek K, Lee SY, Shih W, Jung YS (2016) 3D Cross-Point Plasmonic Nanoarchitectures Containing Dense and Regular Hot Spots for Surface-Enhanced Raman Spectroscopy Analysis Adv Mat 28:8695–8704.

[6]   Hong KY, Menezes JW, Brolo AG (2018) Template-Stripping Fabricated Plasmonic Nanogratings for Chemical Sensing. Plasmonics 13:231–237.

[7]   Horák M, Bukvišová K, Švarc V, Jaskowiec J, Křápek V, Šikola T (2018) Comparative study of plasmonic antennas fabricated by electron beam and focused ion beam lithography. Sci Rep 8:9640.

[8]   Scheible MB, Pardatscher G, Kuzyk A, Simmel FC (2014) Single molecule characterization of DNA binding and strand displacement reactions on lithographic DNA origami microarrays. Nano Lett 14:1627–1633

[9]   Genslein C, Hausler P, Kirchner E, Bierl R, Baeumner AJ, Hirsch T (2016) Graphene-enhanced plasmonic nanohole arrays for environmental sensing in aqueous samples. Beilstein J Nanotechnol 7:1564–1573.

[10] Sarkar B, Alexandridis P (2015) Block copolymer–nanoparticle composites: Structure, functional properties, and processing. Prog Polym Sci 40:33–62.

[11] Boles MA, Engel M, Talapin DV (2016) Self-Assembly of Colloidal Nanocrystals: From Intricate Structures to Functional Materials. Chem Rev 116:11220–11289.

[12] Paik T, Yun H, Fleury B, Hong S, Jo PS, Wu Y, Oh S, Cargnello M, Yang H, Murray CB, Kagan CR (2017) Hierarchical Materials Design by Pattern Transfer Printing of Self-Assembled Binary Nanocrystal Superlattices. Nano Lett 17:1387–1394.

[13] Hwang SH, Jeon S, Kim MJ, Choi D, Choi J, Jung J, Kim K, Lee J, Jeong JH, Youn JR (2017) Covalent bonding-assisted nanotransfer lithography for the fabrication of plasmonic nano-optical elements. Nanoscale 9:14335–14346.

[14] Yim S, Jeon S, Kim JM, Baek KM, Lee GH, Kim H, Shin J, Jung YS (2018) Transferrable Plasmonic Au Thin Film Containing Sub-20 nm Nanohole Array Constructed via High-Resolution Polymer Self-Assembly and Nanotransfer Printing. ACS Appl Mater Interfaces 10:2216–2223.

[15] Weidman MC, Nguyen Q, Smilgies D, Tisdale WA (2018) Impact of Size Dispersity, Ligand Coverage, and Ligand Length on the Structure of PbS Nanocrystal Superlattices. Chem Mater 30:807–816.

[16] Li A, Tang L, Song D, Song S, Ma W, Xu L, Kuang H, Wu X, Liu L, Chen X, Xu C (2016) A SERS-active sensor based on heterogeneous gold nanostar core-silver nanoparticle satellite assemblies for ultrasensitive detection of aflatoxinB1. Nanoscale 8:1873–1878.

[17] Scarabelli L, Coronado-Puchau M, Giner-Casares JJ, Langer J, Liz-Marzán LM (2014) Monodisperse gold nanotriangles: size control, large-scale self-assembly, and performance in surface-enhanced Raman scattering. ACS Nano 8:5833–5842.

[18] Olson AP, Ertsgaard CT, Elliott SN, Lindquist NC (2016) Super-Resolution Chemical Imaging with Plasmonic Substrates. ACS Photonics 3:329–336.

[19] Bibikova O, Haas J, López-Lorente ÁI, Popov A, Kinnunen M, Ryabchikov Y, Kabashin A, Meglinski I, Mizaikoff B (2017) Surface enhanced infrared absorption spectroscopy based on gold nanostars and spherical nanoparticles. Anal Chim Acta 990:141–149.

[20] Hu Y, López-Lorente ÁI, Mizaikoff B (2018) Versatile Analytical Platform Based on Graphene-Enhanced Infrared Attenuated Total Reflection Spectroscopy. ACS Photonics 5:2160–2167.

[21] Proll G, Markovic G, Fechner P, Proell F, Gauglitz G (2017) Reflectometric Interference Spectroscopy. Methods Mol Biol 1571:207–220.

[22] Lin D, Wu Z, Li S, Zhao W, Ma C, Wang J, Jiang Z, Zhong Z, Zheng Y, Yang X (2017) Large-Area Au-Nanoparticle-Functionalized Si Nanorod Arrays for Spatially Uniform Surface-Enhanced Raman Spectroscopy. ACS Nano 11:1478–1487.

[23] Nicolosi V, Chhowalla M, Kanatzidis MG, Strano MS, Coleman JN (2013) Liquid Exfoliation of Layered Materials. Science 340:1226419.

[24] Ossonon BD, Bélanger D (2017) Functionalization of graphene sheets by the diazonium chemistry during electrochemical exfoliation of graphite. Carbon 111:83–93.

[25] Anker JN, Hall WP, Lyandres O, Shah NC, Zhao J, van Duyne RP (2010) Biosensing with plasmonic nanosensors. Nature Mat 7:308–319.

[26] Wu S, Duan N, Shi Z, Fang C, Wang Z (2014) Simultaneous aptasensor for multiplex pathogenic bacteria detection based on multicolor upconversion nanoparticles labels. Anal Chem 86:3100–3107.

[27] Jin B, Wang S, Lin M, Jin Y, Zhang S, Cui X, Gong Y, Li A, Xu F, Lu TJ (2017) Upconversion nanoparticles based FRET aptasensor for rapid and ultrasenstive bacteria detection. Biosens Bioelectron 90:525–533.

[28] Henry A, Sharma B, Cardinal MF, Kurouski D, van Duyne RP (2016) Surface-Enhanced Raman Spectroscopy Biosensing: In Vivo Diagnostics and Multimodal Imaging. Anal Chem 88:6638–6647.

[29] Ayas S, Cinar G, Ozkan AD, Soran Z, Ekiz O, Kocaay D, Tomak A, Toren P, Kaya Y, Tunc I, Zareie H, Tekinay T, Tekinay AB, Guler MO, Dana A (2013) Label-free nanometer-resolution imaging of biological architectures through surface enhanced Raman scattering. Sci Rep 3:2624

[30] Wei L, Hu F, Shen Y, Chen Z, Yu Y, Lin CC, Wang MC, Min W. Live-cell imaging of alkyne-tagged small biomolecules by stimulated Raman scattering. Nat Methods 11:410.

[31] Zhang X, Wang L, Lu Q, Kaplan DL (2018) Mass Production of Biocompatible Graphene Using Silk Nanofibers. ACS Appl Mater Interfaces in press 10.1021/acsami.8b04777

[32] Adato R, Altug H (2013) In-situ ultra-sensitive infrared absorption spectroscopy of biomolecule interactions in real time with plasmonic nanoantennas. Nat Commun 4:2154.

[33] Lohumi S, Lee S, Lee H, Cho B (2015) A review of vibrational spectroscopic techniques for the detection of food authenticity and adulteration. Trends Food Sci Technol 46:85–98.

[34] Ballard ZS, Shir D, Bhardwaj A, Bazargan S, Sathianathan S, Ozcan A (2017) Computational Sensing Using Low-Cost and Mobile Plasmonic Readers Designed by Machine Learning. ACS Nano 11:2266–2274.

[35] Belushkin A, Yesilkoy F, Altug H (2018) Nanoparticle-Enhanced Plasmonic Biosensor for Digital Biomarker Detection in a Microarray. ACS Nano 12:4453–4461.

[36] Couture M, Live LS, Dhawan A, Masson J (2012) EOT or Kretschmann configuration? Comparative study of the plasmonic modes in gold nanohole arrays. Analyst 137:4162–4170.

[37] Lee K, You M, Tsai C, Lin E, Hsieh S, Ho M, Hsu J, Wei P (2016) Nanoplasmonic biochips for rapid label-free detection of imidacloprid pesticides with a smartphone. Biosens Bioelectron 75:88–95

[38] Jaque D, Martínez Maestro L, del Rosal B, Haro-Gonzalez P, Benayas A, Plaza JL, Martín Rodríguez E, García Solé J (2014) Nanoparticles for photothermal therapies. Nanoscale 6:9494–9530.

[39] Tittl A, Leitis A, Liu M, Yesilkoy F, Choi D, Neshev DN, Kivshar YS, Altug H (2018) Imaging-based molecular barcoding with pixelated dielectric metasurfaces. Science 360:1105–1109.

[40] High AA, Devlin RC, Dibos A, Polking M, Wild DS, Perczel J, Leon NP de, Lukin MD, Park H (2015) Visible-frequency hyperbolic metasurface. Nature 522:192–196.

[41] Luo X, Chang X (2015) A novel data fusion scheme using grey model and extreme learning machine in wireless sensor networks. Int J Control Autom Syst 13:539–546.

[42] Kubota KJ, Chen JA, Little MA (2016) Machine learning for large-scale wearable sensor data in Parkinson's disease: Concepts, promises, pitfalls, and futures. Mov Disord 31:1314–1326.

[43] Mayer M, Baeumner AJ (2018) ABC Spotlight on Analytics 4.0. Anal Bioanal Chem 410:5095-5097

[44] Zou T, Wang Y, Wang M, Lin S (2017) A Real-Time Smooth Weighted Data Fusion Algorithm for Greenhouse Sensing Based on Wireless Sensor Network. Sensors 17:2555.

7 Summary

The thesis describes the fabrication, functionalizing and (bio)analytical applications of nanostructured surfaces based on plasmonic effects. In **Chapter 1** a review of the physical requirements of plasmons and as well as design and fabrications concepts are provided with emphasis on nanostructured platforms. Sensor applications of plasmonic nanostructured surfaces are introduced. The aim of this work is outlined in **Chapter 2** to investigate nanostructured gold surfaces in their sensing capabilities in SPR and utilizing the hot spots of such structures in other optical transducing techniques.

The fabrication of nanohole arrays with different hole sizes *via* a modified nanosphere lithography is reported in **Chapter 3**. Nanostructured surfaces were modified with reduced graphene oxide (rGO) as a thin receptor layer via spin-coating. In a comparison to a continuous film, nanohole arrays displayed a 250 - 350% higher shift in the SPR angle. The capabilities of nanohole arrays modified with rGO were investigated with the detection of the plasticizer diethyl phthalate in water. With the analysis of a small analyte binding to graphene *via* π-stacking on nanohole arrays with varying hole diameter, the effect of the plasmonic field on (bio)sensors was studied. For the nanohole array with a diameter-to-periodicity ratio of 0.43 roughly 12-fold enhancement of the maximum signal response was observed and a 10-times better LOD of ~20 nM was determined. The feasibility of the rGO-modified nanohole array as sensor platform was demonstrated with the analysis of environmental water samples without pre-treatment. Surprisingly the combination of the graphene with gold nanostructures resulted in further signal enhancement compared to continuous gold films. This effect can be assigned to an additional plasmonic enhancement by the 2D carbon nanomaterial itself.

Chapter 4 deals with a more detailed investigation of the graphene receptor layer. The modification and sensing properties of differently prepared graphene, which differ in flake size, number of layers and numbers of defects types was studied on nanostructured surfaces. A wet transfer method for chemical vapor deposition (CVD) graphene was introduced. The more homogenous and reproducible graphene films on nanohole arrays were yielded for CVD graphene when compared to rGO with Raman spectroscopy. The higher signal response for CVD graphene is attributed to less defects and a large uniform layer. A 7-fold lower LOD 0.9 µM for a CVD-modified nanohole array for the detection of adenine with SPR revealed the enhanced sensing performance.

In **Chapter 5** the enhanced luminescence of NIR to UV upconversion at a nanostructured surface is described. An nanoengineered interface consisting of NaYF$_4$:Yb,Tm

upconversion nanoparticles and a gold nanotriangle array was fabricated by a self-assembly method. Upconversion nanomaterials are known for low quantum efficiency which clearly hinders a wider impact of these materials in many applications. Hot spots of the nanostructured surface provided a local electromagnetic field enhancement, that improved the 4-photon upconversion process at 345 nm with an about six-times higher emission intensity. For UCNPs dispersed in solution, this emission is usually too weak to be used in any analytical application. Assembled as a nanoengineered interface a sensor for the detection of vitamin B12 in serum was constructed. A LOD of 0.6 ± 0.2 nM was found. The strong enhancement in the UV emission at a very low laser density of 13 W·cm^{-2} is outstanding and a very promising fact for the development of miniaturized point-of-care diagnostics.

Challenges of nanostructured surfaces are addressed in **Chapter 6.** Preliminary results of a designed transmission setup for nanostructured surfaces are presented. Nanohole arrays are capable of extraordinary optical transmission and can significantly improve (bio)sensors based on transmission. Future directions and perspectives of nanostructured surfaces are highlighted.

8 Zusammenfassung

Die vorliegende Dissertation beschreibt die Fabrikation, Funktionalisierung und (bio)analytische Anwendungen von nanostrukturierten Oberflächen. **Kapitel 1** gibt einen Überblick der physikalischen Voraussetzungen von Plasmonen sowie Design- und Fabrikations-Konzepte mit dem Schwerpunkt auf nanostrukturierte Plattformen. Sensorische Anwendungen dieser Strukturen werden vorgestellt. Die wissenschaftliche Fragestellung dieser Arbeit wird in **Kapitel 2** beschrieben. Nanostrukturierte Oberflächen sollen hinsichtlich ihrer sensorischen Eigenschaften mit SPR untersucht werden. Eine weitere mögliche Anwendung wäre das Ausnutzen der Hotspots dieser Strukturen mit anderen optischen signalübertragenden Techniken.

Die Herstellung von Nanohole Arrays mit unterschiedlichen Lochgrößen über eine Nanokugel-Lithographie wird in **Kapitel 3** beschrieben. Über Rotationsbeschichtung werden die nanostrukturierten Oberflächen mit reduziertem Graphenoxid (rGO), das eine dünne Rezeptorschicht bildet, modifiziert. Im Vergleich zu einem kontinuierlichen Film, zeigen Nanohole Arrays eine 250 - 300% größere Verschiebung des SPR Winkels. Die Einsatzmöglichkeit von rGO-modifizierten Nanohole Arrays wurde mit der Detektion des Weichmachers Diethylphthalat in Wasser gezeigt. Der Effekt des plasmonischen Feldes auf (Bio)sensoren wurde durch die Veränderung der Lochgröße mit der Analyse der Bindung eines kleinen Moleküls über π-π-Wechselwirkungen an Graphen untersucht. Ein Nanohole Array mit einem Durchmesser-zu-Periodizität-Verhältnis von 0.43 zeigte ungefähr eine 12-fache Verstärkung in der maximalen Signalantwort und eine 10-fach geringere Nachweisgrenze wurde festgestellt. Die Umsetzbarkeit der rGO-modifizierten Nanohole Arrays als Sensorplattform wurde mit einer Analyse von nicht vorbehandelten ökologischen Wasserproben untersucht. Überraschenderweise, zeigte die Kombination von Graphen und Gold Nanostrukturen eine weitere Signalverstärkung im Vergleich zu einem kontinuierlichen Gold Film. Dieser Effekt lässt sich einer zusätzlichen plasmonischen Verstärkung durch das 2D-Kohlenstoff-Nanomaterial zuordnen.

Kapitel 4 untersucht die Graphen Rezeptorschicht im Detail. Die Modifikations- und Sensor-Eigenschaften von unterschiedlich hergestelltem Graphen, welche in ihrer Flockengröße, der Anzahl der Lagen und der Anzahl an Defekten variieren, wurden auf nanostrukturierten Oberflächen untersucht. Durch chemische Gasphasenabscheidung (CVD) hergestelltes Graphen wurde über eine Nasstransfer Methode aufgebracht. Ein

homogenerer und reproduzierbarer Graphen Film auf Nanohole Arrays wurde für CVD Graphene gefunden, durch einen Vergleich zu rGO mittels Raman Spektroskopie. Die gesteigerte Signalantwort für CVD Graphene entsteht durch weniger Defekte und eine größere uniforme Schicht. Eine 7-fach kleinere Nachweisgrenze für CVD-modifizierte Nanohole Arrays für die Detektion von Adenine mit SPR demonstrierte die verstärkte sensorische Leistungsfähigkeit.

Die erhöhte Lumineszenz der NIR zu UV Aufkonvertierung an nanostrukturierten Oberflächen wird in **Kapitel 5** beschrieben. Eine nanokonstruierte Schnittstelle bestehend aus $NaYF_4$:Yb,Tm aufkonvertierenden Nanopartikeln (UCNPs) und einem Gold Nanotriangle Array wurde über Selbstorganisation hergestellt. Die UCNPs zeigen eine geringe Quantenausbeute, welche eine breitere Auswirkung dieser Materialien in vielen Anwendungen deutlich erschwert. Eine lokale Verstärkung des elektromagnetischen Feldes entsteht an den Hotspots der nanostrukturierten Oberfläche. Diese führte zu einer ca. 6-fach größeren Emissionsintensität des 4-Photonen aufkonvertierenden Prozesses bei 345 nm. Für in Lösung dispergierte UCNPs ist diese Emission normalerweise zu schwach um für analytische Anwendungen verwendet zu werden. Die zusammengeführte nanokonstruierte Schnittstelle wurde verwendet, um einen Sensor für Vitamin B12 zu entwickeln. Eine Nachweisgrenze von 0.6 ± 0.2 nM wurde festgestellt. Die große Verstärkung der UV Emission bei einer sehr geringen Laserleistungsdichte von $13\,W \cdot cm^{-2}$ ist hervorragend und eine vielversprechende Gegebenheit für die Entwicklung von miniaturisierter Vor-Ort-Diagnostik.

Kapitel 6 erörtert in einer abschließenden kritischen Diskussion die Herausforderungen an nanostrukturierte Oberflächen. Erste Ergebnisse, die mit einem selbst designten Transmission Messplatzes für nanostrukturierte Oberflächen erzielt wurden, werden vorgestellt. Nanohole Arrays zeigen eine außerordentliche optische Transmission und können (Bio)sensoren, die auf Transmission basieren, verbessern. Es wird ein Ausblick gegeben, als auch die Perspektiven von nanostrukturierten Oberflächen erörtert.

Curriculum Vitae

Personal Data

Name	Christa Genslein
Adress	Rote-Löwen-Straße 11, 93047 Regensburg
Day of Birth	09. August 1987
Place of Birth	Bamberg
Nationality	German

Education

10/2015 – 09/2018

Doctoral Study in Chemistry, University of Regensburg
"Plasmonic (Bio)sensors Based on Nanostructured Metallic Surfaces"
Institute of Analytical Chemistry, Chemo- and Biosensors (Prof. A. J. Baeumner and Dr. Thomas Hirsch), Member of German Science Foundation (DFG) research training group 1570 (Electronic Properties of Carbon-based Nanostructures)

10/2013 - 08/2015

Master of Science in Chemistry, **University of Regensburg**
Master Thesis: *Nanostructured Substrates for Bioanalytical Applications based on Plasmonic Effects*
Institute of Analytical Chemistry, Chemo- and Biosensors (Prof. A. J. Baeumner and Dr. Thomas Hirsch)

10/2010 - 07/2013

Bachelor of Science in Chemistry, University College Dublin (Ireland) and University of Regensburg
Bachelor Thesis: *Synthesis towards Analogues of Goniothalesdiol*
UCD School of Chemistry (Prof. P. Guiry)

09/2007 – 07/2010

Apprenticeship as a Chemical Laboratory Assistant at Friedrich-Alexander-University Erlangen-Nürnberg, Chair of Separation Science & Technology

09/1998 – 07/2007

Friedrich-Rückert Grammar School, Ebern
Graduation: Allgemeine Hochschulreife (equivalent to A level)

Awards

2017   Travel funding from the "Freunde der Universität Regensburg e.V."

2017   Travel Grant Graphene 2017 (Barcelona)

2016   Travel Grant Graphene 2016 (Genova)

2015   Conference Grant of the GDCh (ANAKON, Graz)

Additional Qualifications

2018   Business Administration for Engineers (Regensburg, Germany)

2017   10th Advanced Study Course on Optical Chemical Sensors - Biochemical Sensors in Medicine (Třešť, Czech Republic)

2016   Quality assurance in analytical chemistry (summer school organized by the GDCh, Berlin, 2016)

2015   "Frühjahrsschule Analytik"; GDCh workshop on analytical chemistry, (Regensburg, Germany)

Publications

7. **C. Genslein,** T. Hirsch, Nano(bio)sensors based on Plasmonic Effects of Nanostructured Metallic Surfaces: Concept, Fabrication and Applications, *invited to be submitted to Microchimica Acta.*

6. L. Wiesholler*, **C. Genslein***, A. Schroter, T. Hirsch, Plasmonic Enhancement of NIR to UV Upconversion by a Nanoengineered Interface Consisting of NaYF$_4$:Yb,Tm Nanoparticles and a Gold Nanotriangle Array for Optical Detection of Vitamin B12 in Serum, *submitted to Analytical Chemistry.*

5. **C. Genslein**, P. Hausler, E.-M. Kirchner, R. Bierl, A. J. Baeumner, T. Hirsch, Detection of small molecules with surface plasmon resonance by synergistic plasmonic effects of nanostructured surfaces and graphene, *SPIE BiOS. International Society for Optics and Photonics*, **2017**, 100800F-100800F-7, doi: 10.1117/12.2252256.

4. **C. Genslein**, P. Hausler, E.-M. Kirchner, R. Bierl, A. J. Baeumner, T. Hirsch, Graphene-enhanced plasmonic nanohole arrays for environmental sensing in aqueous samples, *Beilstein Journal of Nanotechnology*, **2016**, 7(1), 1564-1573, doi:10.3762/bjnano.7.150.

3. C. Fenzl, **C. Genslein**, C. Domonkos, K. Edwards, Th. Hirsch, A.J. Baeumner**,** Investigating non-specific binding to chemically engineered sensor surfaces using liposomes as models. *Analyst*, **2016**, 141(18), 5265-5273, doi:10.1039/C6AN00820H.

2. **C. Genslein,** 11th International Workshop on Biosensors and Bioanalytical Microtechniques for Environmental, Food and Clinical Analysis in Regensburg, Germany. Analytical and Bioanalytical Chemistry, **2016**, 408(6), 1533, doi: 10.1007/s00216-015-9252-7.

1. C. Fenzl, **C. Genslein**, A. Zöpfl, A. J. Baeumner, T. Hirsch, A photonic crystal based sensing scheme for acetylcholine and acetylcholinesterase inhibitors. *Journal of Materials Chemistry B.*, **2015**, 3(10), 2089-2095, doi: 10.1039/C4TB01970A.

Presentations

Oral Presentations

2017 SPIE. Photonic WEST, San Francisco, USA
Detection of small molecules with surface plasmon resonance by synergistic plasmonic effects of nanostructured surfaces and graphene

2017 Graphene, Barcelona, Spain
Synergistic Plasmonic Effects of Nanostructured Gold Surfaces in Combination with 2D Nanomaterials for Sensing Applications of Biomarkers

2017 Internal Workshop GRK 1570, Rattenberg, Germany
Two-Dimensional Carbon-Based Nanomaterials for Label-Free Biosensing

2017 11th Interdisciplinary PhD Seminar, Berlin, Germany
Plasmonic effects of nanostructured gold surfaces covered by 2D-nanomaterials for sensing applications

2016 Internal Workshop GRK 1570, St. Oswald, Germany
Molecular Interactions of Graphene for Bioanalytical Applications based on Plasmonic Effects

2016 Europt(r)ode XIII, Graz, Austria (Short Poster Talk)
Hybrid Plasmon-Graphene System for Determination of Adenine

Poster Presentations

2018 Europt(r)ode XIV, Naples, Italy
Plasmonic Nanomaterials for Surface-Enhanced Optical Sensors

2016 Graphene, Genova, Italy
Nanohole Arrays Combined with Chemically Rreduced Graphene Oxide for Sensing

2016 Europt(r)ode XIII, Graz, Austria
Hybrid Plasmon-Graphene System for Determination of Adenine

2015 Deutsches BioSensor Symposium, Munich
Sensing of Acetylcholine and Acetylcholinesterase Inhibitors Based on Three-Dimensional Photonic Crystals

2015 ANAKON, Graz, Austria
3-D Photonic Crystal Sensor for Acetylcholine and Acetylcholinesterase Inhibitors

2015 11th International Workshop on Biosensors and Bioanalytical Microtechniques for Environmental, Food and Clinical Analysis, Regensburg, Germany
Electrochemical and Surface Plasmon Resonance Sensors Based on Graphene

EIDESSTATTLICHE ERKLÄRUNG

Ich erkläre hiermit an Eides statt, dass ich die vorliegende Arbeit ohne unzulässige Hilfe Dritter und ohne Benutzung anderer als der angegebenen Hilfsmittel angefertigt habe; die aus anderen Quellen direkt oder indirekt übernommenen Daten und Konzepte sind unter Angabe des Literaturzitats gekennzeichnet.

Weitere Personen waren an der inhaltlich-materiellen Herstellung der vorliegenden Arbeit nicht beteiligt. Insbesondere habe ich hierfür nicht die entgeltliche Hilfe eines Promotionsberaters oder anderer Personen in Anspruch genommen. Niemand hat von mir weder unmittelbar noch mittelbar geldwerte Leistungen für Arbeiten erhalten, die im Zusammenhang mit dem Inhalt der vorgelegten Dissertation stehen.

Die Arbeit wurde bisher weder im In- noch im Ausland in gleicher oder ähnlicher Form einer anderen Prüfungsbehörde vorgelegt.

Ort, Datum   Unterschrift